Hybrid Monte Carlo-Gear's Solver to Retrieve the Vertical Profiles of Minor Atmospheric Constituents for Cloud Microphysical Modelling

A thesis submitted to the

Indian Institute of Space Science and Technology

Valiamala P.O., Thiruvananthapuram – 695 547, Kerala, India

For the Ph.D degree in Earth and Space Sciences

Kavita Patnaik

(SC19D019)

Under the joint supervision of

Dr. Amit P. Kesarkar

Scientist/ Engineer- SF

NARL, Gadanki

Dr. Chandrasekar A.

Outstanding Professor

IIST, Thiruvananthapuram

Research work carried out at

National Atmospheric Research Laboratory

Department of Space, Government of India, Gadanki, India- 517 112

Certificate

This is to certify that the thesis entitled 'Hybrid Monte Carlo-Gear's Solver to Retrieve the Vertical Profiles of Minor Atmospheric Constituents for Cloud Microphysical Modelling' submitted by Kavita Patnaik to the Indian Institute of Space Science and Technology, Thiruvananthapuram in partial fulfillment for the award of the degree of Doctor of Philosophy is a bonafide record of research work carried out by her under our supervision. In full or in parts, the contents of this thesis have not been submitted to any other Institution or University for the award of any degree or diploma.

(Amit P. Kesarkar) (A. Chandrasekar)

NARL Supervisor IIST, Supervisor

Dr.. Rama Rao Nidamanuri

Professor &Head

Dept. Of Earth and Space Sciences

IIST

Declaration

I declare that this thesis, 'Hybrid Monte Carlo-Gear's Solver to Retrieve the Vertical Profiles of Minor Atmospheric Constituents for Cloud Microphysical Modelling' submitted in partial fulfillment of the degree of Doctor of Philosophy, is a record of original work carried out by me under the supervision of Dr. Amit P Kesarkar and Prof. A Chandrasekar, has not formed the basis for the award of any other degree or diploma, in this or any other Institution or University. In keeping with the ethical practice of reporting scientific information, due acknowledgments have been made wherever the findings of others have been cited.

Thiruvananthapuram-695547 Kavita Patnaik

Oct 2023 (SC19D019)

Acknowledgments

I would like to thank my supervisors, Dr. Amit P. Kesarkar and Prof. A. Chandrasekar, for their guidance, constant support, and constructive criticism throughout my Ph.D. tenure. Their immense experience and knowledge have encouraged me during my research life. Besides my advisors, I would like to thank Mr. Subhrajit Rath, Mr. Abhishek Panchal, and Dr. Jyoti N. Bhate for their persistent support throughout my research work.

I am fortunate to be part of NARL, and I would like to thank Dr. Amit Kumar Patra, the Director of the National Atmospheric Research Laboratory (NARL), for this opportunity. I am thankful to the NARL administration and other staff for the support I have received throughout my tenure. I would like to thank Dr. S. Unnikrishnan Nair, the Director of the Indian Institute of Space Science and Technology (IIST), for the opportunity to pursue PhD at the institute.

I sincerely acknowledge the European Centre for Medium-Range Weather Forecasts (ECMWF) for providing the ERA5 temperature datasets, which have been used to initialize the temperature the solver developed in this work, and NASA for making the CLIMCAPS dataset available on the website which has been used to initialize the solver and validate its output. I am also thankful to the Ministry of Environment, Forest and Climate Change for providing the sectoral emissions over four megacities viz Delhi, Kolkata, Chennai, and Mumbai. I would like to acknowledge the Indian Meteorological Department (IMD) for providing the rain gauge observations. I am also thankful to ECMWF for making the CAMS model data available on their website, which has been used to validate the 1-D solver output.

I would like to appreciate the love and support I received from all my friends. I have enjoyed the journey with my friends Dr. Arpita Munsi, Dr. Meenakshi S, and Dr. Swetha Singh, who have made my NARL life fun-filled and cheerful. My batch mates and lab mates Arun Kumar Panda, Akash Biswal, Donali Gogoi, Renju Nandan, Sritam Hajra, Reetambhara Dutta, and Debojit Sarkar have made my Ph.D. journey memorable and colorful. Moreover, I would like to extend my thanks to all members of the WCRG group, especially Mrs. Hema Lakshmi.

It is most difficult to overstate my gratitude to my family, particularly my husband, M. Naresh, and parents, M. Prameela and MV Ramana. They have given me unceasing support for all my decisions concerning my education and career. Moreover, they always motivated, encouraged, and guided me to do my best in all aspects of day-to-day life to be a better human being in society. Finally, I thank the almighty for all the blessings.

Kavita Patnaik

Abstract

Determining the number concentration of minor constituents in the atmosphere is very important as it controls the chemistry processes of the entire troposphere. These constituents may act as cloud condensation nuclei (CCN) and ice nuclei (IN), impacting heterogeneous nucleation inside the cloud. However, the estimations of the number concentration of CCN/IN in cloud microphysical parameters are associated with uncertainties. In the present work, a hybrid Monte Carlo Gear solver has been developed to retrieve profiles of CH_4, N_2O, and SO_2. The idealized experiments have been carried out using this solver to retrieve the vertical profiles of these constituents over four megacities, viz., Delhi, Mumbai, Chennai, and Kolkata. Community Long-term Infrared Microwave Coupled Atmospheric Product System (CLIMCAPS) dataset around 0800 UTC (2000UTC) has been used for initializing the number concentration of CH_4, N_2O, and SO_2 for daytime (nighttime). The daytime (nighttime) retrieved profiles have been validated using 2000 UTC (next day 0800 UTC) CLIMCAPS products. ERA5 temperature dataset has been used to estimate the kinematic rate of reactions with 1000 perturbations determined, using Maximum Likelihood Estimation (MLE). The retrieved profiles and CLIMCAPS products are in very good agreement, as evidenced by the percentage difference between them, within the range of 1.3×10^{-5} – 60.8 %, and the coefficient of determination mainly within the range between 81-97 %. However, during the passage of tropical cyclone and western disturbance, its value became as low as 27% and 65% over Chennai and Kolkata, respectively. The development of synoptic scale systems, such as western disturbances, tropical cyclone Nivar, and easterly waves, led to disturbed weather over these megacities. The retrieved profiles during disturbed weather conditions have large deviations in vertical profiles of N_2O. However, the profiles of CH_4 and SO_2 showed lower deviation. It is inferred that incorporating the above methodology in the dynamical model will help simulate the realistic vertical profiles of the minor constituents in the atmosphere.

The accurate forecast of the diurnal cycle of the number concentration of trace gases is vital due to their influence on precipitation processes, where they control the number concentration of cloud condensation nuclei (CCN). A 1-D hybrid Monte Carlo-Gear solver was developed to retrieve vertical profiles of the number concentration of CCNs,

for microphysics modeling has been tested for representation of the diurnal cycle in this study. The retrieved profiles of CH_4 and SO_2 have been tested with the Copernicus Atmosphere Monitoring Service (CAMS) model at 3-hour time intervals over four megacities for rainy and non-rainy days. The retrieved profiles have shown diurnal variation up to 18 UTC at all pressure levels with either lead or lag time, similar to the CAMS model. After 18 UTC, there is observed a rapid increase in the number concentrations.

During non-rainy days, the 1-D model slightly overestimated (underestimated) the maximum (minimum) number concentrations of CH_4 over Delhi, whereas concentrations are overestimated over Kolkata, Chennai, and Mumbai. Forecasted CH_4 has a good (weak) correlation over Chennai (Mumbai), respectively. The 1-D model overestimated (overestimated) the maximum (minimum) number concentrations of SO_2 over Delhi. However, the maximum (minimum) concentrations are underestimated (overestimated) in Kolkata, Chennai, and Mumbai. The number concentrations of SO_2 have shown a good correlation for all megacities except Delhi. CH_4 number concentration is overestimated during rainy days. Delhi and Kolkata show a good correlation of CH_4 during rainy days. SO_2 during rainy days is underestimated, except over Chennai, and both models show a good correlation, except over Mumbai. Overall, it can be stated that the 1-D hybrid solver successfully simulates the monthly mean diurnal variation of vertical profiles of CH_4 and SO_2.

A hybrid Monte-Carlo Gear solver, developed earlier, has been improved to retrieve the vertical profiles of CH_4 and N_2O during disturbed weather situations, such as western disturbances, tropical cyclones, and heavy rainfall events, over the four megacities. Due to rapid changes in the temperature, during the passage of these systems over megacities, the percentage differences of CH_4 and N_2O number concentrations were large as compared to the Community Long-term Infrared Microwave Coupled Atmospheric Product System (CLIMCAPS). Hence, the hybrid solver has been modified by improving the maximum likelihood estimates of vertical temperature profiles. The number concentrations of CH_4 and N_2O during these weather events since 2012 have been obtained from the CLIMCAPS dataset for bias correction. It was found that the modified methodology has improved the retrieval of CH_4 and N_2O vertical profiles by reducing the error percentages during daytime and nighttime over these megacities. The percentage

error in the estimated number concentrations of CH_4 and N_2O is decreased significantly during (i) the passage of the western disturbance and rainy days of August 2020 over Delhi, (ii) the rainy days of June 2020 over Kolkata, (iii) the influence of supercyclonic storm Nivar (24 and 25 Nov 2020) over Chennai and (iv) rainy days of July 2020 over Mumbai. Implementing the above solver in the global model may lead to more accurate retrievals of the vertical profiles of the number concentrations.

Contents

List of Figures

List of Tables

Abbreviations

AIRS	Atmospheric Infrared Sounder
ASIS	Adaptive Semi-Implicit Scheme
AMSU	Advanced Microwave Sounding Unit
ATMS	Advanced Technology Microwave Sounder
ACE-FTS	Atmospheric Chemistry Experiment Fourier Transform Spectrometer
AIRS	Atmospheric Infrared Sounder
BC	Black Carbon
CAABA	Chemistry As A Box model Application
CCN	Cloud Condensation Nuclei
CSET	Cloud System Evolution in the Trades
CAM5	Community Atmosphere Model
CLIMCAPS	Community Long-term Infrared Microwave Coupled Atmospheric Product System
CMAQ	Community Multiscale Air Quality
UTC	Coordinated Universal Time
CAMS	Copernicus Atmosphere Monitoring Service
CrIS	Cross Track IR Sounder
DCA	Dicarboxylic acids
DSMC	Direct Simulation Monte Carlo
ENC	estimated number concentrations
ECMWF	European Centre for Medium-Range Weather Forecasts
ERA5	European Centre for Medium-Range Weather Forecasts Reanalysis
FTS	Fourier Transform Spectrometer
FTIR	Fourier transforms infrared
GCMs	Global Circulation Models
GWP	Global Warming Potential
GEOS-Chem	Goddard Earth Observing System - Chemistry

GHG	Green House Gases
HOLODEC	Holographic Detector for Clouds
HULIS	humic-like substances
IN	Ice Nuclei
IMD	Indian Meteorological Department
ISRO-GBP	Indian Space Research Organization's Geosphere-Biosphere Programme
IST	Indian Standard Time
INDCM	Indoor Detailed Chemical Model
IPPU	Industrial Processes and Product Use
IASI	infrared atmospheric sounding interferometer
IR	Infrared Radiation
IFS	Integrated Forecasting System
JPSS	Joint Polar Satellite System
LULUCF	Land Use, Land Use Change, and Forestry
LBLRTM	Line-by-Line Radiative Transfer Model
ML	Machine Learned
MBL	Marine Boundary Layer
MCM	Master Chemical Mechanism
MLE	Maximum Likelihood Estimation
MSA	Methane Sulphonic Acid
MW	Microwave
MoEFCC	Ministry of Environment, Forest and Climate Change
MECCA	Module Efficiently Calculating the Chemistry of the Atmosphere
MCA	Mono Carboxylic Acids
MSEA	MSA and methane sulphinic acid
MAX-DOAS	Multi-axis Differential Optical Absorption Spectroscopy
NASA	National Aeronautics and Space Administration
NOAA	National Oceanic and Atmospheric Administration
NPP	National Polar-orbiting Partnership
NDACC	Network for the Detection of Atmospheric

	Composition Changes
NRMS	Normalized Root-Mean-Square Error
NCCD	Number Concentrations from the CLIMCAPS Dataset
ODEs	Ordinary Differential Equations
OC	Organic Carbon
PDNC	Percentage Difference of Number Concentration
PSCF	Potential Source Contributing Factors
RH	Relative Humidity
SOFRID	Software for the Retrieval of IASI Data
SMOG	Surface Meteorology and Ozone Generation
UV	Ultraviolet
UNFCC	United Nations Framework Convention on Climate Change
VOC	Volatile Organic Compounds

List of symbols

s	Order of approximation
$N_{i,t}$	Concentration for individual species at a time 't'
$\widehat{N}_{i,t}$	Set of species.
Γ	Gamma function for bias adjustments
Jt	Jacobian matrix
$N_{i,t-jh}$	Concentration of species at a time (t-jh)
CH_4	Methane
N_2O	Nitrous Oxide
SO_2	Sulphur Dioxide
O(1D)	First excited state of oxygen
NO_3	Nitrate ion
F	Fluorine
Cl	Chlorine
FO_2	Dioxygen monofluoride
CF_3O	Trifluoromethanolate
NH_2	Amine
O	Oxygen atom
HO_2	Hydroperoxyl radical
SO	Sulfur monoxide
N_2	Nitrogen
NO_2	Nitrogen Dioxide
O_2	Oxygen
O_3	Ozone
H_2O_2	Hydrogen peroxide
CH_2OH	Methanol
HCHO	Methanal
H_2O	Water
HNO_3	Nitric acid
HF	Hydrogen fluoride
HCl	Hydro Chloric Acid

CF_3OH	Trifluoromethyl alcohol
SO_3	Sulfur Trioxide
$HOSO_2$	Hydroxysulfonyl radical
H_2SO_3	Sulfurous acid
CH_3	Ethane
H_2	Hydrogen
NO	Nitric oxide
CO	Carbon Monoxide

Chapter-1

1. Introduction

The atmosphere is a dynamic system in which gases are continuously exchanged with vegetation, oceans, and biotic organisms. Also, the atmosphere is crucial in supporting life on Planet Earth. Nitrogen (78% by volume) and oxygen (21% by volume) are present in significant amounts in Earth's atmosphere. Due to their modest amounts, the remaining 1% of atmospheric gases are called "trace gases." In the atmosphere, trace gases are created by chemical reactions, occurring in the gas phase with chemical components that may be sourced through biogenic processes, volcanic, lightning activities, forest fires, oceanic emissions, radioactive decay, or anthropogenic activities, such as burning of biomass, mining for fossil fuels, industrial activity, etc. These gases are released into the atmosphere via chemical reactions, ecological cycles, and physical processes, such as forming new particles, deposition, and absorption by oceans and land.

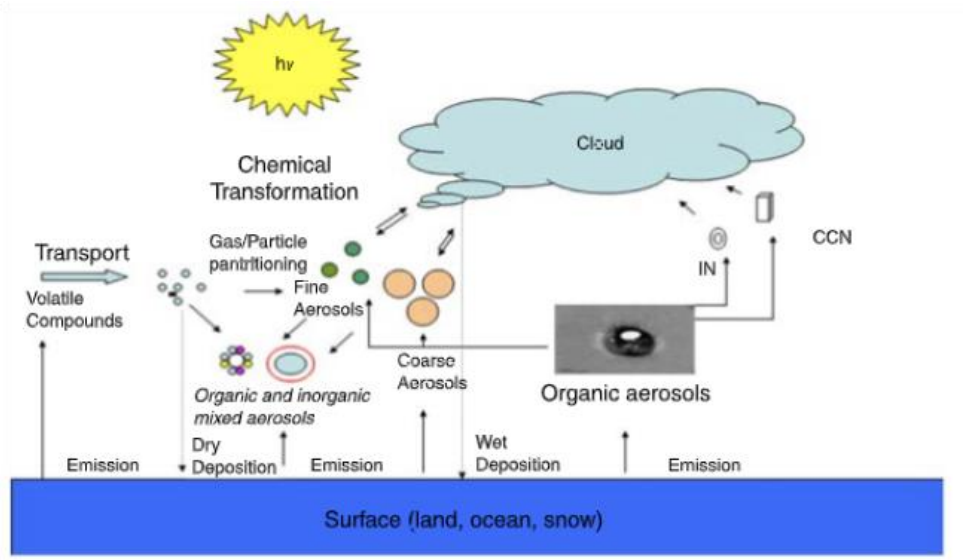

Figure 1.1. Schematic of Organic aerosol Transformation and processes in the atmosphere leading to CCN and IN (Ice Nuclei) and cloud formation (J. Sun & Ariya, 2006)

Direct emissions and the gas-to-particle conversion of vapor precursors are the two primary sources of atmospheric particles known as Aerosols. Most atmospheric aerosols typically contain a mixture of inorganic and organic species in their chemical

composition. Organic particulate matter can be a complex combination of organic carbon (OC) that is either biogenic or non-biogenic, as shown in Figure 1.1. Studies on aerosols in the atmosphere reveal that organic aerosols constitute a significant part of the overall cloud condensation nuclei (CCN) budget. Their activation potential is believed to be comparable to that of sulphate aerosols, the most efficient of all CCN.

The lifetime of a gas molecule released in the atmosphere may vary widely between seconds and millions of years, depending on the efficiency of removal processes. Natural or anthropogenic sources of various species are considered air pollutants over the region where their concentrations exceed significantly from normal values. The species' lifecycles are intricately linked; therefore, the chemical components of the atmosphere do not go through their lifecycles independently. As a result, a perturbation in one component can result in substantial, nonlinear changes in other components and feedback that can either amplify or dampen the original perturbation. It is, therefore, necessary to understand the atmospheric cycles and transformations of trace gases, including natural and anthropogenic sources, and the predominant removal mechanisms to assess the potential impact of these emissions on the atmosphere. Moreover, the analysis of the air trapped in ice cores shows that the long-lived "greenhouse gases," such as carbon dioxide (CO_2), methane (CH_4), and nitrous oxide (N_2O), have increased their amounts dramatically over time. The above indicates that the composition and amounts of atmospheric constituents are changing (Seinfeld and Pandis, 2006) with time.

The Northern Hemispheric regions have experienced a sharp rise in tropospheric ozone (O_3) and sulphate SO_4^{2-} aerosol concentrations throughout the past century, affecting the atmosphere's fundamental chemistry (Seinfeld and Pandis, 2006). Except for the most inert molecules, all other chemicals are expected to engage in some chemical reaction while transported through the atmosphere. The above products may be removed from the atmosphere in a way very different from that of their precursors. When a substance originally released as gas has been successfully converted into particle form, the overall removal is usually accelerated since particles can be removed more readily from the air than gases. It is convenient to classify the atmospheric scales of motion into four broad groups, namely, (i) Microscale (0–100 m, e.g., chimney plumes, wakes, etc.), (ii) Mesoscale (tens to hundreds of kilometers, e.g., land-sea breezes, mountain–valley winds etc.), (iii) Synoptic Scale (hundreds to thousands of kilometers, e.g., motions of whole

weather systems) and (iv) Global Scale (> 5 × 10^3 km) (Seinfeld and Pandis, 2006) as shown in Figure 1.2. An intrinsic relationship between the chemical lifetimes and the scales of atmospheric motion influences the spatial range of the various minor constituents present in the atmosphere.

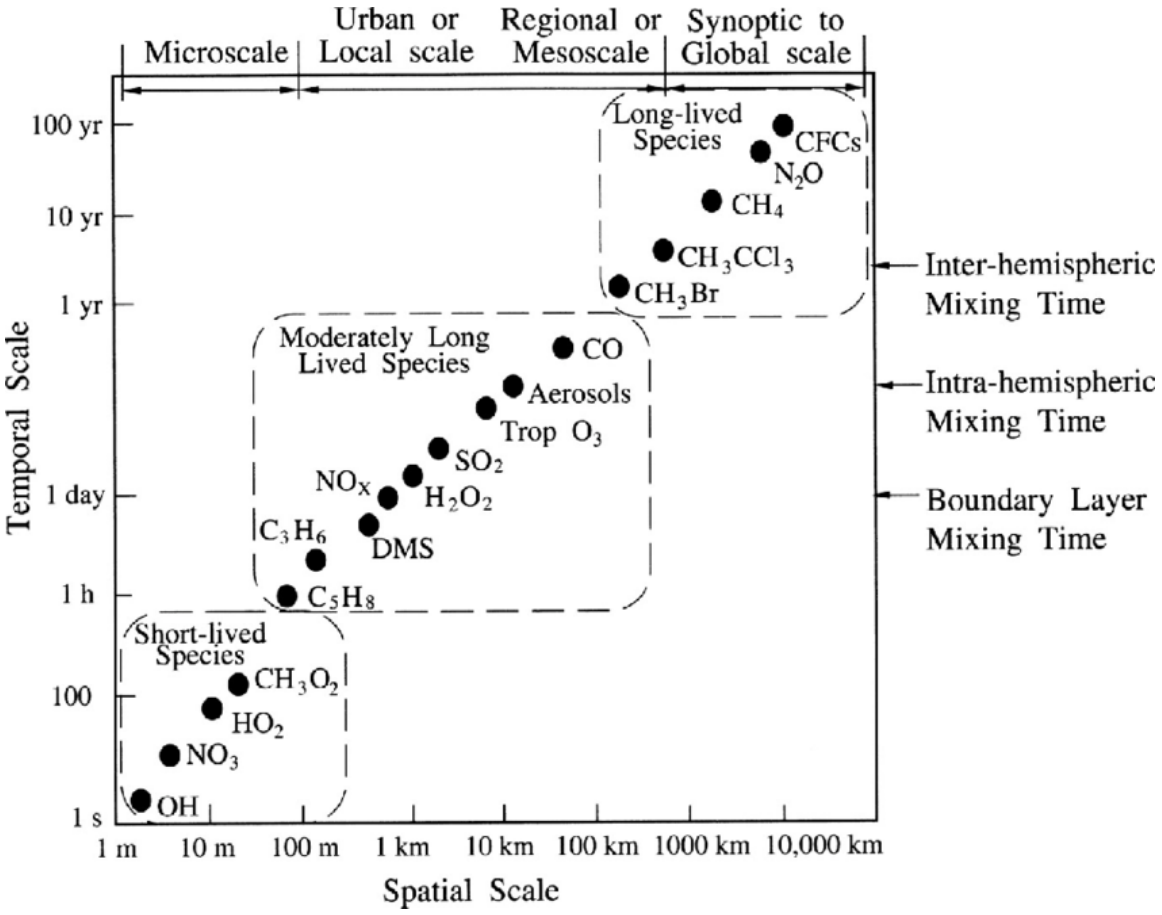

Figure 1.2. Spatial and temporal scales of variability of minor atmospheric constituents (Seinfeld and Pandis, 2006).

Aerosols can be classified in many ways, such as based on (i) generation mechanism: Primary and Secondary Aerosols, (ii) Sources: Natural and Anthropogenic, and (iii) Affinity towards water: Hygroscopic and Hydrophobic. Aerosols are typically polydisperse in nature, with the size of aerosols varying from 1nm (0.001 μm) to 10000 nm (10μm) and their varying residence times. Aerosol particles with a size range between 1nm to 10 nm are called the "nucleation mode particles," while the particles with a size range between 10 nm to 100 nm are the "Aitken mode particles." The residence time of nucleation and Aitken mode particles may vary from minutes to hours since they undergo different processes, such as gas-to-particle conversion and coagulation. Aerosol particles

of size between 100 nm to 1000 nm are called the "accumulation mode particles," and their residence time varies from days to weeks as they are subjected to wet/dry deposition. Aerosol particles between 1000 nm and 10000 nm are called the "coarse mode particles," and their residence time varies from minutes to days as they settle down due to gravity, i.e., the dry deposition of particles. Furthermore, aerosols can be classified based on their physical, chemical, and optical properties. The aforementioned physical properties may include measures such as particle size distribution, number and mass concentrations, aging of aerosols, and transportation of aerosols.

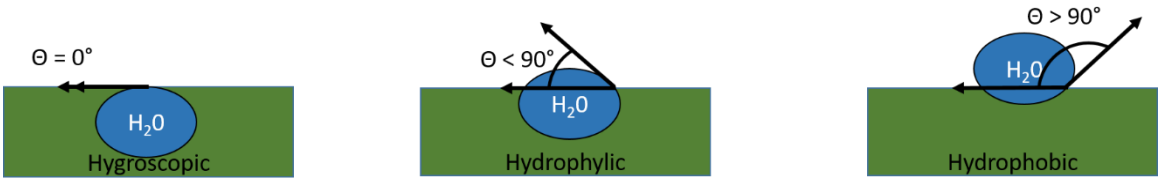

Figure 1.3. Schematic figure of contact angle of hygroscopic, hydrophilic, and hydrophobic surfaces.

Chemical properties may include solubility, hygroscopicity, mixing, etc. Also, optical properties may be characterized by the absorption and scattering of aerosol particles. The contact angle (θ) between the water droplet and the surface of aerosols shows the wettability properties, such as hygroscopic, hydrophilic, and hydrophobic. An aerosol is called "hygroscopic" when it absorbs moisture from the air, resulting in the contact angle (θ) becoming 0°. However, when the contact angle (θ) is less than 90°, aerosols tend to attract water droplets, and such an aerosol is termed "hydrophilic." For contact angle (θ) greater than 90°, water droplet is not absorbed, and such aerosols are called "hydrophobic." Figure 1.3 shows a schematic diagram of the contact angle (θ). of hygroscopic, hydrophilic, and hydrophobic surfaces

Table 1.1 presents the chief characteristics of various aerosols in terms of size, affinity towards water, and potential transformations to CCN. Sun and Ariya (2006) have discussed the role of organic aerosols and their transformation to CCN, as indicated schematically in Figure 1.1. It is suggested that various types of mono- and dicarboxylic acids (MCA and DCA) are the primary components of the organic CCN. Sun and Ariya (2006) have also hypothesized that humic-like substances (HULIS) might influence CCN

production and aerosol hygroscopicity. McMeeking et al. (2011) have studied the role of Black Carbon (BC) in the atmosphere and opined that although BC is essentially hydrophobic in nature, it has the potential to serve as CCN by acquiring hygroscopic coatings. Ming & Russell (2001) have studied the growth of hygroscopic sea salt aerosol in Marine Boundary Layer (MBL). DeMott et al. (2003) investigated the nucleation efficiency of African dust aerosols and confirmed that dust aerosols contribute to the formation of ice nuclei, even at larger distances from their sources. Koehler et al. (2009) have studied the hygroscopicity and CCN activity over different locations and found that the mineral dust particles can be activated to CCN at relative humidity less than 90 % ($RH \leq 90\%$). Mochida et al. (2011) measured the CCN activation diameters and studied the hygroscopic growth factors simultaneously in the marine boundary layer over the western North Pacific from August to September 2008. Mochida et al. (2011) found that Sulphate aerosols of small diameters can act as CCN. The results of the study by Ishizaka & Adhikari (2003) indicate that sulphates and nitrates contribute greatly to the formation of CCN, while there is minimal contribution by soot particles towards the formation of CCN.

Moreover, ambient measurements only partially capture atmospheric conditions at a specific time and location. Such observations are frequently challenging to interpret without a precise conceptual model of atmospheric dynamics. Furthermore, decision-makers cannot directly use observable measurements to plan efficiently to resolve air quality issues. Understanding particular atmospheric processes (such as chemistry, transport, removal, etc.) does not fully comprehend the system as a whole. The integration of our knowledge of many atmospheric processes can be utilized using mathematical models to unravel the relationship between the various atmospheric processes.

1.1. Atmospheric chemical transport model

Establishing a useful relationship between the air quality at a given location and the impact of the emissions on cloud formations requires atmospheric chemical transport modeling. It provides for descriptions and distribution of emission sources, weather patterns, chemical reactions, and removal mechanisms (Figure 1.4).

Table 1. 1. Characteristics of different aerosols.

Aerosols		Size (Diameter)	Hygroscopic	Hydrophobic	CCN	IN	References
Carbonaceous Aerosol	Organic Carbon	0.1-10 µm	✓		✓		(J. Sun & Ariya, 2006)
	Black Carbon	0.1-10 µm		✓			(McMeeking et al. 2011)
Sea Salt		0.05-10 µm	✓		✓		(Ming & Russell, 2001)
Soil dust or Mineral dust		0.1-10 µm	✓		✓	✓	(DeMott et al. 2003) (Koehler et al. 2009)
Sulphates		0.1-10 µm	✓		✓		(Ishizaka & Adhikari, 2003, Mochida et al. 2011)
Nitrates		0.1-10 µm	✓		✓		(Ishizaka & Adhikari, 2003)

Such a model provides for a relationship between changes in emission brought about by source control measures and subsequent changes in airborne concentrations that affect precipitation and cloud formation. Transport, physicochemical changes, and species emissions comprise the three main parts of the atmospheric chemical transport model. It is important to emphasize how closely modeling efforts, laboratory testing, and ambient monitoring contribute to and supplement one another. Whether routine or intensive, the end result of ambient monitoring of the atmosphere is used to assess the atmospheric conditions and provide the information necessary to utilize and evaluate atmospheric models. Models can be simply defined as the unifying system that organizes the understanding of atmospheric processes. The evaluation of model results frequently reveals a gap in our understanding that will lead to greater laboratory and field measurements, followed by further improved model development.

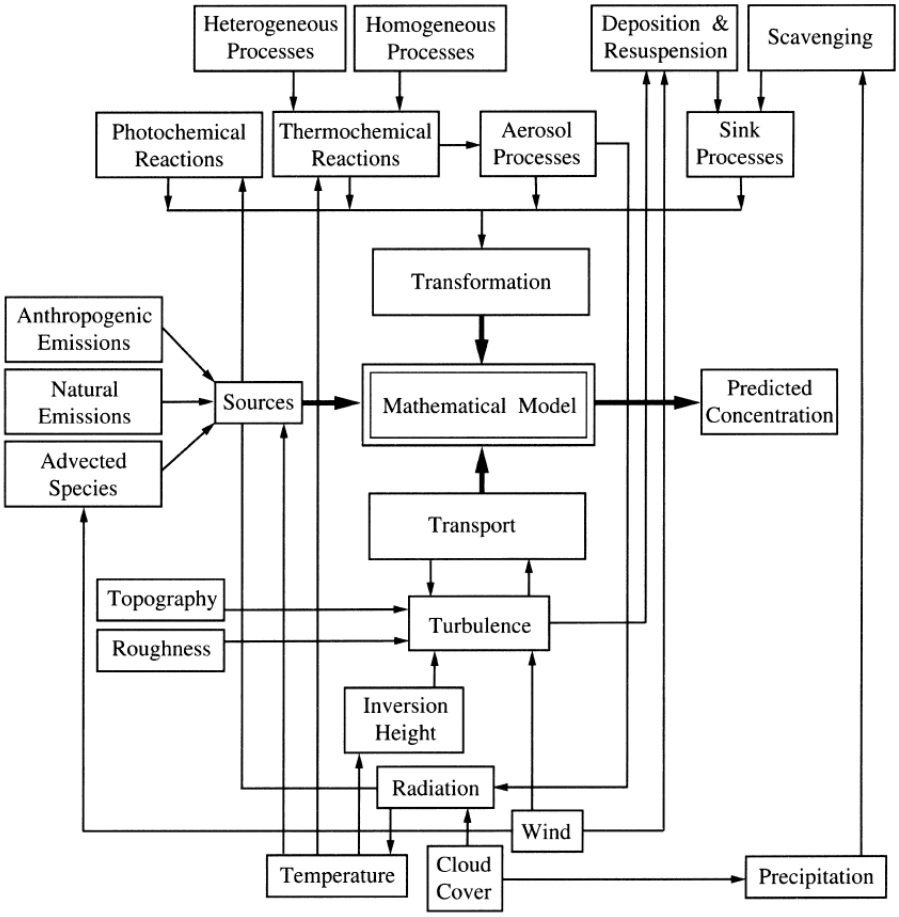

Figure 1.4. Flowchart of atmospheric chemical transport model (Seinfeld and Pandis, 2006).

There are essentially two types of atmospheric models: (i) physical model and (ii) mathematical model. Physical models have limited utility since they cannot accurately reproduce and replicate the atmosphere's motion on a real scale. Hence, mathematical models are normally employed to investigate the atmospheric processes and dynamics. In general, there are two types of mathematical models that provide for the evolution of atmospheric behavior: (i) simulations based on fundamental principles of atmospheric physical and chemical processes and (ii) models that are developed using statistical data analysis.

Furthermore, atmospheric models vary in complexity based on the dimensionality of the model, such as zero-dimensional (0-D), one-dimensional (1-D), two-dimensional (2-D), and three-dimensional (3-D) models, as shown in Figure 1.5. The concentration of

species (c_i) in 0-D models are a function of only time (t). 1-D models, also known as column models, have a concentration of species as a function of height (h) and time ($c_i(h,t)$). In 2-D models, the species concentrations are considered uniform along one dimension, generally the longitude, and are, hence, functions of latitude, height, and time ($c_i(x,h,t)$). In 3-D models, the species concentrations are considered to be functions of three-dimensional space and time ($c_i(x,y,h,t)$).

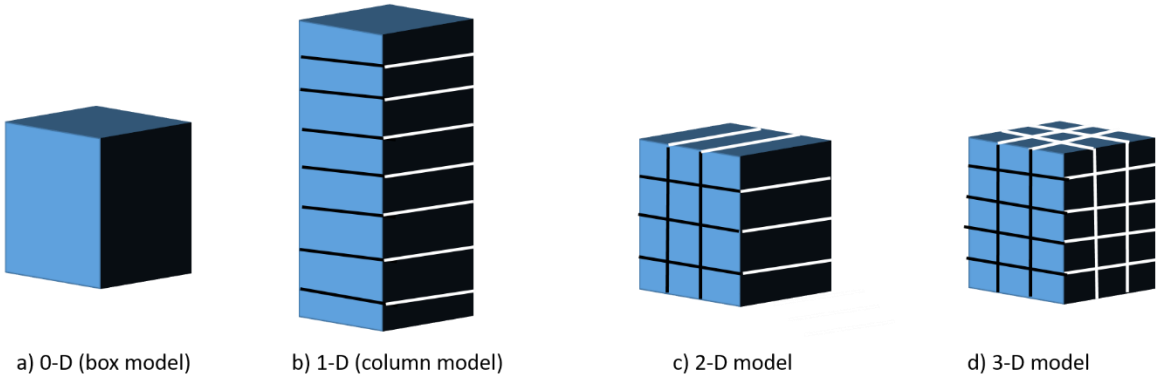

Figure 1.5. Representation of 0-D model, 1-D model, 2-D model and 3-D model.

1.2. Monte Carlo Simulations

Monte Carlo simulations are based on repeated random sampling and statistical analysis and aim to compute the possible outcomes of random experiments with unknown results (Raychaudhuri, 2008). The Monte Carlo algorithm involves the following few steps. The statistical properties of model inputs are determined and then employed to generate random sample input to calculate the model output. Further, the model output is compared to observations for validation. If there is a reasonable match between the model output and the observations, the model output is subjected to statistical analysis. Otherwise, the above steps are repeated to generate random sample input to compute the model output, as shown in Figure 1.6.

Several studies have used the Monte Carlo algorithm to investigate atmospheric chemistry and cloud microphysics processes. CAABA (Chemistry As A Box model Application) and MECCA (Module Efficiently Calculating the Chemistry of the Atmosphere) have used chemistry in multiple aerosol-sized bins and performed automatic multiple simulations that reach a steady state, Monte Carlo simulations with randomly

varying rate coefficients within their experimental uncertainty, employ Lagrangian trajectories, mercury chemistry, etc. in their calculations, in the updated model version (Sander et al. 2011).

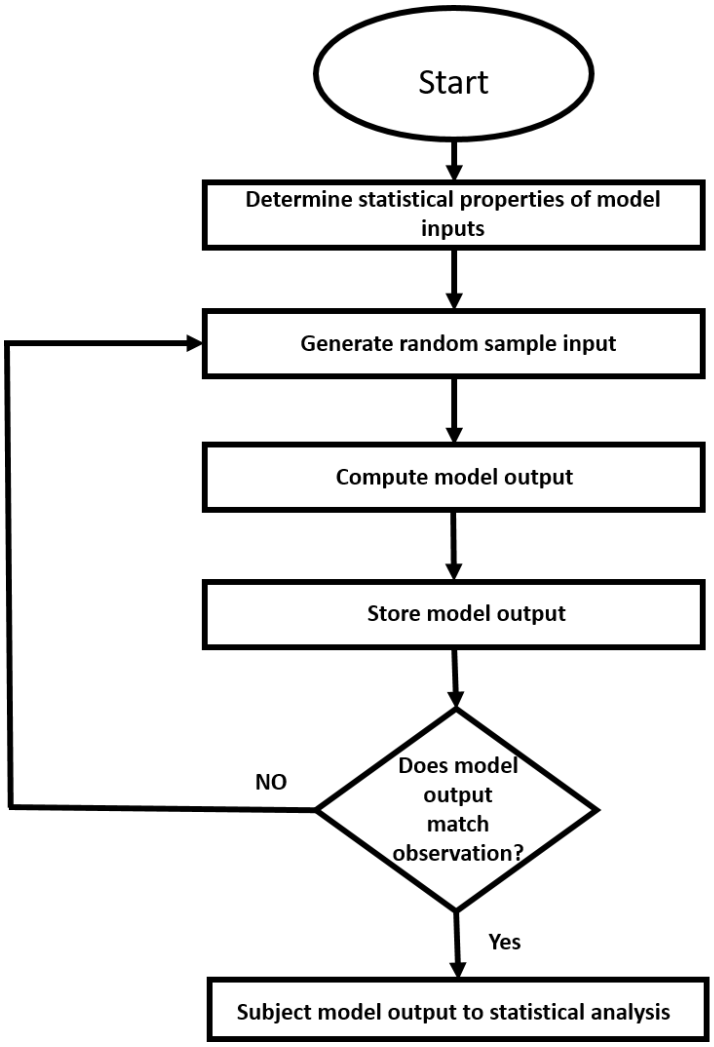

Figure 1.6. Algorithm of Monte Carlo Simulations.

(2015) have developed a parametric sensitivity analysis framework to examine the aerosol climate effects on East Asian Monsoons. Yan et al. (2015) employed the Community atmosphere model (CAM5), integrated with the quasi-Monte Carlo parameter sampling method and a surrogate model. Yan et al. (2015) performed 256 CAM5 simulations in total to evaluate the model response to the unknown cloud microphysics parameterizations, aerosol emission variables, such as sulfate, black carbon (BC), and dust, as well as their interactions. The results of Yan et al. (2015) indicated

that the impact of sulfate, BC, and dust aerosols on the East Asian Monsoon through cloud-radiation interactions are different from one another due to the variations in their optical, microphysical, and spatial distribution. Jaruga & Pawlowska (2018) have developed a novel method, which is available in the libcloudph++ library of algorithms, for simulating cloud microphysics to represent aqueous-phase chemical reactions within water drops, in the particle-based microphysics scheme. The above method extends the libcloudph++ particle-based microphysics approach to include a Monte Carlo coalescence for the aqueous-phase chemical reactions inside the cloud droplets. Kruza et al. (2021) have employed the INdoor Detailed Chemical Model (INDCM) to perform a Monte Carlo simulation, where a large but realistic range of model input parameters are varied stochastically over 1000 model runs. Kruza et al. (2021) suggest that the model output defines the likely range of model performance and directly correlates the input parameter values with predicted indoor air species concentrations.

La et al. (2022) investigated the effects of entrainment and the subsequent mixing of free-tropospheric and cloudy air on cloud microphysical properties of marine stratocumulus clouds during the Cloud System Evolution in the Trades (CSET) campaign over Northern California and Hawaii. Due to its ability to provide 3-D positions and sizes of droplets within a sample volume on a centimeter scale, the data measured by Holographic Detector for Clouds (HOLODEC) were widely employed. The above allowed for the analysis of the 3-D spatial distribution of droplets, which would not have been possible with conventional cloud probes earlier. The study of La et al. (2022) focused on analyzing the visual characteristics of 3-D spatial distribution and inhomogeneous mixing of droplets and quantified the relationship between 3-D spatial distribution and inhomogeneous mixing characteristics by comparing the following two spatial distributions, namely, (i) the measured spatial distribution of the droplets and (ii) the generation of randomly distributed droplets using a Monte Carlo approach.

1.3. Gear's Solver

The first-order homogeneous ordinary differential equation (ODE) of the first degree is used to describe the chemical reactions in the gas phase. In sets of gas-phase reactions, the chemical e-folding lifetimes of individual gases vary by many orders of magnitude, making them stiff. Some classical numerical approaches do not help solve stiff chemical

ODEs. The explicit methods, such as the fourth-order Runge–Kutta method and the Richardson extrapolation/Bulirsch–Stoer method, are slow and provide inefficient solutions to stiff ODEs. Due to the above reasons, a semi-implicit solver such as Gear's solver is usually employed to solve stiff ODEs (Jacobson, 2005).

Santillana et al. (2010) presented a computationally efficient adaptive method to calculate the temporal evolution of chemical species concentrations in global 3-D atmospheric chemistry models. Santillana et al. (2010) divided the computational domain into fast and slow regions for each chemical species at each time step. Subsequently, Santillana et al. (2010) grouped the fast species and solved for their concentration in a coupled manner. Slow species concentrations, however, were calculated using a simple semi-implicit formula. Santillana et al. (2010) performed a one-year simulation of global tropospheric ozone-NO_x-VOC aerosol chemistry using the GEOS-Chem model. Their results showed a 50% improvement in the computational power of the chemical solver without significant additional error.

Cariolle et al. (2017) have developed and tested an Adaptive Semi-Implicit Scheme (ASIS) solution for simulating atmospheric chemistry to solve systems of ordinary differential equations involving species concentrations' temporal evolution. ASIS adopts a one-step linearized implicit system that considers the Jacobian of chemical fluxes. It conserves mass and has a time-stepping module that controls the accuracy of the numerical solution. In idealized box model simulations, ASIS provides results similar to higher-order implicit schemes derived from Rosenbrock’s and Gear's methods, requiring less computation and runtime with the reasonable accuracy required for atmospheric applications. Kelp et al. (2022) highlighted and identified the greatest computational difficulty in the global modeling of atmospheric chemistry. Kelp et al. (2022) suggested that the numerical integration of the coupled kinetic equations poses the greatest computational difficulty and developed a machine-learned (ML) solver that captures surface ozone's diurnal and synoptic variability at polluted and clean locations. Kelp et al. (2022) opined that Gear high-order implicit solvers can integrate the system of stiff coupled differential equations and provide accurate solutions.

1.4. Motivation

There is considerable uncertainty in our knowledge and understanding of how anthropogenic emissions from industry, fossil fuels, and biomass affect the atmosphere's oxidation chemistry. The aforementioned emissions release trace substances that are likely to decrease the oxidative capacity of the atmosphere by acting as a sink for hydroxyl radicals and also increase the oxidative capacity through a series of tropospheric ozone (O_3) formation reactions. The lifetime of a trace element such as CH_4 and CO that impacts climate change and human health is determined by atmospheric oxidative capacity. It is paramount to develop strategies for mitigating greenhouse gases and air pollution to understand how anthropogenic activities impact their atmospheric oxidation capacity on a regional scale (Alexander et al. 2004). Gaur et al. (2014) analyzed the variations of SO_2, NO_x, CO, and O_3 at an urban location in Kanpur in Northern India from June 2009 to May 2013 using long-term near-surface measurements. Gaur et al. (2014) have indicated that scientists in India were interested in trace gas observations around the beginning of the 1990s. Gaur et al. (2014) suggest that the goal of the Indian Space Research Organization's Geosphere-Biosphere Programme (ISRO-GBP) is to understand better atmospheric trace gases, including their chemistry, transportation paths, and modeling over the Indian subcontinent. Gaur et al. (2014) have also highlighted that several long-term studies based on near-surface in-situ observations over the Indian subcontinent have been conducted, and the majority of these studies only focused on O_3 data, and none of them reported SO_2 data.

Modeling and estimating the uncertain climate impacts of aerosols across Asia requires a regional-scale analysis that considers all aerosols' physical, optical, chemical, and radiative properties. Therefore, It is essential to undertake a quantitative analysis of columnar physical, optical and chemical aerosol characteristics to embark on a mission to improve air quality and mitigate air pollution (S. Ramachandran & Rupakheti, 2022).

1.5. Scope of Thesis Study

The study of the thesis has been scoped as below to develop a hybrid solver for obtaining vertical profiles of the minor constituents of the atmosphere.

1. The vertical stratification of trace gases undergoes chemical transformations and impacts the availability of CCN and IN, which affect the growth of clouds and precipitation.
2. Hybrid Monte Carlo Gear's Solver is employed to simulate vertical profiles of minor constituents of the atmosphere, its diurnal variation, and their concentration during disturbed weather situations.

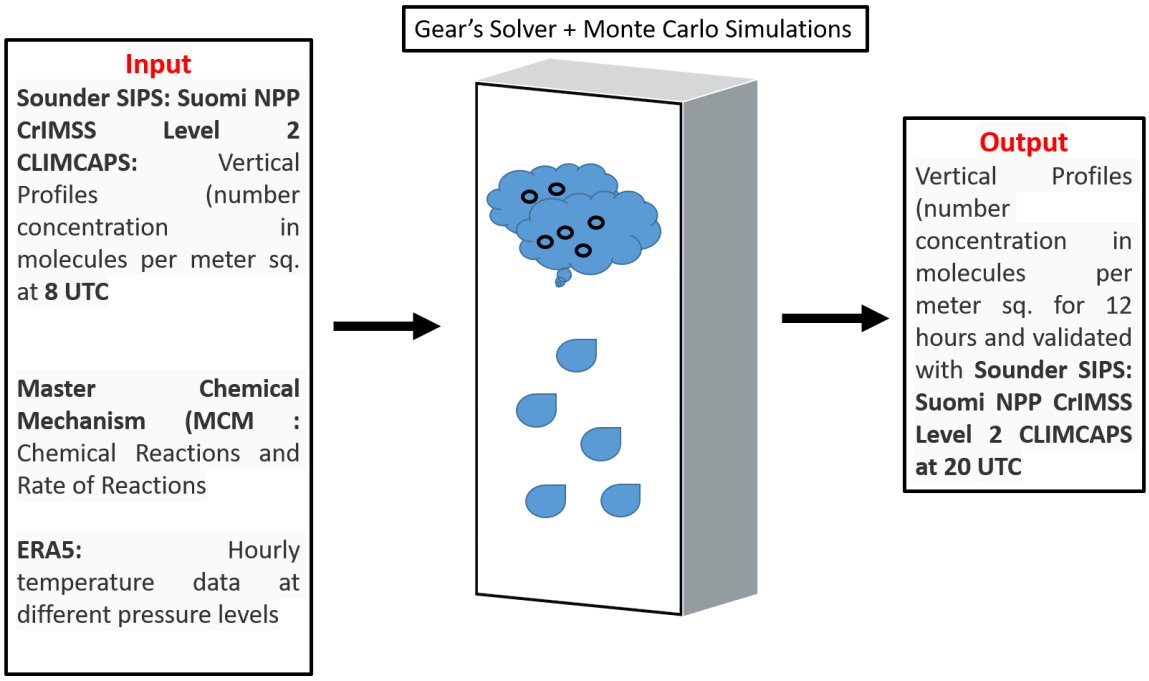

Figure 1.7. Schematic of 1-D hybrid Monte Carlo Gear Solver.

1.6. Thesis objectives

The objective of this thesis study is to develop a 1-D model

(i) to develop a 1-D hybrid Monte Carlo-Gear's Solver.

I. (ii) to retrieve the vertical profiles of minor atmospheric constituents using the 1-D hybrid solver.

II. (iii) to simulate and validate the diurnal variation of minor constituents using the 1-D hybrid solver.

III. (iv) to improve the 1-D hybrid model for better retrieval of the vertical profiles of minor constituents during disturbed weather situations.

Chapter 2

2. Data and Methodology

2.1 Site selection

The locations of the four megacities chosen for this thesis study are shown in Figure 2.1. The four megacities are Delhi (28.56°N, 77.11°E), Kolkata (22.65°N, 88.45°E), Chennai (13.04°N, 80.17°E), and Mumbai (18.90°N, 72.81°E) are part of the golden quadrilateral, a national roadway project. The Golden Quadrilateral, with 5846 km, is a national highway network connecting several major industrial, agricultural, and cultural centers of India that forms a quadrilateral with all the four major metro cities of India forming the vertices, viz. Delhi (north), Kolkata (east), Mumbai (west), and Chennai (south). These megacities together have a population of about 56 million. Delhi is the capital of India and is located in northern India; Kolkata, situated near the Bay of Bengal, is home to over 14 million people. Delhi and Kolkata are also part of the Indo-Gangetic Plain and are one of India's industrial belts (Ojha et al. 2020). Mumbai is located on the west coast of India, off the Arabian Sea, and has the largest population of all megacities, of about 18 million, while Chennai is on the southeast coast, off the Bay of Bengal. Delhi is landlocked and has a temperate climate without dry seasons and hot summers (Peel et al. 2007). The stations Mumbai, Chennai, and Kolkata are coastal cities, and the weather over these cities is influenced by coastal phenomena such as sea breeze. The cities of Chennai and Kolkata have tropical savannah climates (Peel et al. 2007), while the climate of Mumbai city is tropical rainforest type (Peel et al. 2007).

All four megacities are characterized by distinct weather phenomena depending on the seasons. During the southwest monsoon season (JJAS), the south-westerly wind flows in the lower troposphere from the equatorial Indian Ocean, bringing ample moisture over the continent as it progresses from the southern peninsula to northern latitudes. The southernmost city, Chennai, is unaffected by the southwest Indian monsoon as the eastern Ghat mountains block the monsoon winds. Mumbai receives the highest amount of rainfall among the four cities. The coastal town of Kolkata also gets significant rain during the southwest Indian monsoon season. The southwest Indian monsoon reaches Delhi by the end of June or early July. Delhi receives maximum rainfall during the southwest monsoon season (June-September), with the highest rainfall in August,

followed by July. Kolkata and Mumbai cities, however, receive most of their rainfall during the southwest Indian monsoon season, with maximum rainfall during June and July for Kolkata, followed by August and June for Mumbai.

The withdrawal of the southwest monsoon season changes the lower tropospheric winds from the southwest to the northeast direction. The northeast monsoon season (OND) prevails over the southern peninsula from October to December. The transition begins from the northern latitude towards the southern direction. The transition is characterized by thunderstorms all over India, especially in Chennai city. The northeast monsoon season brings maximum rainfall over Chennai in November, followed by October. The occurrence of tropical cyclones over the Bay of Bengal and Arabian Sea also marks this season. Most Bay of Bengal cyclones cross the east coast, contributing to heavy rainfall over Chennai. Mumbai has fair weather during this season (October to December), except for a few thunderstorms at the beginning of October. Kolkata also receives good rain during October, followed by November and December. Delhi experiences rainfall due to Western disturbances during January, followed by cold wave conditions.

In the winter months (January and February), cold temperatures characterize the weather over Mumbai, with north-westerly winds. During January and February, the passage of western disturbances and the upper air trough in easterlies caused fog over Delhi/Kolkata regions and cold wave conditions over Delhi, Kolkata, and Mumbai. In these winter months (January and February), the Chennai region observes fair weather conditions with moderate air temperatures. Climatologically, cold temperatures prevail over Delhi during the November-March months and warm temperatures in the other months (Figure. 2.1 a).

In the pre-monsoon (MAM) season, the anticyclone in the lower troposphere is observed over the Arabian Sea and the Bay of Bengal. April and May are the hottest months in the Indian region; hence, all four cities experience hot weather conditions during April and May. Delhi has an extreme maximum air temperature during this season; however, June is the warmest month in Delhi. Pre-monsoon dust, storms, thunderstorms, and squalls are observed over Delhi and Kolkata. Thunderstorms followed by rainfall and hail are observed over Mumbai and Chennai cities. May is the warmest month for Chennai (Figure 2.1c), Kolkata (Figure 2.1b), and Mumbai (Figure 2.1d).

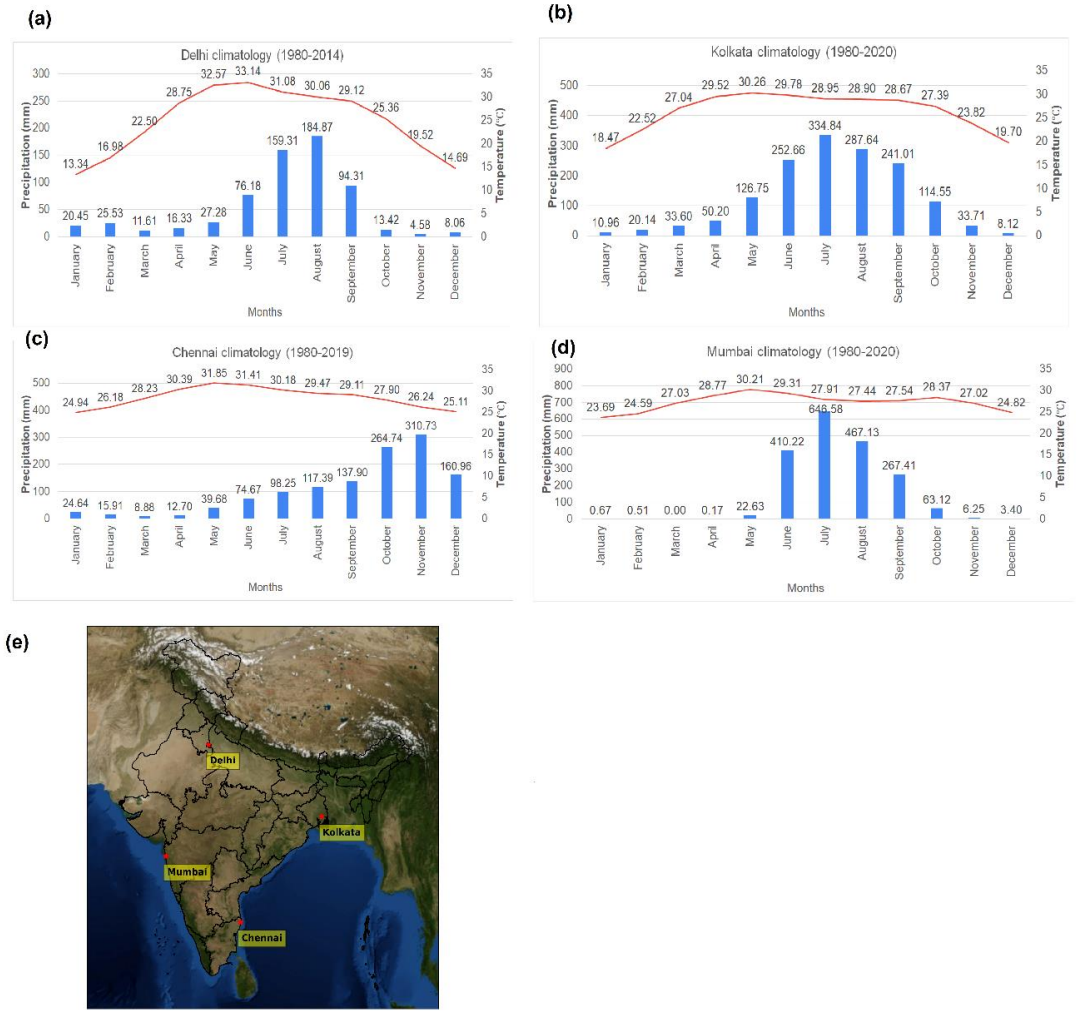

Figure 2.1. Climatology of monthly averaged temperature and rainfall over (a) Delhi, (b) Kolkata, (c) Chennai, and (d) Mumbai. (e) India map indicating locations of four megacities selected for the solver validation using satellite dataset.

2.2. Potential local sources for emissions of minor constituents

The survey of sectoral emissions for the whole of India (Figure 2.2 a) by MoEFCC (2021) indicated a reduction in emissions from the agriculture sector since 2014. The land use, land use change, and forestry (LULUCF) sector is a net sink for emissions in India. A slight increase in the Industrial Processes and Product Use (IPPU) sector has been observed since 2014. The major emissions are from the energy sector (75%), and total national emissions have increased by 9.75% since 2014.

The national capital of India, Delhi, is the largest commercial hub and also the largest center of small-scale industries. Conversely, Mumbai has several engineering, oil refineries, thermal power plants, manufacturing and food processing sectors, and textile Industries (point source). Kolkata is primarily a commercial and financial hub of eastern India, having various industrial sectors, including steel, heavy engineering, mining, minerals, cement, pharmaceuticals, food processing, agriculture, electronics, textiles, and jute. Chennai is the commercial capital of south India and has the largest industrial sector, comprising software, electronics, construction, and automobiles.

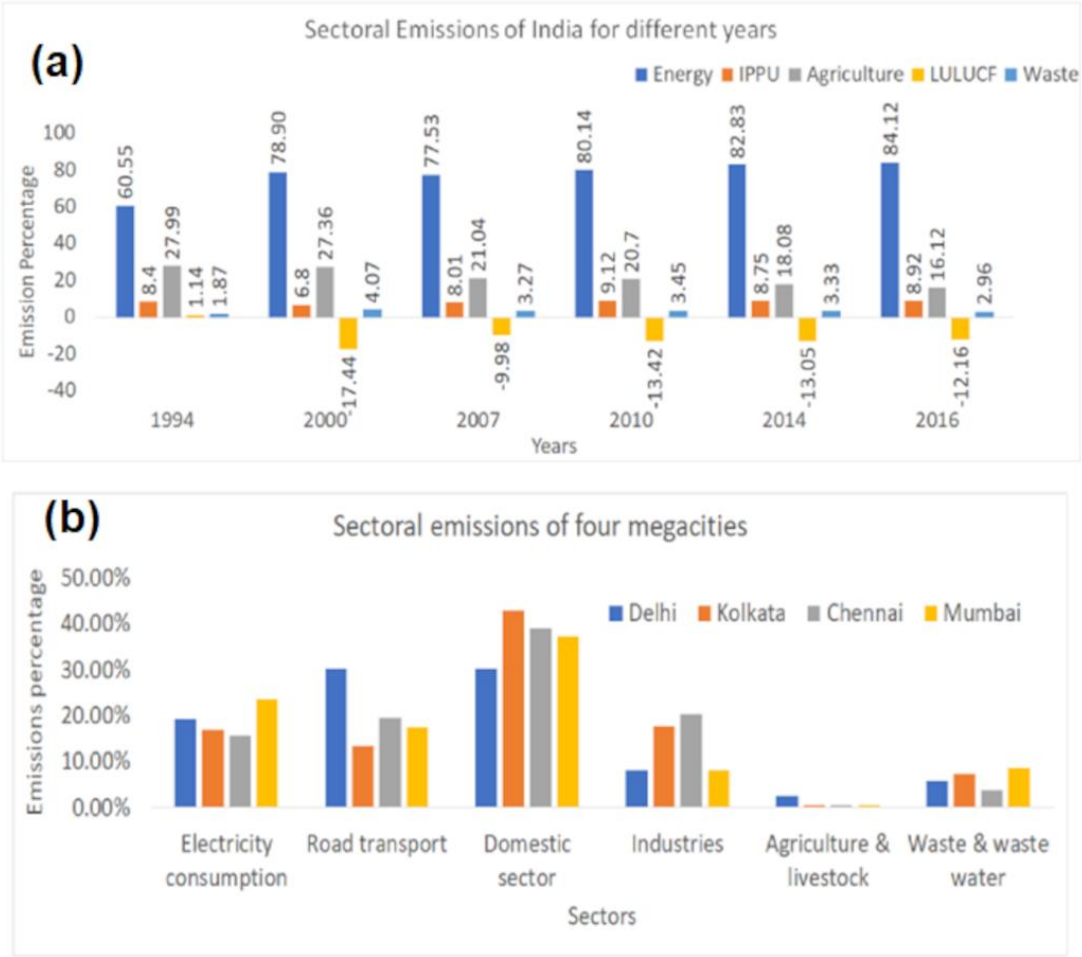

Figure 2.2. (a) Sectoral emission of India for different years (MoEFCC, 2021) and (b) sectoral emissions over four megacities (A. Ramachandran & Anushiya, 2015)

Ramachandran and Anushiya, 2015 estimated the emissions of greenhouse gases in Indian cities. Their study indicated that Delhi has maximum emissions from road transport (32.08%), followed by the domestic sector (30.26%), electricity consumption (19.28%), industries (9.789%), waste and wastewater (5.78%), and agriculture and

livestock (2.49%). Kolkata has maximum emissions from the domestic sector (42.78%), industries (17.66%), electricity consumption (17.04%), road transport (13.30%), waste and wastewater (7.18%), and agriculture and livestock (0.22%). In comparison, Chennai has maximum emissions from the domestic sector (39.01%), followed by industries (20.25%), road transport (19.50%), electricity consumption (15.77%), waste and wastewater (3.72%), and agriculture and livestock (0.05%). However, Mumbai has maximum emissions from the domestic sector (37.20%), electricity consumption (23.44%), road transport (17.41%), waste and wastewater (8.46%), industries (7.89%), and agriculture and livestock (0.12%). Singh et al. (2021) also indicated that the transport sector has a dominant contribution to total emissions in these megacities.

2.3. Master Chemical Mechanism (MCM)

MCM (http://mcm.york.ac.uk/) describes a series of primary emitted volatile organic compounds (VOCs) and gas-phase chemical processes that cause tropospheric degradation. MCM was initially developed to provide accurate, up-to-date, and robust information on the role of specific organic compounds at the ground level. MCM additionally offers a research tool for investigating different areas in which an in-depth illustration of the chemistry is required, e.g., generating distributions of speciated radical and closed-shell intermediates formed during VOC degradation. This dataset contains thermal and photochemical reactions and corresponding temperature-dependent reaction rates for gas-phase atmospheric constituents (Atkinson et al. 2004). The details of MCM version 3.3.1 for (i) non-aromatic schemes have been discussed in Jenkin et al. (1997) and Saunders et al. (2003); for aromatic schemes have been discussed in Jenkin et al. (2003), and Bloss et al. (2005); for (iii) β-caryophyllene scheme has been discussed in Jenkin et al. (2012); and for (iv) isoprene scheme has been discussed in Jenkin et al. (2015).

In the present work, we have used MCM version 3.3.1 to select chemical reactions and kinematic reaction rates. While the number concentration of O_3, CO, CH_4, N_2O, HNO_3, H_2O, and SO_2 are available from the Community Long-term Infrared Microwave Coupled Atmospheric Product System (CLIMCAPS) dataset for model initialization, the chemical reactions, as well as the rate of reactions for these atmospheric constituents, have been obtained from MCM dataset. The chemical reactions and corresponding reaction rates are

indicated in Table 2.1. These reaction rates have been used to estimate the vertical profile of the changes in the number concentration of chemical species at temperatures corresponding to the heights (Patnaik et al. 2023).

Table 2.1. Reactions and rate of reactions used in the solver and obtained from MCM

Reactants	**Products**	**Rate Coefficients**
$O(1D) + CH_4$	$HO + CH_3$	1.5×10^{-10}
$O(1D) + CH_4$	$CH_2OH + H$	1.5×10^{-10}
$O(1D) + CH_4$	$HCHO + H_2$	1.5×10^{-10}
$HO + CH_4$	$H_2O + CH_3$	$1.85 \times 10^{-12} \times \exp(-1690/T)$
$NO_3 + CH_4$	$HNO_3 + CH_3$	1×10^{-18}
$F + CH_4$	$HF + CH_3$	$1.3 \times 10^{-10} \times \exp(-215/T)$
$Cl + CH_4$	$HCl + CH_3$	$6.6 \times 10^{-12} \times \exp(-1240/T)$
$FO_2 + CH_4$	products	4.1×10^{-15}
$CF_3O + CH_4$	$CF_3OH + CH_3$	$2.6 \times 10^{-12} \times \exp(-1420/T)$
$O(1D) + N_2 + M$	$N_2O + M$	2.8×10^{-36}
$O(1D) + N_2O$	$N_2 + O_2$	$4.3 \times 10\text{-}^{11}$
$O(1D) + N_2O$	2NO	7.6×10^{-11}
$O(1D) + N_2O$	$O(3P) + N_2O$	6.0×10^{-12}
$NH2 + NO_2$	$N_2O + H_2O$	$2 \times 10^{-11} \times (T/298)^{-1.3}$
$O + SO_2 + M$	$SO_3 + M$	1.1×10^{-14}
$HO + SO_2 + M$	$HOSO_2 + M$	9.3×10^{-13}
$HO_2 + SO_2$	products	1×10^{-18}

$NO_3 + SO_2$	products	1×10^{-19}
$SO + O_2$	$SO_2 + O$	$1.6 \times 10^{-13} \times \exp(-2280/T)$
$SO + O_3$	$SO_2 + O_2$	$4.5 \times 10^{-12} \times \exp(-1170/T)$
$SO + NO_2$	$SO_2 + NO$	1.4×10^{-11}
SO_2 + ice	products	$7.3 \times 10^{-4} \times \exp(2065/T)$
$SO_2 + H_2O_2$ - doped ice	products	$2.9 \times 10^{-15} \times \exp(2065/T)$
SO_2 + mineral oxide (dust) surfaces	products	
$SO_2 + H_2O$ (l)	H_2SO_3(aq)	$5 \times 10^{6} \times \exp(-2300/T)$

2.4. Rain gauge observations

Daily rainfall data was obtained from the Indian Meteorological Department (IMD) for the four megacities during summer and rainy days in 2020 (Figure 2.3). As seen from Figure 2.1, climatologically, most rainfall occurs in August, November, June, and July for Delhi, Chennai, Kolkata, and Mumbai, respectively. Hence, the months mentioned above in 2020 are selected to validate the methodology developed in this study for a rainy month. The daily rainfall that occurred in these months is shown in Figure 2.3. The average annual rainfall for Delhi, Mumbai, Kolkata, and Chennai are 79.4 cm, 212.3 cm, 172 cm, and 140.4 cm, and the average annual rainy days are 39, 73, 83, and 59, respectively. The ever-recorded heaviest rainfalls in 24 hours over Delhi, Mumbai, Kolkata, and Chennai are 184 mm (on 02 August 1961), 94.4 cm (on 26 July 2005 at Santacruz, Mumbai), 38.3cm (on 06 June 1984) and 80cm (on 12 November 1991) respectively.

For validating the methodology, presented in this work for non-rainy months, the simulations have been carried out in April for the Delhi location and in May for the other places. During May, no rainfall was recorded at Santacruz station in Mumbai, Dum Dum station in Kolkata, and 5.2 mm rainfall at Minambakkam, Chennai. For April 2020, Safdarjung station in Delhi received 9 mm of rainfall. The maximum rainfall was found

to be 54.53 mm (13 August 2020) over Delhi, 124.80 mm (28 June 2020) over Kolkata, 156.40 mm (24 November 2020) over Chennai, and 244.40 mm (16 July 2020) over Mumbai. Delhi received rather heavy rainfall of 54.53 mm on 13 August 2020 and 40.60 mm on 20 August 2020 and moderate rain between 10.50 mm to 23.13 mm on 6, 14, 18, and 29 August 2020. Kolkata received heavy rainfall of 124.80 mm on 28 June 2020 and rather heavy rain of 39.10 mm on 12 June 2020, as well as 37.40 mm on 21 June 2020 and 40.50 mm on 27 June 2020. Kolkata received moderate rain between 9.90 mm and 17.40 mm on the 7, 11, 13, 16, and 23 of Jun 2020. Chennai received heavy rain of 156.40 mm on 24 November 2020 and, 141.90 mm on 25 November 2020, and rather heavy rain of 38.70 mm on 16 November 2020. Chennai received moderate rain between 14.30 mm and 33.70 mm on November 11, 12, 15, and 26 of 2020. Mumbai received very heavy rainfall of 244.4 mm on 16 July 2020, heavy rainfall of 125.7 mm on 03 July 2020, 182.2 mm on 04 July 2020, and 137.6 mm on 05 July 2020, and the remaining days it received light to moderate rain. Thus, selected non-rainy months for simulations have very little monthly observed rainfall in contrast to rainy months, the latter having a relatively large amount of rainfall. The above indicates that the sample selected represents rainy and non-rainy months for testing the methodology proposed in this work (Patnaik et al., 2023).

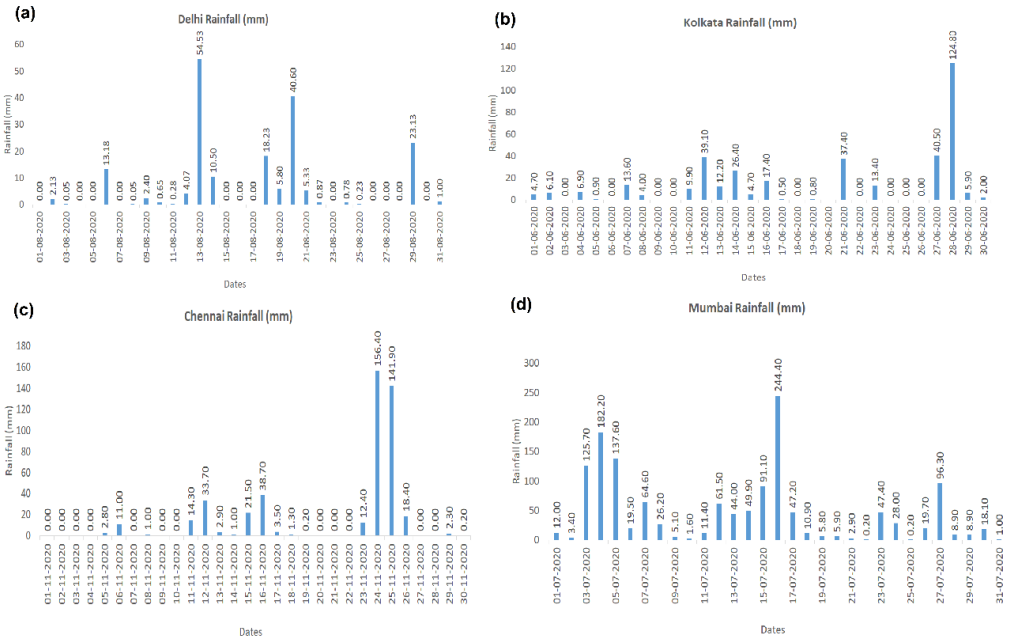

Figure 2.3. The daily rainfall (mm) during months selected for studies of the year 2020 over four megacities viz. (a) Delhi, (b) Kolkata, (c) Chennai, and (d) Mumbai.

2.5. CLIMCAPS Datasets

CLIMCAPS Version 2 Level-2 (**https://disc.gsfc.nasa.gov**) datasets provided by NASA since 2012 contain a variety of geophysical parameters derived from IR/MW sounder measurements on board polar-orbiting satellites, such as AIRS/AMSU on Aqua, CrIS/ATMS on Suomi NPP, and NOAA20. CLIMCAPS contains a variety of geophysical parameters, such as profiles of temperature, water vapor, and trace gas species (O_3, CO, CH_4, N_2O, HNO_3, and SO_2) as well as clouds and surface properties for six minutes of instrument observation at a time. Also, data from the National Aeronautics and Space Administration (NASA) system for sounder instruments on the polar-orbiting satellites Aqua (2002–present), Suomi NPP (2012–present), and NOAA20 (2017–present), that is, the first of the Joint Polar Satellite System (JPSS) series of four satellites scheduled to maintain operational orbit through 2040 (Smith and Barnet 2020), is available. In addition, the Cross Track IR Sounder (CrIS) sensor provides more accurate, detailed atmospheric temperature, moisture, and greenhouse gas observations for weather and climate applications. Its performance is best in clear to partly cloudy conditions, as infrared energy does not penetrate thick clouds. Hence, it works along with the Advanced Technology Microwave Sounder (ATMS) since microwave energy from this instrument can penetrate the cloud cover. This product has been used to initialize O3, CH4, N2O, HNO3, and SO2 concentrations on 37 fixed-pressure layers in the vertical direction during summer and rainy days in selected locations. This satellite has an overpass over India twice a day at around 0800 UTC (1330 IST) and 2000 (0130 IST) UTC. In this chapter, we have utilized the 0800 UTC dataset for initialization and the 2000 UTC dataset to validate the method.

2.6. ERA5 Reanalysis Dataset

ERA5 estimates the various atmospheric, terrestrial, and oceanic climatic variables hourly. The data covers the Earth with a 30km grid and breaks down the atmosphere into 137 levels from the surface to an altitude of 80km (Bell et al. 2021; Hersbach et al. 2020). It is based on the Integrated Forecasting System (IFS) Cy41r2. The ERA5 dataset also provides information about uncertainties for all variables at reduced spatial and temporal resolutions. In this work, we have used vertical profiles of temperature at 37 pressure levels for the days of the simulation months, as mentioned above. These temperature

profiles form the input to Monte Carlo simulations and are used in calculating thermal reaction rates of chemical reactions considered in this work.

2.7. CAMS

Since 2003, CAMS (http://atmosphere.copernicus.eu) has provided global estimates of atmospheric composition, which includes seven different aerosols such as desert dust, sea salt, organic matter, black carbon, sulphate, nitrate, and ammonium aerosol and includes more than 50 chemical species. CAMS has been generated through data assimilation. The initial conditions of each forecast are generated by fusing prior forecasts with recent satellite measurements. CAMS provides the best estimate of the state of the atmosphere at the first forecast time step and offers a globally complete and consistent dataset. CAMS also provides estimates of atmospheric pollutants in areas with poor observation data coverage at 3-hourly intervals.

2.8. Methodology

2.8.1 Monte Carlo simulations

Monte Carlo simulations are computational algorithms that leverage randomness to obtain deterministic results. These algorithms are used to handle uncertainties in the estimates of the deterministic problem by initializing a number of most likely initial conditions. For this purpose, these methods are initialized by random seeds in the permissible range, and multiple probabilistic simulations are carried out to estimate the outcome. The vertical profiles of the number concentration of the minor atmospheric constituents are obtained by simulating atmospheric chemistry (Table 2.1), in general, and chemistry processes at cloud levels. As reaction rates of chemical reactions depend on ambient temperature, we have generated 1000 random samples by perturbing temperature obtained from the ERA5 dataset at 37 pressure levels. Thus, 1000 samples of chemical reaction rates are available at 37 pressure levels.

The uncertainties in the number concentrations of minor atmospheric constituents can be estimated by perturbing reaction rates (depending on temperature) for suitable samples with an appropriate range. Therefore, obtaining probabilistic estimates of the maximum likely temperature profiles in the atmosphere will be helpful. Maximum likelihood estimation is a suitable method to obtain these probabilistic estimates, as it maximizes a likelihood function for a given statistical model and observed data. Raychaudhuri (2008)

has described this method in detail. This work uses Gaussian distribution as a statistical model and the ERA5 temperature dataset from 2000 – 2020 for each location. The 1000 vertical profiles of maximum estimates for ambient temperature have been obtained, and 24 reaction rates have been calculated at 37 pressure levels for 1000 profiles. Figure 2.4 shows the maximum likelihood best estimates for temperature (K) derived from the ERA5 dataset of 2000-2020 and sample random values estimated at different pressure levels for 0800 UTC of Delhi on 01 April 2020 (Patnaik et al. 2023).

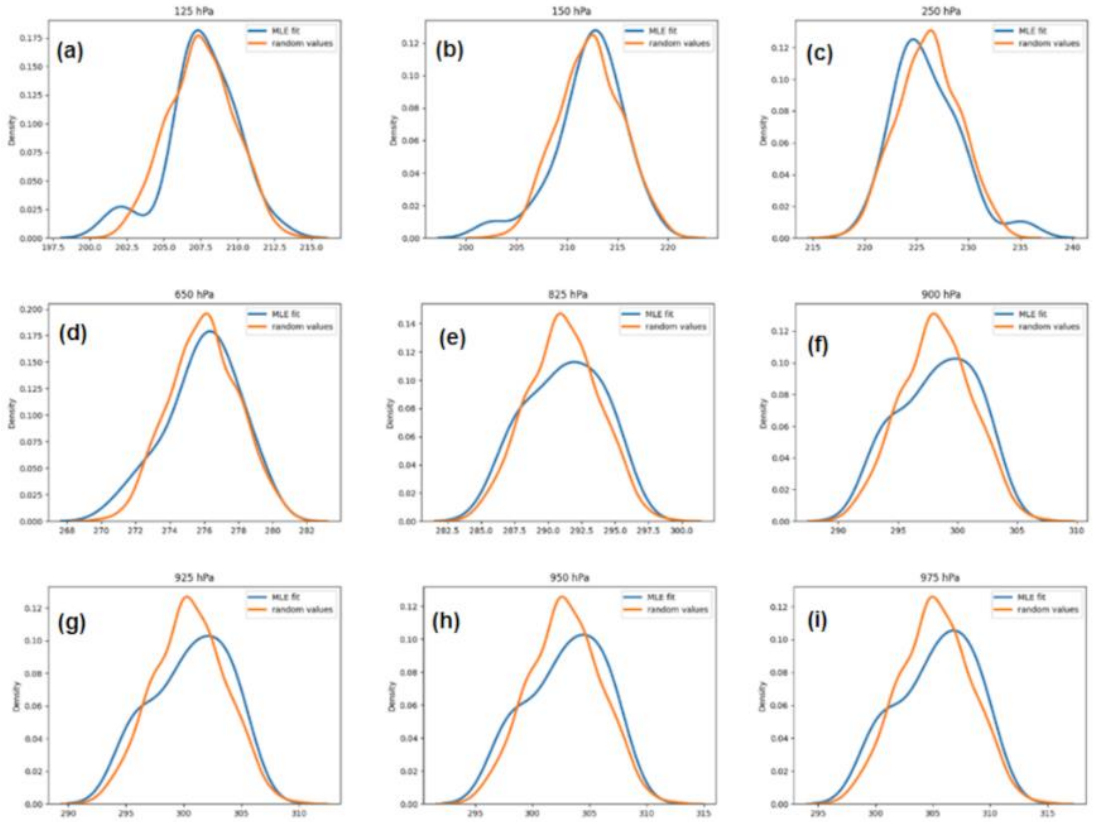

Figure 2.4. MLE and Random values of Temperature values at different pressure levels

2.8.2 Gear's solution method

Gear's solver (Jacobson, 2005) has been used to determine the concentration of CH4, N2O, and SO2 molecules at each pressure level to solve ordinary chemical differential equations. This method uses the backward differentiation formula (2.1)

$$\frac{dN_{i,t}}{dt} = \frac{N_{i,t} - \alpha_{s,1}N_{i,t-h} - \alpha_{s,2}N_{i,t-2h} \ldots\ldots \alpha_{s,s}N_{i,t-sh}}{h\beta_s} = \frac{N_{i,t} - \sum_{j=1}^{s} \alpha_{s,j}N_{i,t-jh}}{h\beta_s} \ldots\ldots\ldots (2.1)$$

s is the order of approximation of the method, and α and β are scalar multipliers, j=1,2,…,s. $N_{i,t}$ is the concentration for individual species i at a time 't' and $\widehat{N}_{i,t}$ is for the set of species. $N_{i,t-jh}$ is the concentration of species i at a time (*t-jh*).

Solving formula (2.1), we obtain formula (2.2) for a set of species.

$$0 = -\widehat{N}_t + \sum_{j=1}^{s} \alpha_{s,j} \widehat{N}_{t-jh} + h\beta_s \frac{d\widehat{N}_t}{dt} \quad \ldots\ldots\ldots (2.2)$$

The solution to the above equation we get

$$\text{Pt } \Delta\widehat{N}_{t,m} = \hat{B}_{\text{t,m}} \ldots\ldots\ldots (2.3)$$

$$\hat{B}_{\text{t,m}} = -\widehat{N}_{t,m} + \sum_{j=1}^{s} \alpha_{s,j} \widehat{N}_{t-jh} + h\beta_s \frac{d\widehat{N}_{t,m}}{dt} \quad \ldots\ldots\ldots\ldots\ldots\ldots (2.4)$$

where Pt is the Predictor Matrix, and it expands to Pt = I – $h\beta_s$Jt…. (2.4), I is the Identity matrix, Jt is the Jacobian matrix given by Jt $= \left[\frac{\partial^2 \widehat{N}_{i,t,m}}{\partial N_{k,t,m} \partial t}\right]_{i,k=1}^{k,k}$, $\Delta\widehat{N}_{t,m} = \widehat{N}_{t,m+1} - \widehat{N}_{t,m}$ and $\hat{B}_{t,m} = -\widehat{N}_{t,m} + \sum_{j=1}^{s} \alpha_{s,j} \widehat{N}_{t-jh} + h\beta_s \frac{d\widehat{N}_{t,m}}{dt}$ at iteration m. Once $\Delta\widehat{N}_{t,m}$ is solved, concentrations for the next iteration is calculated by the formula (2.5)

$$\widehat{N}_{t,m+1} = \widehat{N}_{t,m} + \Delta\widehat{N}_{t,m} \quad \ldots\ldots\ldots (2.5)$$

After each iteration, we have checked the local error. Furthermore, upon the satisfaction of the local error test, a global error test is performed to ascertain if the cumulative normalized root-mean-square error (NRMS) obtained exceeds another parameterized value, depending on the order of approximation considered. If the global error check fails, a new time step has to be considered, with one order of lower approximation. If the global test succeeds, the time step is successful, and $N_{t,m+1}$ values from the last iteration are set to final concentrations. If the global error check fails, the time step continues to be reduced. If needed, after every few successful time steps, the time step value and the order of approximation are re-evaluated with any time step estimation method.

Chapter 3

3. Formulation and validation of 1-D Model to Retrieve the Vertical Profiles of Minor Atmospheric Constituents

3.1. Introduction

The minor constituents determine the tropospheric chemistry processes in the atmosphere; hence, their behavior influences the state of the atmosphere and, therefore, the air quality. Furthermore, the air quality in urban areas poses a major threat to human health (Singh et al. 2021). Thus, observations of the chemical components in the atmosphere are crucial for a better understanding of the chemistry, mixing effects, radiative forcing, and transport of atmospheric constituents in the atmosphere (Tsai et al., 2012). However, there needs to be more in-situ observations globally. Furthermore, monitoring the minor constituents in the atmosphere is extremely challenging due to the complexities of various processes involving them. Also, the temporal and spatial resolutions of such measurements from remote sensing platforms such as satellites are limited, considering these sensors are presently on board and are present in low-earth orbiting satellites. Atmospheric constituents, such as Sulfur dioxide (SO_2), may exert a significant cooling effect on climate in the Northern Hemisphere through the backscattering of solar radiation (Chin et al. 2000), whereas methane (CH_4) and Nitrous Oxide (N_2O) provide a warming effect (Bange et al. 2019; Moumen et al. 2016).

Due to the rapid development of cities and the associated construction of multi-storied buildings, anthropogenic influences are gradually expanding from the ground to greater heights (Hong et al. 2021), together with impacts on the sources and sinks, rates of chemical reactions, and spatial distribution of SO_2, CH_4, and N_2O at various altitudes. For example, SO_2 oxidizes rapidly in the atmosphere, causing aerosol formation and acid rain (Yoo et al. 2014). In contrast, N_2O and CH_4 concentrations in the atmosphere must be regulated by the Kyoto Protocol for their role in global warming (UNFCC, 1998). Both molecules also show a uniform distribution in the troposphere. Although N_2O occurs in the troposphere at low concentrations [~320 ppbv], compared to other greenhouse gases, its particularly long lifetime (120 years) makes it a potent molecule for global warming (Tsai et al. 2012). Since methane is rapidly transported to

the upper troposphere, an inaccurate representation of the vertical methane distribution may cause discrepancies in global model estimates. Infact, simulations of surface methane mixing ratios (Locatelli et al. 2015) occurring at certain levels of the atmosphere can overlook or not consider a methane plume. Hence, it is important to understand the vertical distribution of these minor atmospheric constituents, especially over megacity regions, where the population is more than 10 million people and the city is associated with urban agglomeration.

Numerical models have been developed in the literature to simulate the vertical distribution of minor atmospheric constituents. For example, Hov (1983) developed a one-dimensional vertical model for Ozone, Sulphur dioxide, Nitrogen dioxide, and hydrocarbons and studied the impact of variation of the boundary layer on their concentration. The results from their study indicated that NO_x prevents the ozone from reaching the ground, and it is removed by dry deposition. As a result, maximum hydroxyl radical concentrations are observed, where nitrogen oxides, hydrocarbons, and sulphur dioxide emissions occur. This model also simulated the nighttime accumulation of nitrogen dioxide, sulphur dioxide, and hydrocarbons in the shallow nocturnal boundary layer. Jonson and Isaksen (1992) have studied the modification of SO_2 and hydrogen peroxide inside the cloud as well as in the precipitation process. They have shown that the levels of hydrogen peroxide are high at the cloud top and are depleted at lower levels due to high amounts of SO_2. The depletion of SO_2 is mainly due to deposition and gas-to-liquid conversion. Hertel (1994) has studied marine biogenic sulfur compounds to investigate the decomposition of DMS emissions into methane sulphonic acid (MSA) and sulphate aerosols. They have shown that the concentration of NO_x largely controls the concentrations of MSA and methane sulphinic acid (MSEA), which vary due to tidal shifting effects.

Fitzgerald et al. (1998a) and Gelbard et al. (1998) have developed a one-dimensional, multicomponent sectional model to simulate the spatiotemporal variations of the vertical profile of aerosol size distribution (sulphates) and their composition in the marine boundary layer (MBL). The above model could simulate the shirking and swelling of the aerosol as it travels through a humidity gradient in the atmosphere and its impact on particle size distribution inside the cloud. Thus, the above formulation is useful for integrating the impact of aerosol size distribution on nucleation processes (Fitzgerald et al. 1998b) and particle growth mechanisms (Gelbard et al. 1998). Caffrey et al. (2006)

have simulated the dynamics of aerosols in the marine boundary layer with a one-dimensional, multi-component, sectional aerosol model, using vertical profiles of turbulence, relative humidity, temperature, vertical velocity, cloud cover, and precipitation provided by 3-D mesoscale meteorological model output. They have discussed the surface relative contribution of free-tropospheric sulphate particles, and sea-salt aerosol, to CCN concentration. They have shown that sulphate mass splits under moderate wind speed, contributing to the cloud processes, whereas the higher sea-salt flux enhances heterogeneous nucleation processes under large wind speed conditions. Wang et al. (2018) studied the black carbon (BC) dome effect, its key influencing factors, and its impact on atmospheric boundary layer height using a one-dimensional model. They have indicated that the presence of BC near the capping inversion layer suppresses the atmospheric boundary layer height and weakens the turbulent mixing, resulting in hazy weather, especially in winter.

Most of the studies discussed above have indicated that one-dimensional models are useful to simulate the atmospheric chemical processes that influence complex phenomena such as the evolution of boundary layers, cloud development, and rain processes. Further, the cloud microphysics parameterizations are one-dimensional parameterizations embedded in the global or regional dynamical cores. However, chemical solvers are the most expensive components of chemical transport models (Eastham et al., 2018). Therefore, most models use higher-order implicit algorithms, such as the Gear method, which is optimized both for accuracy and speed. Jacobson and Turco (1994) have developed an efficient Gear solver to integrate ordinary differential equations to simulate the evolution of the number concentration of chemical species in the atmosphere based on the Gear method (Gear, 1971). This solver uses LU decomposition and the Gauss elimination (back substitution) method to solve ODEs. Sparse matrix techniques can solve large atmospheric problems by saving significant CPU time. Hertel et al. (1993) and Verwer et al. (1996) have indicated that back substitution methods efficiently solve chemistry and vertical turbulent diffusion in a coupled way.

Lu et al. (1997) suggested that this solver is robust, accurate, and efficient for multidimensional atmospheric photochemical problems. This solver has been implemented in many air quality modeling systems, such as the Surface Meteorology and Ozone Generation (SMOG) model (Lu et al. 1997), Community Multiscale Air Quality

(CMAQ) model (Byun & Schere, 2006), (Hakami et al. 2007), Global Earth Observing System (GEOS-CHEM) model (Martin, 2002), Unified General Circulation Model (Liao, 2004). Wagh et al. (2023) studied the Bromine chemistry over the Bharati station, Antarctica, using Multi-axis Differential Optical Absorption Spectroscopy (MAX-DOAS) from December 2018 to February 2020. Further, they used a box model and showed that bromine chemistry at the Bharati Station can deplete ozone by as much as 2.15 parts per billion in a single day on clear days. The above study also indicated that it does not lead to total ozone depletion over Bharati.

These one-dimensional chemical solvers are initialized using the known vertical profiles of the number concentration of some minor constituents (CH_4, N_2O, H_2O, SO_2, CO, HNO_3) observed through satellite platforms at the time of satellite overpass. Once initialized, these solvers can be used to generate vertical profiles of chemical constituents of the atmosphere based on chemical kinematics. However, there are uncertainties in prediction because only a few minor components are initiated using observations, while the remaining are initiated using random numbers, within some limit of number concentrations. Further, the kinematic reaction rates can change with sub-grid-scale temperature and pressure variations. The Monte-Carlo method (Kroese et al. 2014) is popularly used to address such uncertainties in the initialization and prediction. Also, these methods can be used in terms of Direct Simulation Monte Carlo (DSMC) methods for simulating the distribution of chemical components (Bird, 1976). The DSMC methods have also been applied to aerosol dynamics by Bird (1976). A direct simulation was developed by Smith and Matsoukas (1998) in which the Monte Carlo (DSMC) method was used, where collision pairs are chosen through the known collision rates and not by the trajectory of the particles. Using this DSMC method, several versions of the Monte Carlo method have been developed to study particle size distribution, undergoing coagulation and/or aggregation (Gooch and Hounslow, 1996), crystallization (Mitchell and Frenklach, 2003), and aggregation with simultaneous surface growth (Efendiev and Zachariah, 2002). A hierarchical hybrid Monte Carlo method was developed to study aerosol coagulation and phase segregation (Z. Sun et al. 2004). An improved Monte Carlo method was developed by Zhao and Zheng (2006) in which the moving bins were integrated to simulate a process involving simultaneous condensation and coagulation. Furthermore, the Monte Carlo method has also been used to solve the general dynamic

equation for removing aerosols to investigate the wet scavenging process of aerosols (Fitzgerald et al. 1998a).

In the present work, a hybrid solver has been developed to simulate the evolution of the minor constituents of the atmosphere. These minor constituents form CCN when they undergo a chemical transformation in the atmosphere. Gear's solver provides an efficient and accurate method to predict the number concentration of the minor constituents. The chemical kinematic reaction rates at different levels of the atmosphere depend on the vertical temperature profiles and initial number concentration. However, these two parameters are uncertain. The Monte-Carlo methods are useful to determine the impact of uncertainties in initial parameters on outcomes. Hence, we have developed a hybrid solver based on the Gear solution method (Jacobson and Turco, 1994) and the Monte-Carlo method (Raychaudhuri, 2008). We used this hybrid solver to integrate the gas-phase chemistry of CH_4, N_2O, and SO_2 and validated them using a merged product derived from satellite observations. To the author's knowledge, this is the first attempt to combine atmospheric chemical solvers developed to predict the number concentration of minor atmosphere constituents through an efficient algorithm, such as Gear solution, that provides for estimating uncertainties in the prediction using Monte-Carlo simulations. Furthermore, this solver has been used to determine the vertical profiles of the number concentration of SO_2, CH_4, and N_2O during summer and rainy days over the following megacities viz. Delhi, Kolkata, Chennai, and Mumbai. The study aimed to develop a robust chemical solver to simulate changes in the number concentration of the atmospheric constituents. It is expected that the hybrid solver will help address the research problems of chemical evolution in the changing atmosphere (Patnaik et al., 2023).

3.2 Proposed method to obtain vertical profiles of minor constituents of the atmosphere

As discussed in section 1.2, the Monte Carlo method handles uncertainties elegantly and adds robustness to this proposed method. Gear solvers are efficient in solving chemical ODEs. Therefore, we have combined the Monte Carlo approach with the Gear Solver to obtain the vertical profiles of CH_4, N_2O, and SO_2 molecules at each pressure level. This

approach combines the advantages of both the Monte Carlo method and Gear solver. The Monte Carlo method is designed to tackle uncertainties by maximizing the likelihood of estimate (number concentration), while the Gear solution method provides an efficient solution by optimizing errors for predicting number concentrations using the predictor-corrector method. In addition, we have combined the gamma mapping technique (Thom, 1958) provided by the equation 3.1.

$$f_\gamma(x) = \frac{1}{\beta^\gamma \Gamma(\gamma)} x^{\gamma-1} e^{\frac{-x}{\beta}} \quad \ldots.(3.1)$$

where x = random variable (number of molecules), β is the scale parameter, γ is the shape parameter, Γ is the gamma function for bias adjustments to improve the estimation.

After testing several bias correction techniques, such as normal mapping, quantile mapping, and gamma mapping, we found that the gamma mapping technique outperforms the other methods. Also, several studies discussed by Modala (2017) indicate that the gamma mapping method is most suitable for correcting biases of meteorological parameters. Thus, the proposed approach combines the Monte Carlo, Gear solver, and gamma-mapping methods to estimate the vertical profile of the number concentration of CH_4, N_2O, and SO_2 molecules at 37 pressure levels.

Idealized experiments have been carried out during the rainy and non-rainy months over Delhi, Kolkata, Chennai, and Mumbai. In two sets of simulation experiments, we used CLIMCAPS data of number concentration around 0800 (2000) UTC for initialization, and vertical profiles of number concentrations were estimated for each hour till up to 12 hours, and the simulated results have been validated with 2000 (0800) UTC. The combined approach used is depicted in Figure 3.1. In addition, the number concentrations from the CLIMCAPS dataset (NCCD) and estimated number concentrations (ENC) have been used to calculate the percentage difference of number concentrations (PDNC) using the following equation 3.2.

$$PDNC\ (\%) = 100\left(\frac{NCCD-ENC}{NCCD}\right) \ldots (3.2)$$

In this thesis, we have proposed a new methodology based on the hybrid Monte Carlo and Gear'solution method to retrieve vertical profiles of minor constituents of the atmosphere.

The validation of the retrieved profiles has been carried out both for rainy and non-rainy months (Patnaik et al., 2023).

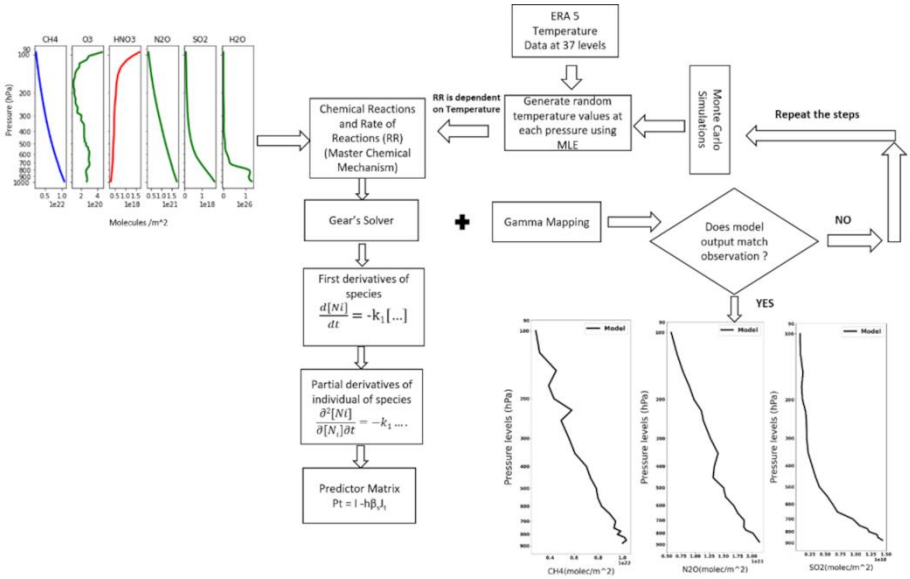

Figure 3.1. Flow chart of the methodology used to retrieve minor constituents of the atmosphere

3.3 Validation during non-rainy months

3.3.1 Delhi

Figure 3.2 shows the day and night-time profiles of CH_4, N_2O, and SO_2 molecules during the summer of April 2020. It shows that the proposed methodology in this work successfully determines the number concentration of CH_4 and N_2O during daytime based on the following observations. The estimated Percentage Difference of Number Concentrations (PDNC) for CH_4 (1st row) varies between -24.18% and 0.86% during daytime over Delhi, except on 23 April 2020 for almost all pressure levels. PDNC for CH_4 showed a variation in the range of -18.49 % to -26.4 % for pressure levels 400 hPa to 100 hPa on 23 April 2020. PDNC for N_2O (2nd row) showed a variation of -26.47% to 6.49% and for pressure levels between 350-300 hPa on all days except 23 April 2020, the latter ranging between -18.52% to -26.47 %. PDNC of SO_2 (3rd row) shows more variation for almost all pressure levels, and its magnitude range is between -39.33% to -26.8%. The night-time simulations showed that during the non-rainy month of April, the PDNC for CH_4 varies from -60.83% to 3.284%. On 22 April 2020 at 2100 hours, the

values of PDNC were found to be between -60.8 % and -56.78% for pressure levels 850 hPa and 825 hPa, respectively. PDNC for N_2O shows a variation of -65.43% to 1.03%. On 23 April 2020, at night-time, PDNC is minimum for N_2O, i.e., in the range of -63.8 % to -65.43 %. PDNC of SO_2 varies between -67.45% to -26.79%. At 175 hPa, the PDNC at night for SO_2 is minimum on 22, 27, 16, and 11 April. The coefficient of determination (R2) was calculated for each case (Table 3.1). The range of $R^2_{minimum}$ to $R^2_{maximum}$ indicated that they range between 97-99%, 82-99%, and 100% for CH_4, N_2O, and SO_2, respectively. It suggests that the proposed methodology successfully simulated the variation in vertical profiles of these components qualitatively with high values of R^2 (Patnaik et al., 2023).

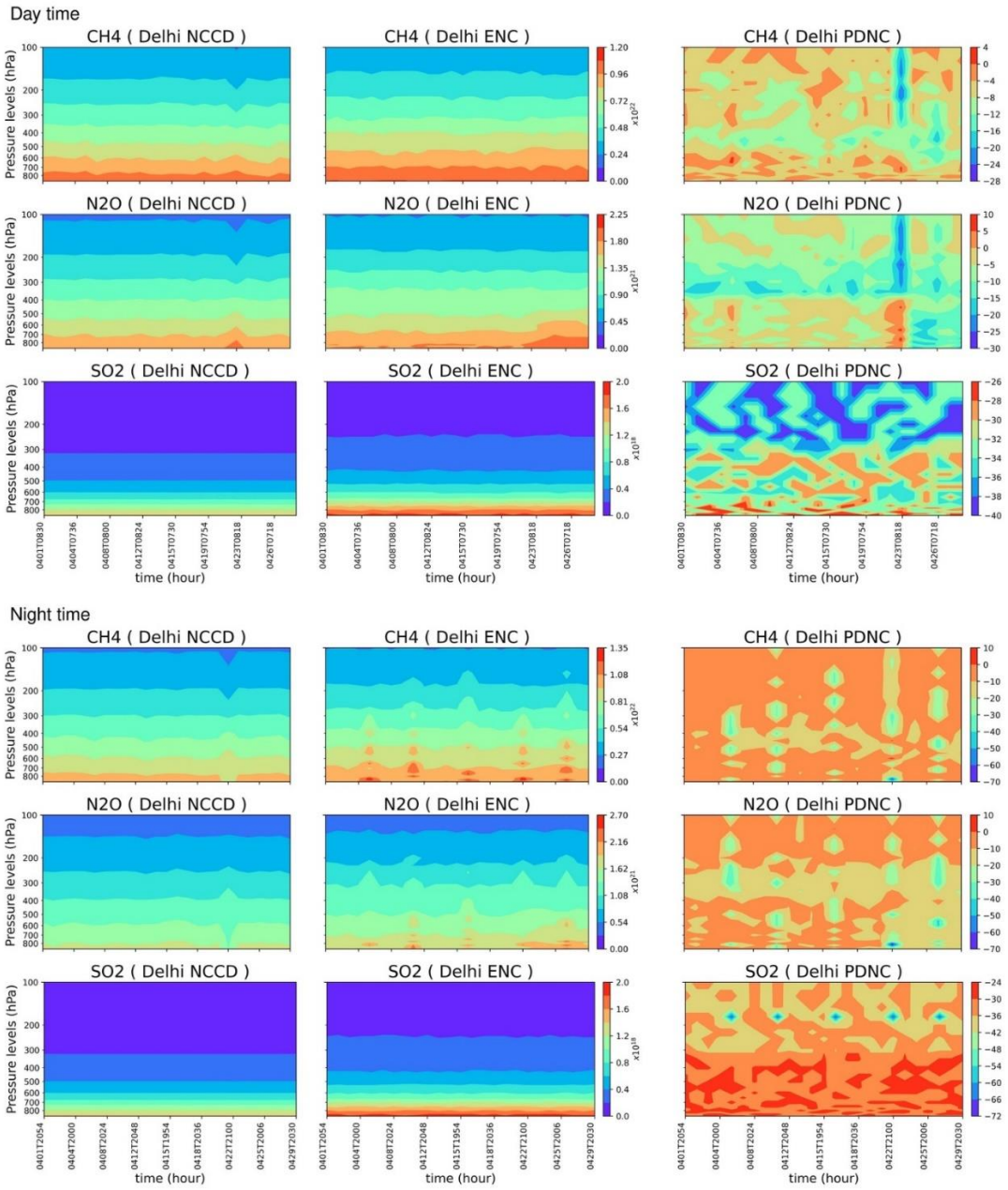

Figure 3.2. Vertical profile of NCCD, ENC, and PDNC of CH_4, N_2O, and SO_2 over Delhi during April 2020.

3.3.2 Kolkata

Figure 3.3 shows the vertical profiles of Number Concentration from the CLIMCAPS Dataset (NCCD), Estimated Number Concentrations (ENC), and PDNC of CH_4, N_2O, and SO_2 over Kolkata during the day and night-time of May 2020. PDNC of CH_4 varies between -17.63% and 1.69%, and the minimum value has been found at 350 hPa on 18 May 2020. PDNC of N_2O varies between -31.93% to -7.10% and has a minimum error

between 350-100 hPa on 21 May 2020, i.e., about -31.93 %. During the day, the PDNC of SO_2 lies in the range of -85.39% to -63.75%, and it was found to be minimum at 350-100 hPa ranging between -85.29 % to -85.39 %. The night-time simulations showed that during the non-rainy month of May 2020, the PDNC of CH_4 varies between -34.96% to -0.36% and minimum PDNC is observed at 125 hPa on 05 May 2020. PDNC of N_2O lies in the range of -35.15% to -3.41% and has lower PDNC between 100 hPa to 350 hPa on 20 May 2020. During the night, the PDNC of SO_2 varies between -85.38% to -64.4%, and the minimum is observed at 350 hPa to 100 hPa, ranging between -84.98 % to -85.38 %. The range of $R^2_{minimum}$ to $R^2_{maximum}$ indicated that the above ratio ranges between 96-99%, 91-98%, and 100% for CH_4, N_2O, and SO_2, respectively (Patnaik et al., 2023).

3.3.3 Chennai

Figure 3.4 shows the vertical profiles of NCCD, ENC, and PDNC of CH_4, N_2O, and SO_2 over Chennai during the day and night-time of May 2020. PDNC of CH_4 varies between -29.66% and -0.55%, and a minimum (-29.66 %) was found on 20 May 2020 at 450 hPa. PDNC of N_2O varies between -15.07% and -0.28% and is found to have a minimum on 16 May 2020 at 150 hPa. During the day, the PDNC of SO_2 lies in the range of -6.08% to 0.12%.

The night-time simulations showed that during the non-rainy month of May 2020. PDNC of CH_4 varies between -43.4% and 5.25%. Minimum PDNC was found during the night on 18 May 2020 at 150 hPa. PDNC of N_2O varies between -57.46% and 31.38%. Minimum PDNC was found on 18 and 20 May 2020, with magnitude -46.6 % (at 875 hPa) and -57.46% (at 250 hPa), respectively. PDNC of SO_2 lies between -25.72 and 6.19×10^{-5}%, with numerical values between 150 hPa and 200 hPa.The range of $R^2_{minimum}$ to $R^2_{maximum}$ indicated that the above ratio ranges between 94-99%, 81-99%, and 100% for CH_4, N_2O, and SO_2, respectively (Patnaik et al., 2023).

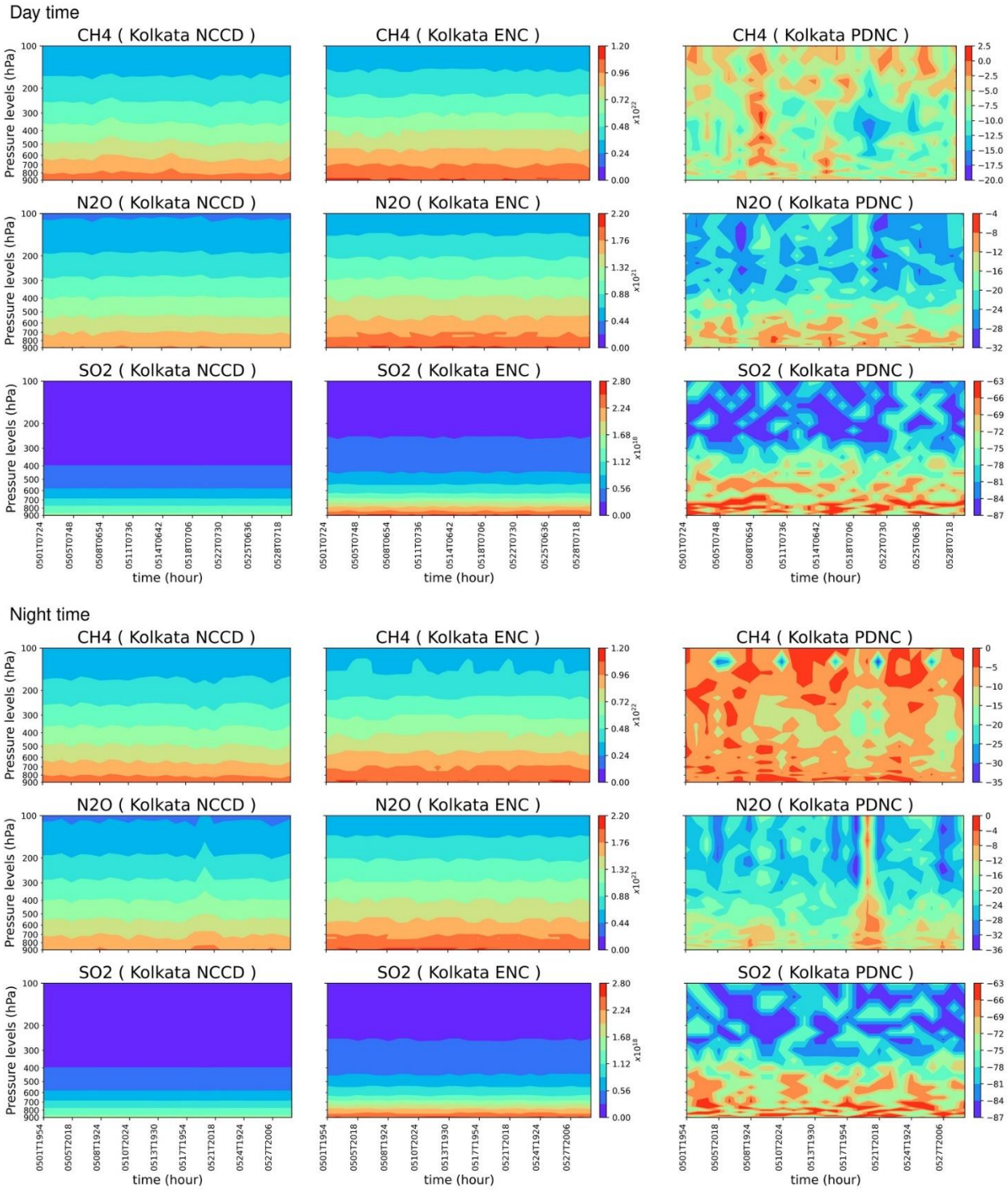

Figure 3.3. Vertical profile of NCCD, ENC, and PDNC of CH_4, N_2O, and SO_2 over Kolkata during May 2020.

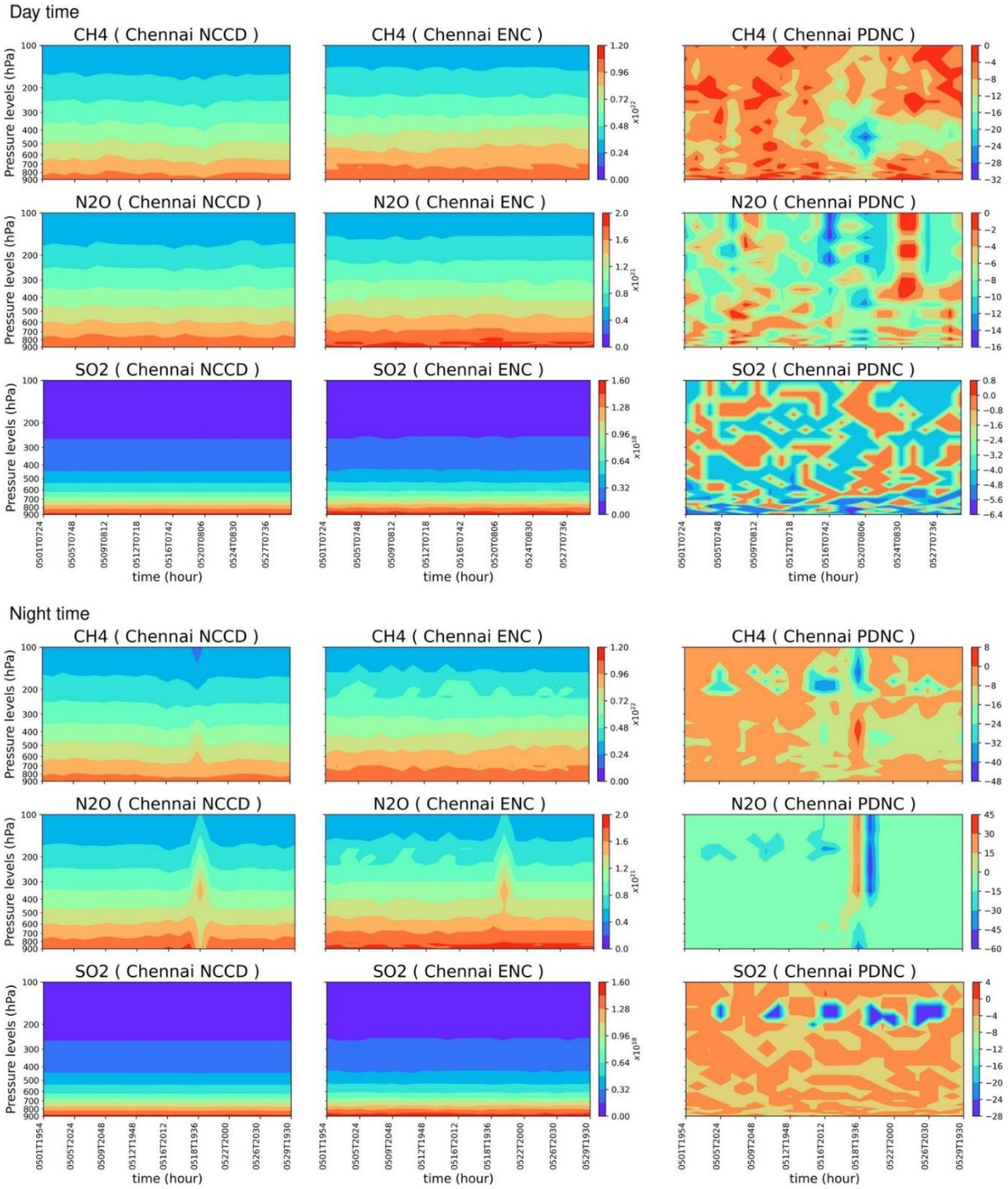

Figure 3.4. Vertical profile of NCCD, ENC, and PDNC of CH_4, N_2O, and SO_2 over Chennai during May 2020.

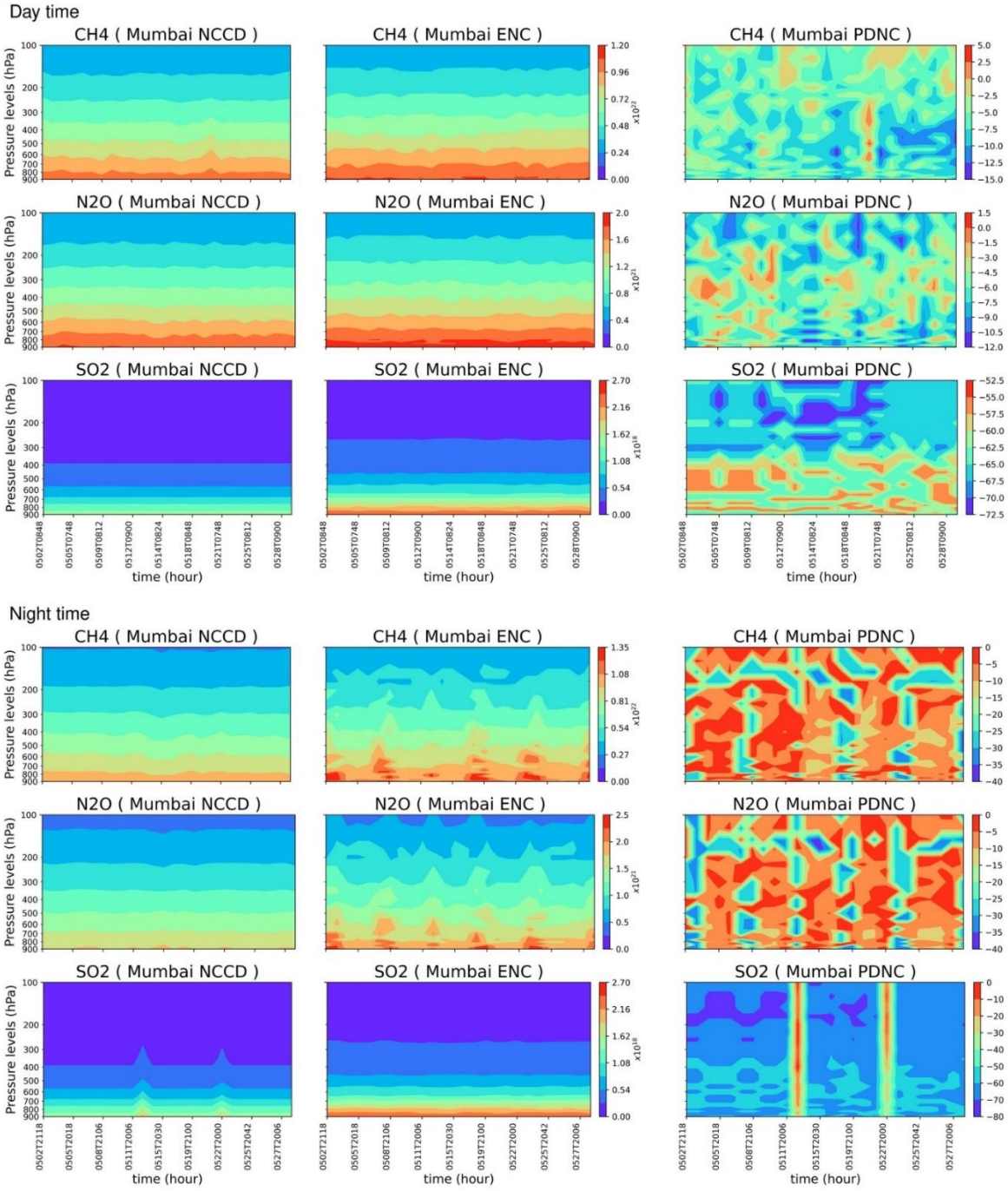

Figure 3.5. Vertical profile of NCCD, ENC, and PDNC of CH_4, N_2O, and SO_2 over Mumbai during May 2020.

3.3.4 Mumbai

Figure 3.5 shows the vertical profiles of NCCD, ENC, and PDNC of CH_4, N_2O, and SO_2 over Mumbai during the day and night-time of May 2020, while the PDNC of CH_4 varies between -14% and 3.177%. PDNC of N_2O varies between 0.016% and -11.67%, and PDNC of SO_2 lies in the range of -71.92% and -54.8%. During the daytime, between 100

hPa and 350 hPa, PDNC has a minimum that lies in the range of -71.9 % and -66.2 %. The night-time simulations showed that during the non-rainy month of May 2020, the PDNC of CH_4 varies between -38.75% and -0.51%, and on 29 May 2020, the PDNC of CH_4 is lower (- 38.75 % to -27.84 %) between 400 hPa to 900 hPa. PDNC of N_2O varies between -37.89% and -1.25%, and during night-time, PDNC of N_2O is minimum with a range of (- 37.89 % to -37.55 %) on 15 May 2020 between 150 hPa to 175 hPa. PDNC of SO_2 lies between -71.9% and -2.3%. While the PDNC of SO_2 is higher on 13 May 2020, i.e., between -2.3% and -33.96 %, For the other days, the PDNC of SO_2 lies in the range of -55.29 % to -66.8 %. During the day, the PDNC of CH_4 and N_2O is considerably lower than at night-time. The range of $R^2_{minimum}$ to $R^2_{maximum}$ indicated that the above ratio ranges between 85-99%, 85-99%, and 100% for CH_4, N_2O, and SO_2, respectively (Patnaik et al., 2023).

Table 3.1. Number of retrieved profiles of CH_4, N_2O, and SO_2 and Coefficient of Determination (R^2) between NCCD and ENC profiles during non-rainy days.

Regions	Number of profiles during non-rainy days and Coefficient of Determination (R^2)					
	Methane (CH_4)	$R^2_{minimum}$-$R^2_{maximum}$	Nitrous Oxide (N_2O)	$R^2_{minimum}$-$R^2_{maximum}$	Sulphur Dioxide (SO_2)	$R^2_{minimum}$-$R^2_{maximum}$
Delhi	49	0.97-0.99	49	0.82-0.99	49	1.0
Kolkata	53	0.96-0.99	53	0.91-0.98	53	1.0
Chennai	49	0.94-0.99	49	0.81-0.99	49	1.0
Mumbai	52	0.85-0.99	52	0.85-0.99	52	1.0

3.4 Validation during rainy months

3.4.1 Delhi

Figure 3.6 shows the vertical profiles of NCCD, ENC, and PDNC of CH_4, N_2O, and SO_2 over Delhi during the day and night-time of August 2020. PDNC of CH_4 varies between -29.82% and 0.88%. During rainy days, the model underestimates and has a PDNC of -29.62% to -17.68% between 500 hPa and 100 hPa on 18 August 2020 and 19 August 2020. PDNC of N_2O varies between -110.96% and 3.91%, and PDNC of N_2O is least on

the pressure levels 350 hPa-100 hPa on 13 August 2020 and 18 August 2020. PDNC of SO_2 lies in the range of -6.31% to 0.0083 %, and SO_2 is predicted well at all levels, with the minimum having values below 850 hPa and a range between -5.78 % and -5.11%. The night-time simulations showed that during the rainy month of August 2020, the PDNC of CH_4 varies between -34.35% and 2.71%. On 18 August 2020, the PDNC of CH_4 is minimum. PDNC of N_2O varies between -94.01% and -2.62%. During the night, the PDNC of N2O is a minimum between 350 and 100 hPa. PDNC of SO_2 lies in the range of -27.9% and 2.3×10^{-4} %. SO_2 has a minimum PDNC between 175 and 100 hPa, i.e., between -27.9 % and -25.7 %. The range of $R^2_{minimum}$ to $R^2_{maximum}$ indicated that the above ratio ranges between 90-99%, 71-83%, and 100% for CH_4, N_2O, and SO_2, respectively (Table 3.2) (Patnaik et al. 2023).

3.4.2 Kolkata

Figure 3.7 shows the vertical profiles of NCCD, ENC, and PDNC of CH_4, N_2O, and SO_2 over Kolkata during the day and night-time of June 2020. PDNC of CH_4 varies between -23.6% - -0.23%, and PDNC of CH_4 on 15 June 2020 is found to have a minimum between 100 hPa to 175 hPa and a range between (-23.18 % to -19.01%). PDNC of N_2O varies between -19.86% and 46.38%, and on 15 June 2020, the PDNC of N_2O is maximum between 300 and hPa-100 hPa. PDNC of SO_2 lies in the range of -6.75% to -1.2×10^{-5} %, and SO_2 is predicted well at all levels.

The night-time simulations showed that during the rainy month of June 2020, the PDNC of CH_4 varies between -36.41% and -0.54%, while minimum PDNC of -36.4% and -29.1% is estimated on 27 June 2020 and 28 June 2020, respectively, at 150 hPa. PDNC of N_2O varies between -44.39% and 4.57%. During the nighttime, the PDNC of N2O is at a minimum of 150 hPa. PDNC of SO_2 lies in the range of -25.72% to -9.3×10^{-5}%, and SO_2 has the least PDNC and is estimated well during the daytime and night-time. The range of $R^2_{minimum}$ to $R^2_{maximum}$ indicated that the above ratio ranges between 97-99%, 65-99%, and 100% for CH_4, N_2O, and SO_2, respectively (Patnaik et al., 2023).

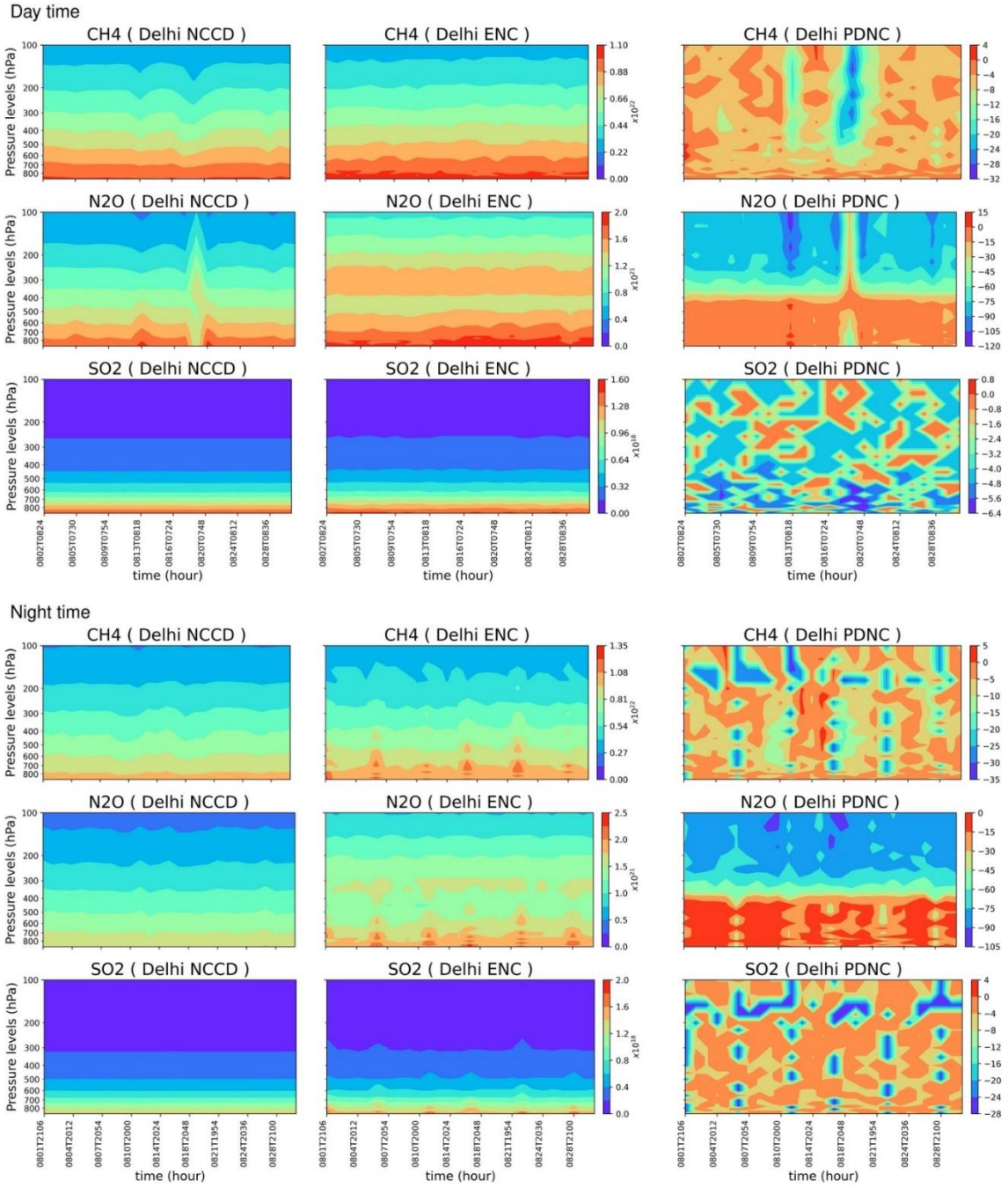

Figure 3.6. Vertical profile of NCCD, ENC, and PDNC of CH4, N2O, and SO2 over Delhi during August 2020.

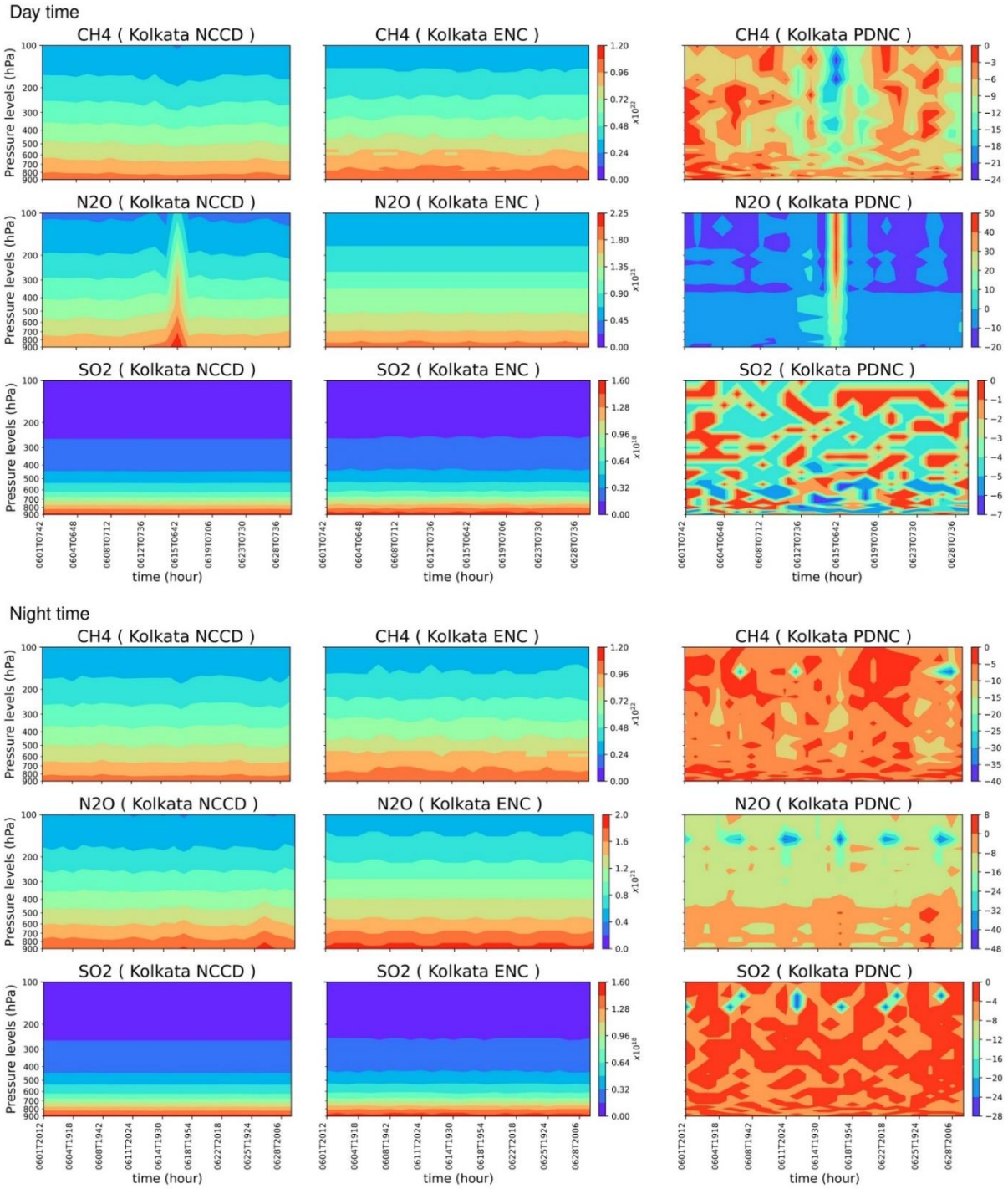

Figure 3.7. Vertical profile of NCCD, ENC, and PDNC of CH_4, N_2O, and SO_2 over Kolkata during June 2020.

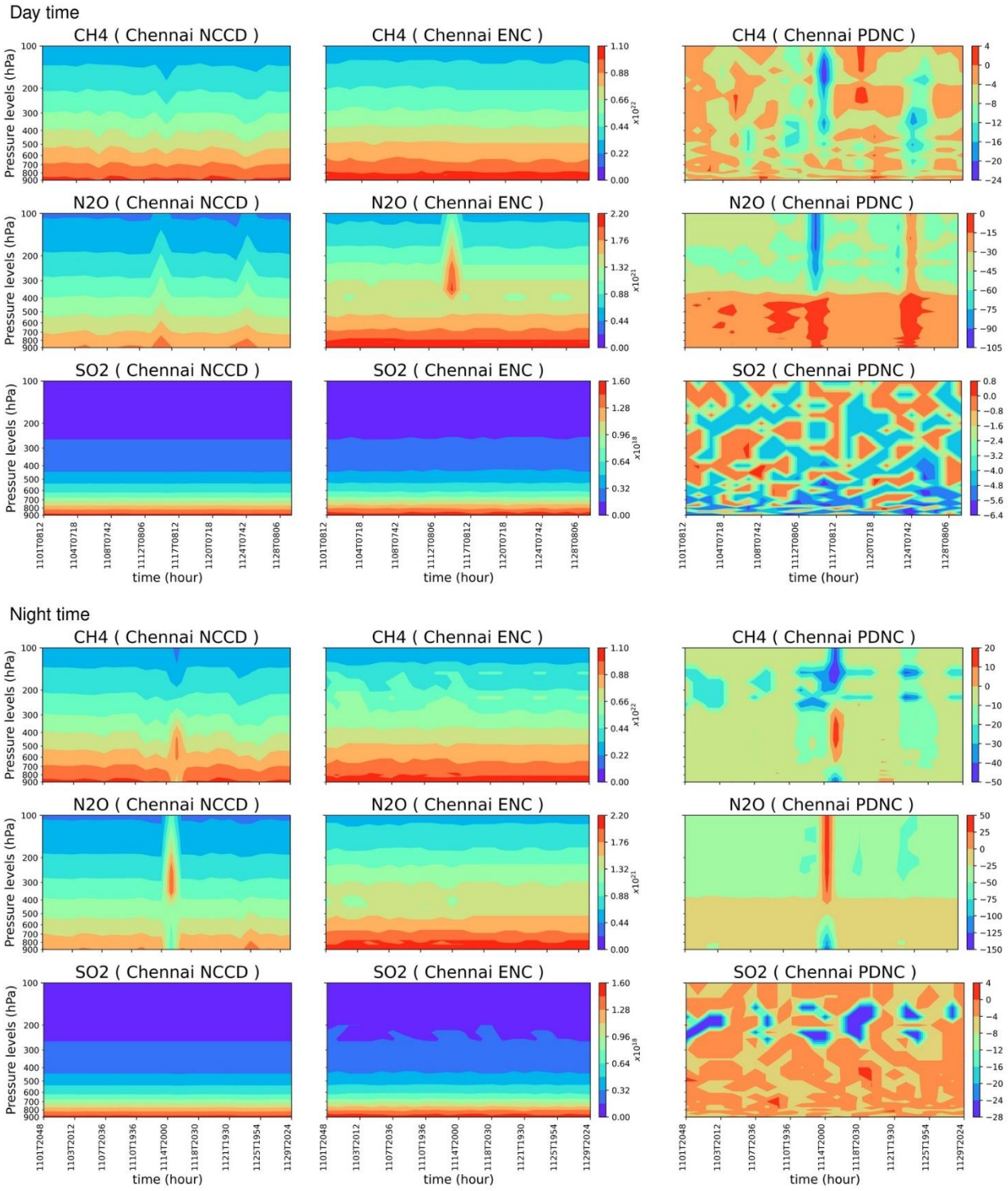

Figure 3.8. Vertical profile of NCCD, ENC, and PDNC of CH_4, N_2O, and SO_2 over Chennai during November 2020.

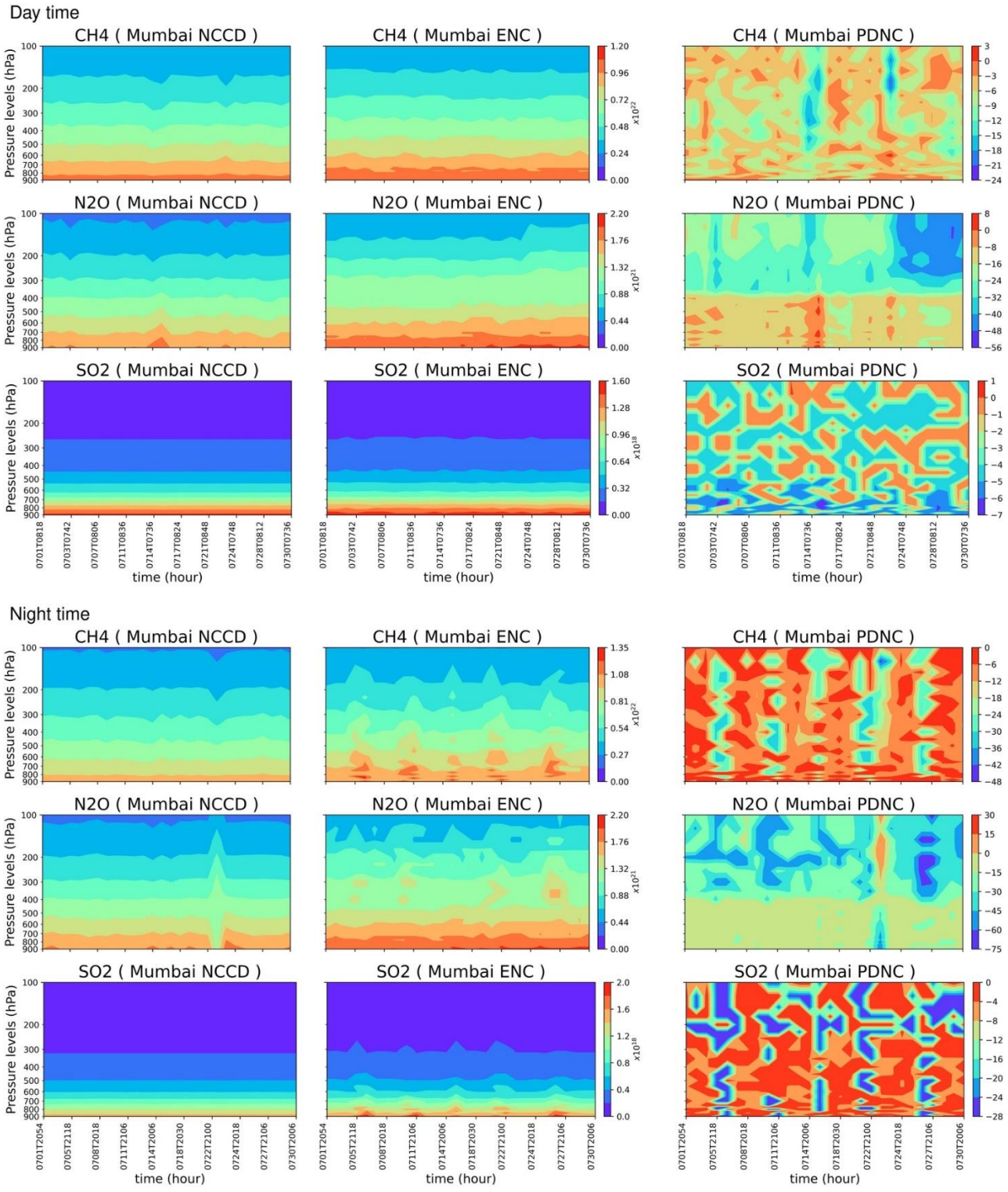

Figure 3.9. Vertical profile of NCCD, ENC, and PDNC of CH_4, N_2O, and SO_2 over Mumbai during July 2020.

3.4.3 Chennai

Figure 3.8 shows the vertical profiles of NCCD, ENC, and PDNC of CH_4, N_2O, and SO_2 over Chennai during the day and night-time of November 2020. PDNC of CH_4 varies between -23.8% and 1.1%, while PDNC of CH_4 is minimum on 16 November 2020, between 400 hPa and 100 hPa, ranging from -14.21 % to -23.85 %. PDNC of N_2O varies between -94.9% and -1.74%. The minimum PDNC of N_2O is between 350 and 100 hPa (-65.35% and -94.23%) on 16 November 2020. PDNC of SO_2 lies in the range of -6.28% to 0.055%. The night-time simulations show that during the rainy month of November 2020, the PDNC of CH_4 varies between -47.35% and 17.48%. On 15 November 2020, the PDNC of CH_4 has been found to be between -14.74 % and- 43.41% between 225 hPa to 100 hPa, which is the minimum at night. PDNC of N_2O varies between -130.04% and 42.56%. PDNC of N_2O is minimum and ranges between -24.87 % and -130.04 % on 15 November 2020. PDNC of SO_2 lies in the range of -25.7% and 0.27%. Mostly, at all levels, SO_2 has the least PDNC. However, between 150 hPa and 200 hPa, PDNC is lower. The range of $R^2_{minimum}$ to $R^2_{maximum}$ indicated that the above ratio ranges between 87-99%, 27-96%, and 100% for CH_4, N_2O, and SO_2, respectively (Patnaik et al., 2023).

3.4.4 Mumbai

Figure 3.9 shows the vertical profiles of NCCD, ENC, and PDNC of CH_4, N_2O, and SO_2 over Mumbai during the day and night-time of July 2020. PDNC of CH_4 varies between -23% and 1.81%. On 23 July 2020, the PDNC of CH_4 had a minimum between 300 hPa and 100 hPa and was in the range of -11.73% to -21.36%. PDNC of N_2O varies between -48.73% and 3.49%. During day time from 23 July 2020 to 30 July 2020. N_2O has a minimum PDNC between 100 and 350 hPa, ranging between 48.73% and 20.12%. PDNC of SO_2 lies in the range of -6.52% to 3.57×10^{-5}. The night-time simulations showed that during the rainy month of July 2020, the PDNC of CH_4 varies between -45.21% and -0.85%. On 23 July 2020, the minimum PDNC for CH_4 was found to be -45.21% at 125 hPa. PDNC of N_2O varies between -71.85% and 15.18%. The minimum PDNC varies from -56.4 % to -71.85% from 26 to 27 July 2020 (100 hPa to 300 hPa), and on 23 July 2020, PDNC is between -22.52 % -63.31 % and is observed between 950 hPa and 550 hPa. PDNC of SO_2 lies in the range of -27.48% to -4.13×10^{-5}%. The range of $R^2_{minimum}$ to $R^2_{maximum}$ indicated that the above ratio ranges between 89-99%, 74-98%, and 100% for CH_4, N_2O, and SO_2, respectively (Patnaik et al., 2023).

Table 3.2: Number of retrieved profiles of CH_4, N_2O, and SO_2 and Coefficient of Determination (R^2) between NCCD and ENC profiles during rainy days.

Regions	Number of profiles during rainy days and Coefficient of Determination (R^2)					
	Methane (CH_4)	$R^2_{minimum}$-$R^2_{maximum}$	Nitrous Oxide (N_2O)	$R^2_{minimum}$-$R^2_{maximum}$	Sulphur Dioxide (SO_2)	$R^2_{minimum}$-$R^2_{maximum}$
Delhi	51	0.90-0.99	51	0.71-0.83	51	1.0
Kolkata	49	0.97-0.99	49	0.65-0.99	49	1.0
Chennai	48	0.87-0.99	48	0.27-0.96	48	1.0
Mumbai	56	0.89-0.99	56	0.74-0.98	56	1.0

3.5 Comparison with previous studies

Studies exist in the literature where the scientific community has carried out similar investigations. Karppinen et al. (2020) discussed a method that is a valuable addition to obtaining methane profile measurements. The vertical distribution of atmospheric methane (CH_4) has been determined using data from a ground-based Fourier Transform Spectrometer (FTS) in Sodankylä, Northern Finland, for 2009-2018. Karppinen et al. (2020) first extracted the profile information using a dimension reduction retrieval method since each measurement contains approximately three pieces of information about the profile shape between 0 and 40 km. They then compared the retrieved profiles to measurements from the Atmospheric Chemistry Experiment Fourier Transform Spectrometer (ACE-FTS) satellite and the AirCore balloon. In-situ measurements from a 50-meter-high mast were also compared at the lowest tropospheric layer. The ground-based FTS and ACE-FTS profiles agreed within 10% below 20 km and 30% between 20 and 40 km in the stratosphere. The above methodology does not provide the accuracy and vertical resolution of aircraft and balloon measurements. However, the time range is much better. A High-resolution terrestrial Fourier transforms infrared (FTIR) spectrometer has been in operation at Addis Ababa, Ethiopia (9.01◦N, 38.76◦ E, 2443m

from sea level) since May 2009, to collect information on the abundances of columns and the configurations of different components of the atmosphere. Vertical profiles and columnar abundances of methane and nitrous oxide were obtained from solar absorption measurements performed by FTIR during the period May 2009 to March 2013 using the retrieval code PROFFIT (V9.5). The mean of CH_4 and N_2O concentrations, within the sensitivity ranges of the instruments up to about 27 km from the surface, are determined as 2.85×10^{19} molecules cm^{-2} ±5.3% and 5.16×10^{18} molecules cm^{-2} ±6.95%, respectively. The overall contribution of both statistical and systematic errors, i.e., a total error of CH_4 and N_2O from ground-based FTIR, is 3.1 % and 3 %, respectively. In general, the CH_4 and N_2O VMRs and column sets obtained from Addis Ababa in the tropics are in excellent agreement with all simultaneous satellite observations over the 17–27 km altitude range, with a positive average within 20–27 km, while the relative difference and negative average are obtained below 20 km (Yirdaw Berhe et al. 2020). The retrieved daytime (night-time) profiles for the CH_4 using the method proposed in this study have shown PDNC ranging between -24.18% and 0.86% (-60.83% and 3.28%), -17.63% and 1.69% (-34.96% and -0.36%), -29.66% and -0.55% (-43.43% and 5.25%), and -14% and 3.17% (-38.75% and -0.507%) for the locations Delhi, Kolkata, Chennai, and Mumbai, respectively during non-rainy days. Similarly, PDNC for the daytime (night-time) retrieved profiles on rainy days for CH_4 range between -29.82 – 0.88% (-34.35 – 2.71%), -23.6 - -0.23% (-36.41 - -0.54%), -23.8 – 1.1% (-47.35 – 17.48%), and -23 – 1.81% (-45.21 - -0.85%) over the locations Delhi, Kolkata, Chennai, and Mumbai, respectively. For SO_2, PDNC during daytime (night-time) ranges between -39.33 - -26.8% (-67.45 - -26.79%), -85.39 - -63.75% (-85.39 - -64.4%), -6.08 - 0.12% (-25.72 – 0%), and -71.92 - -54.8% (-71.9 - -2.3%) for the locations Delhi, Kolkata, Chennai, and Mumbai, respectively during non-rainy days. Similarly, PDNC during daytime (night-time) for SO_2, ranges between 4 -6.31 - -0.0083% (-27.9 – 2.3×10^{-4} %), -6.75 - -1.2×10^{-5} % (-25.72 - -9.3×10^{-5} %), -6.28 – 0.055% (-25.7 – 0.27%), and -6.52 - -3.57×10^{-5} % (-27.48 – 4.13×10^{-5} %) for the locations Delhi, Kolkata, Chennai, and Mumbai, respectively during rainy days. This method has retrieved daytime and night-time profiles of SO_2, CH_4, and N_2O more accurately than previously described methods. Also, the night-time CH_4 profile percentage error is mostly lower than the daytime concentration profile errors (Patnaik et al., 2023).

3.6. Conclusions

In this chapter, we have developed a one-dimensional model for retrieving the vertical profiles of the number of concentrations of minor constituents of the atmosphere. A hybrid solver has been designed to simulate the gas phase chemistry of CH_4, N_2O, and SO_2. The CLIMCAPS dataset has been used to initialize and validate the retrieved profiles of these constituents. The proposed methodology in this work, which uses a hybrid Gear solver with the Monte Carlo method, is new, as per the author's knowledge.

The idealized experiments have been carried out to retrieve vertical profiles of the number concentrations of minor constituents in the atmosphere. The four megacities in India, viz. Delhi, Kolkata, Chennai, and Mumbai have been selected for validation. The simulations using this hybrid solver have been carried out for non-rainy and rainy months for all four megacities. It has been seen that the retrieved profiles and CLIMCAPS product are in very good agreement on rainy and non-rainy days and also during day and night. This method has retrieved daytime and night-time profiles of SO_2, CH_4, and N_2O with better accuracy than previously described methods. Also, the night-time CH4 profile percentage error is mostly less compared to the daytime concentration profile errors (Patnaik et al., 2023).

Chapter 4

4. Simulation of Diurnal Variations

4.1. Introduction

The concentrations of atmospheric components at a region and at a particular time are determined by the superposition of augmentations from various causes that can contribute to variabilities. Hence, the simulation of different variabilities due to causes such as diurnal, seasonal, annual, decadal, and centennial is vital to determine the number concentration accurately. The diurnal cycle is a prominent mode of atmospheric variability (Bhate et al. 2019), and simulation of the diurnal cycle of atmospheric parameters is crucial to test the skills of the weather and climate models (Bhate & Kesarkar, 2019). The diurnal variations in trace gases, such as Nitrogen species ($NO_{x)}$ and Carbon Monoxide (CO), are the combined effects of local sources, local wind patterns, chemistry, etc., leading to higher values in the morning and evening hours (Lal, 2007). These species greatly influence precipitation and diurnal variation of convection and rainfall, and their impact depends on moisture availability in the atmosphere and the surface heat budget. Assessing their diurnal variation is essential to analyze the time, duration, and amount of precipitation (Trenberth et al. 2003). Rastogi et al. (2021) have investigated the diurnal characteristics of Brown Carbon spectra using online measurements, which include a particle-into-liquid sampler, a portable UV–Visible spectrophotometer with liquid waveguide capillary cell, and a total carbon analyzer over Delhi. They have also highlighted that such studies are essential for climate models. Therefore, it is vital to model the trace gases' diurnal variations to accurately predict the atmospheric parameters. However, due to the sparse surface monitoring of trace gases over the Indian subcontinent, there is a lack of understanding of the key drivers of its diurnal and seasonal variability.

Methane (CH_4) has a prominent role in tropospheric chemistry, and its growth rate and mixing ratio in the atmosphere depend on the balance between the sources and sinks, which are controlled by transport phenomena. Major sources of CH_4 are rice cultivation, freshwater reservoirs, livestock, emissions from fossil fuels, wetlands, oceans, landfills, etc.(Kirschke et al. 2013). However, the sinks of CH_4 are photochemical or biological oxidation, and they are mainly removed by the photolytically produced hydroxyl radical

(OH) in the troposphere (Levy, 1971). It is also the main contributor to the increase in stratospheric water vapor, following the loss by reaction with OH radical (Keppler et al. 2006). The complex interaction between surface emissions, convective transport, and large scale circulation determines the variation of CH_4 in different parts of India (Patra et al. 2009; Lin et al. 2015). Also, the photosynthesis of plants significantly alters the production, oxidation, and transport processes for CH_4, resulting in a diurnal emission change with high peaks at midday and low values only an hour before sunrise on the next day (Wang & Han, 2005).

Sulfur dioxide (SO_2) is the most common pollutant that endangers the environment and human health, and it has been linked to an increase in the number of cases of cardiovascular and respiratory diseases. SO_2 is commonly found in urban areas with other pollutants due to industrial plant emissions and automobile exhaust gases. Sulphate aerosols, in particular, are a vital component of fine particles suspended in urban areas with a longer residence time in the atmosphere. Furthermore, SO_2 plays a significant role in forming acid species and sulphate aerosols, which may increase ice nuclei formation (Liu et al. 2021). The secondary aerosols formed from SO_2 and other precursor species can limit the reduction of fine particle concentrations.

The number concentration of CH_4 and SO_2 varies diurnally at the surface, which can be observed using eddy covariance flux towers or Fourier Transform Infrared Spectrometer. However, vertical profiles of CH_4 and SO_2 are challenging to measure, and therefore, model-determined profiles are used for investigations. Jha et al. (2014) have reported large diurnal variability in CH_4 emissions, as well as flux, using eddy covariance flux tower over Sundarbans mangroves of the Indian subcontinent, which has an unpolluted and undisturbed ecosystem. Huijnen et al. (2019) have compared model results from three chemistry versions as implemented in the European Centre for Medium-Range Weather Forecasts (ECMWF) Integrated Forecasting System (IFS), referred to as IFS(CB05BASCOE), IFS(MOZART) and IFS(MOCAGE) and compared the output with aircraft field campaigns, surface observations, ozone-sondes, and satellite observations. It is seen that the models of NO_2, SO_2, and HNO_3 differ considerably from one another in terms of their effect on secondary chemical production. Over Delhi, a long-term analysis of the SO_2 mixing ratio was carried out by Suneja et al. (2020). Their results indicated that maxima during monsoons and minima during pre-monsoon seasons are observed. In addition, the potential source contributing factors (PSCF) and backward trajectories

analysis also demonstrated that local and regional sources of industrial activity, coal combustion or thermal plants, etc., significantly impact mixing ratios for SO_2 over Delhi. Over the last decades, due to urbanization, energy production, and control measures, a divergence in SO_2 trends has been observed across different world regions (Chutia et al. 2022). In this study, CAMS reanalysis, satellite data, and emission inventories have been used. CAMS results are consistent with satellite observations, but the model results underestimate the growth of SO_2 over East India.

We have retrieved CH_4 and SO_2 concentrations over the megacities of Delhi, Kolkata, Chennai, and Mumbai using the 1-D hybrid solver developed by Patnaik et al. (2023)). The work compares the simulated diurnal variation of the vertical profile of the number concentration of CH_4 and SO_2 by the 1-D hybrid solver and Copernicus Atmosphere Monitoring Service (CAMS) model at 3-hour time intervals (Patnaik et al. 2023).

4.2. Data and Methodology

4.2.1. CAMS

Since 2003, CAMS (http://atmosphere.copernicus.eu) has provided global estimates of atmospheric composition, which includes seven different aerosols such as desert dust, sea salt, organic matter, black carbon, sulphate, nitrate, and ammonium aerosol and includes more than 50 chemical species. CAMS has been generated through data assimilation. The initial conditions of each forecast are generated by fusing prior forecasts with recent satellite measurements. CAMS provides the best estimate of the state of the atmosphere at the first forecast time step and offers a globally complete and consistent dataset. CAMS also provides estimates of atmospheric pollutants in areas with poor observation data coverage at 3-hour intervals.

4.2.2. 1-D Monte Carlo – Gear solver

The 1-D hybrid (1-D Monte Carlo – Gear) solver described in Patnaik et al. (2023) has been used to simulate vertical profiles of CH_4 and SO_2. The 1-D hybrid solver uses ERA5 temperature vertical profiles to calculate the Maximum Likelihood Estimation at 15 different pressure levels by generating 1000 vertical temperature perturbation profiles. The chemical reactions and the rate of reactions have been obtained from the Master Chemical Mechanism (MCM). Since the rates of reactions are temperature-dependent, a Gear solver has been used to estimate the number concentration of CH_4 and SO_2.

Community Long-term Infrared Microwave Coupled Atmospheric Product System (CLIMCAPS) has been used for initialization to predict the number concentration of molecules at each hour of non-rainy days and rainy days. CLIMCAPS satellite provides vertical profiles of atmospheric components around 0800 UTC and 2000 UTC. The hourly profile of the number concentration of CH_4 and SO_2 has been calculated for the non-rainy days and rainy days using the 1-D hybrid solver, respectively. Since the CAMS model generates output every 3 hours, the mean vertical number concentration is calculated for all the non-rainy and rainy days over the megacities of Delhi, Kolkata, Chennai, and Mumbai at these time intervals. As described in Patnaik et al. (2023), the monthly mean number concentrations have been compared with the 1-D hybrid solver's number concentration at every 3-hour time interval, as shown in Figure 4.1.

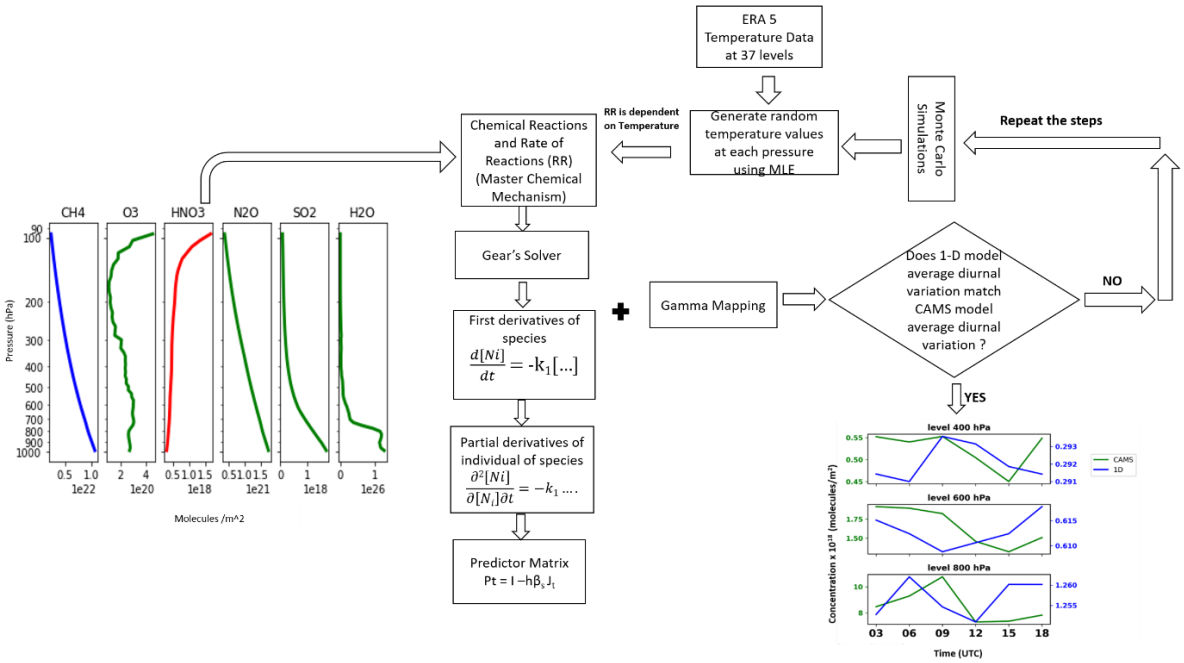

Figure 4.1. Graphical representation of the proposed methodology.

4.3. Results and Discussion

4.3.1 Delhi

The first panel of Figure 4.2 shows the diurnal variation of CH_4 vertical profiles (number concentration) forecasted by the CAMS model and 1-D solver at every 3-hour interval during the non-rainy days of April 2020 over Delhi. The maximum (minimum) CH_4 number concentration value determined by the CAMS model is 8.34×10^{21} molecules m^{-2} (2.89×10^{21} molecules m^{-2}) at 06 UTC (18 UTC) and 700 hPa (100 hPa) pressure level.

The 1-D solver shows the maximum (minimum) CH_4 number concentration value of 10.25×10^{21} molecules m^{-2} (2.67×10^{21} molecules m^{-2}) at 18 UTC (15 UTC) and 800 hPa (100hPa) pressure level. Thus, the maximum number concentration has been over-estimated in the forecast of a 1-D hybrid solver, while both the models simulated minimum number concentrations agree with one another. The number concentration of CH_4 shows diurnal variation in the forecast of both models at all pressure levels. The correlation coefficient (Table 4.1 (a)) between the CAMS model and 1-D hybrid solver is calculated for CH_4. Correlation coefficients at 03, 06, 09, 12, 15, and 18 UTC are 72.68%, 72.63%, 72.96%, 72.64%, 72.30%, and 72.52%, respectively (Patnaik et al., 2023).

The second panel of Figure 4.2 shows the diurnal variation of SO_2 vertical profiles (number concentration) estimated by the CAMS model and 1-D solver at every 3-hour interval during the non-rainy days of April 2020 over Delhi. The maximum (minimum) SO_2 number concentration value determined by the CAMS model is 46.25×10^{18} molecules m^{-2} (1.96×10^{15} molecules m^{-2}) at 09 UTC (03 UTC) and 800 hPa (100 hPa) pressure level. The 1-D solver shows the maximum (minimum) SO_2 number concentration value of 2.29×10^{20} molecules m^{-2} (2.6×10^{15} molecules m^{-2}) at 18 UTC (03 UTC) and 700 hPa (100hPa) pressure level. Thus, the maximum number concentration has been over-estimated in the forecast of a 1-D hybrid solver, while both the models simulated minimum number concentrations agree with one another. The number concentration of SO_2 almost shows diurnal variation in the forecast of both models at all pressure levels. The correlation coefficient (Table 4.1b) between the CAMS model and 1-D hybrid solver is calculated for SO_2. Correlation coefficients at 03, 06, 09, 12, 15, and 18 UTC are 51.48%, 32.89%, 56.65%, 71.20%, 19.31%, and 45.05%, respectively (Patnaik et al., 2023).

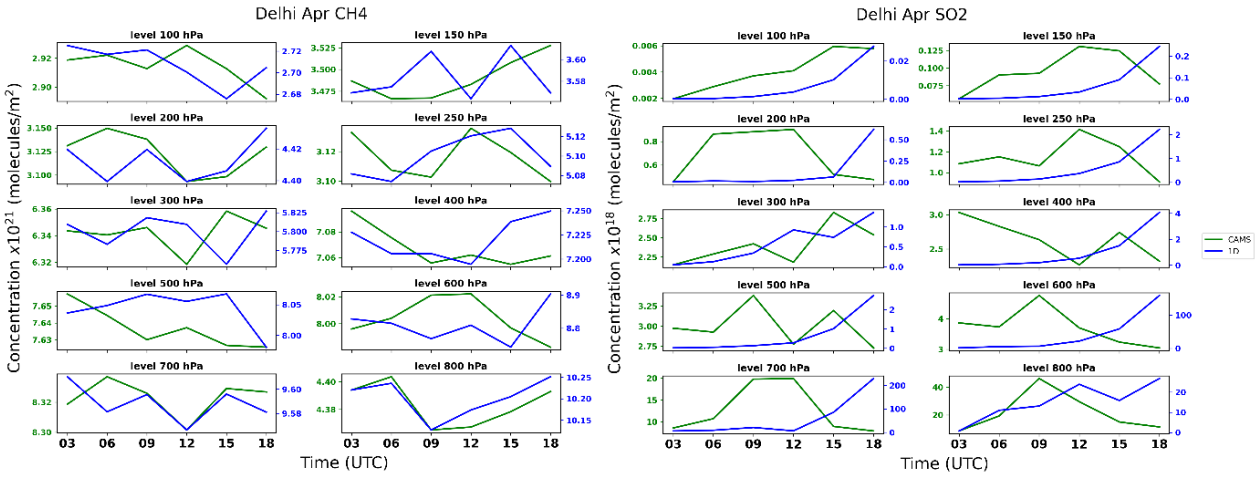

Figure 4.2. Mean diurnal variation of number concentration during non-rainy days over Delhi.

The first panel of Figure 4.3 shows the diurnal variation of CH_4 vertical profiles (number concentration) forecasted by the CAMS and 1-D model at every 3-hour interval during the rainy days of August 2020 over Delhi. The CAMS forecasted maximum (minimum) CH_4 number concentration value is 8.38×10^{21} molecules m^{-2} (2.22×10^{21} molecules m^{-2}) at 700 hPa (100 hPa) pressure level and 03 UTC (12 UTC). The 1-D solver forecasted maximum (minimum) CH_4 number concentration is 9.95×10^{21} molecules m^{-2} (2.77×10^{21} molecules m^{-2}) at 800 hPa (100 hPa) pressure level to be at 06 UTC (06 UTC). The number concentration of CH_4 almost shows diurnal variation in the forecast of both models at all pressure levels. The correlation coefficient (Table 4.1 (c)) between the CAMS model and 1-D hybrid solver is calculated for CH_4. Correlation coefficients at 03, 06, 09, 12, 15, and18 UTC are 74.85%, 74.26%, 75.56%, 75.91%, 75.45%, and 75.18%, respectively (Patnaik et al., 2023).

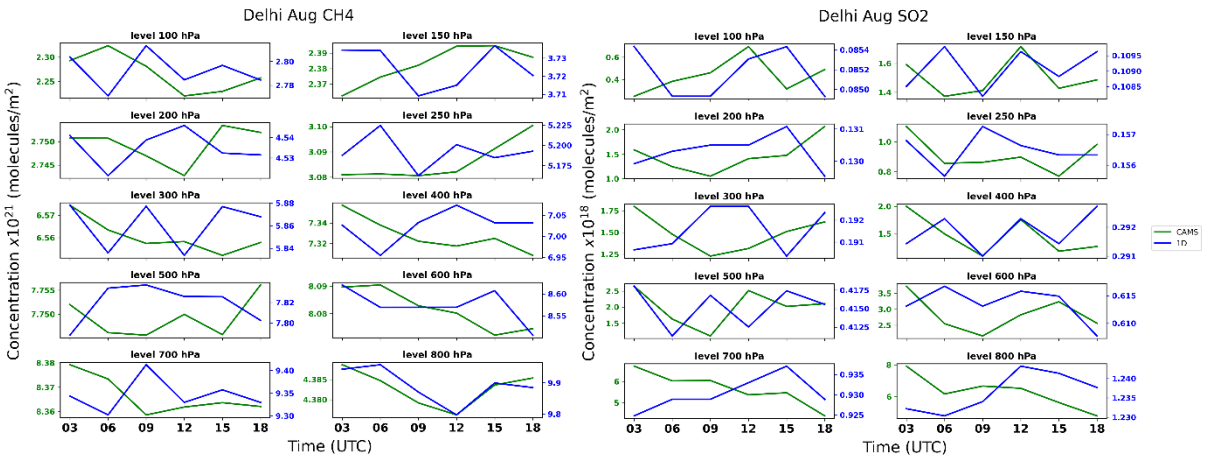

Figure 4.3. Mean diurnal variation of number concentration during rainy days over Delhi.

The second panel of Figure 4.3 shows the diurnal variation of SO_2 vertical profiles (number concentration) predicted by the CAMS model and 1-D solver at every 3-hour interval during the rainy days of August 2020 over Delhi. The maximum (minimum) SO_2 number concentration value determined by the CAMS model is 7.91×10^{18} molecules m^{-2} (2.50×10^{17} molecules m^{-2}) at 03 UTC (03 UTC) and 800 hPa (100 hPa) pressure level. The 1-D solver shows the maximum (minimum) SO_2 number concentration value of 1.24×10^{18} molecules m^{-2} (8.49×10^{16} molecules m^{-2}) at 12 UTC (09 UTC) and 800 hPa (100hPa) pressure level. Thus, the forecast of a 1-D hybrid solver has underestimated the maximum and minimum number concentrations. The number concentration of SO_2 shows diurnal variation in the forecast of both the models at all pressure levels. Correlation coefficients (Table 4.1 (d)) between the CAMS model and 1-D hybrid solver are calculated for SO_2. Correlation coefficients at 03, 06, 09, 12, 15, and 18 UTC are 97.33%, 92.97%, 86.48%, 86.31%, 91%, and 90.28%, respectively (Patnaik et al., 2023).

Table 4.1. Correlation Matrix for Delhi during non-rainy and rainy days. (a) CH_4 (non-rainy) (b) SO_2 (non-rainy) (c) CH_4 (rainy) (d) SO_2 (rainy)

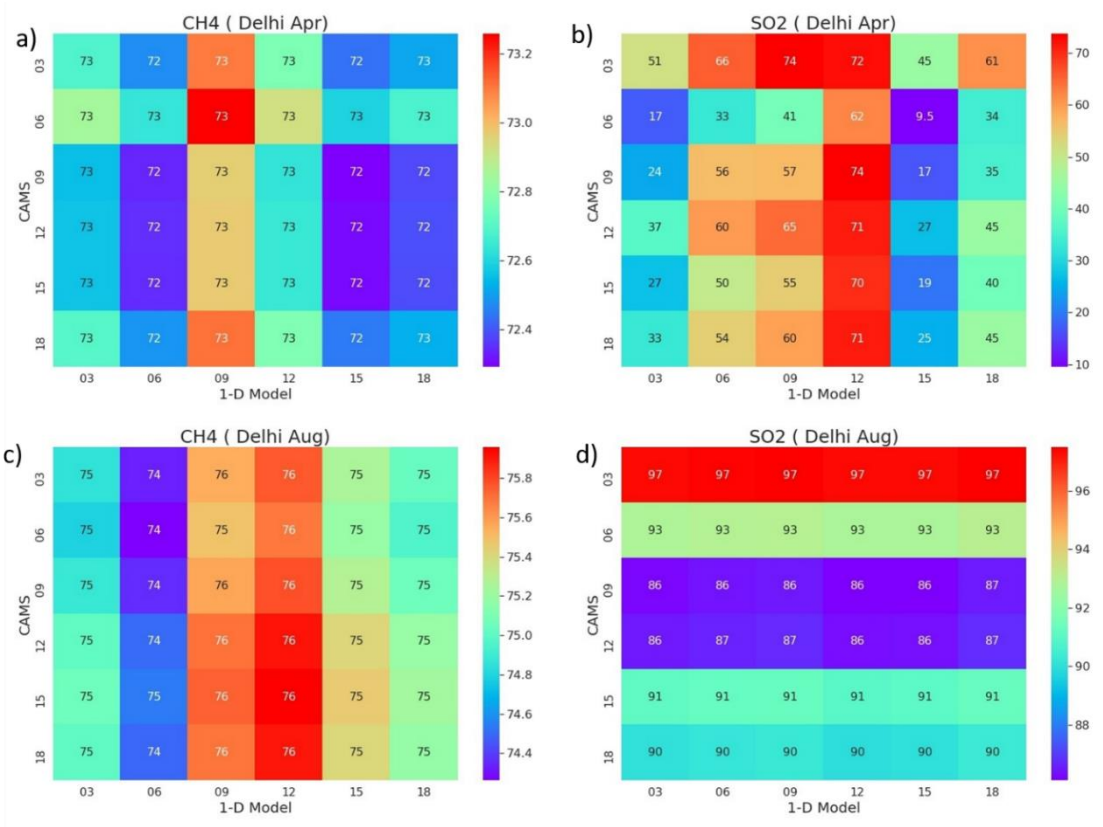

4.3.2. Kolkata

The first panel of Figure 4.4 shows the diurnal variation of CH_4 vertical profiles (number concentration) forecasted by the CAMS model and 1-D solver at every 3-hour interval during the non-rainy days of May 2020 over Kolkata. The CAMS forecasted maximum (minimum) CH_4 number concentration is 8.33×10^{21} molecules m^{-2} (2.37×10^{21} molecules m^{-2}) at 700 hPa (100 hPa) pressure level and 06 UTC (12 UTC). The 1-D solver forecasted a maximum (minimum) CH_4 number concentration of 10.22×10^{21} molecules m^{-2} (2.74×10^{21} molecules m^{-2}) at 800 hPa (100 hPa) and on 09 UTC (03 UTC). The number concentration of CH_4 shows almost a diurnal variation in the forecast of both models. The 1-D hybrid solver slightly overestimated the maximum and minimum number concentration. The correlation coefficient (Table 4.2 (a)) between the CAMS model and 1-D hybrid solver is calculated for CH_4. Correlation coefficients at 03, 06, 09, 12, 15, and 18 UTC are 62.65%, 62.68%, 62.63%, 62.64%, 62.79% and 61.79%, respectively (Patnaik et al. 2023).

The second panel of Figure 4.4 shows the diurnal variation of SO_2 vertical profiles (number concentration) forecasted by the CAMS model and 1-D solver at every 3-hour interval during the non-rainy days of May 2020 over Kolkata. The maximum (minimum) SO_2 number concentration value determined by the CAMS model is 23.18×10^{18} molecules m^{-2} (4.45×10^{16} molecules m^{-2}) at 03 UTC (03 UTC) and 800 hPa (100 hPa) pressure level. The 1-D solver shows the maximum (minimum) SO_2 number concentration value of 2.06×10^{18} molecules m^{-2} (1.49×10^{17} molecules m^{-2}) at 12 UTC (06 UTC) and 800 hPa (100hPa) pressure level. Thus, the maximum number concentration has been underestimated, while the minimum number concentration is overestimated in the forecast of a 1-D hybrid solver. The number concentration of SO_2 shows diurnal variation in the forecast of both the models at all pressure levels. The correlation coefficient (Table 4.2 (b)) between the CAMS model and 1-D hybrid solver is calculated for SO_2. Correlation coefficients at 03, 06, 09, 12, 15, and 18 UTC are 96.58%, 97.82%, 97.25%, 98.39%, 99.2%, and 97.74%, respectively (Patnaik et al., 2023).

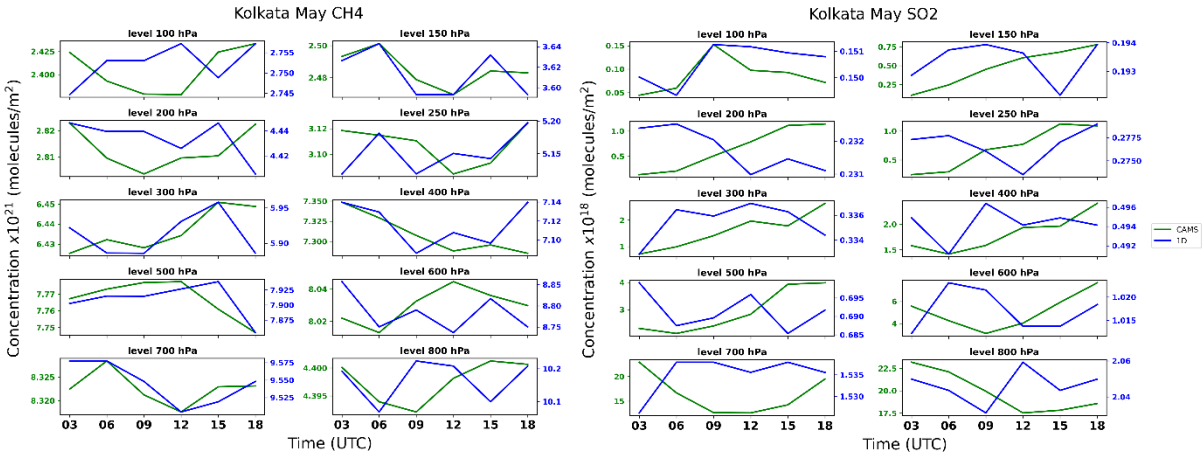

Figure 4.4. Mean diurnal variation of number concentration during non-rainy days over Kolkata.

The first panel of Figure 4.5 shows the diurnal variation of CH_4 vertical profiles (number concentration) forecasted by the CAMS model and 1-D solver at every 3-hour interval during the rainy days of June 2020 over Kolkata. The CAMS forecasted maximum (minimum) CH_4 number concentration is 8.39× 10^{21} molecules m^{-2} (2.19 × 10^{21} molecules m^{-2}) at 700 hPa (100 hPa) pressure level and on 03 UTC (18 UTC). The 1-D solver forecasted maximum (minimum) CH_4 number concentration is 10.11 × 10^{21} molecules m^{-2} (2.70 × 10^{21} molecules m^{-2}) at 800 hPa (100 hPa) pressure level and 06 UTC (03 UTC). The number concentration of CH_4 shows diurnal variation in the forecast of both models at all pressure levels. The correlation coefficient (Table 4.2 (c)) between the CAMS model and the 1-D hybrid solver is calculated for CH_4. Correlation coefficients at 03, 06, 09, 12, 15, and 18 UTC are 62.5%, 62.36%, 61.82%, 61.86%, 62.80%, and 62.96%, respectively (Patnaik et al., 2023).

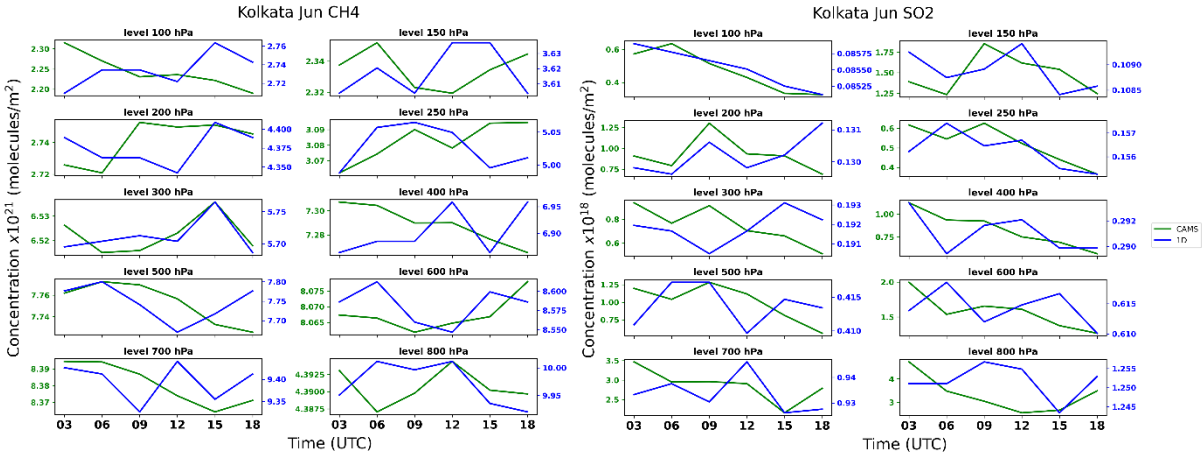

Figure 4.5. Mean diurnal variation of number concentration during rainy days over Kolkata.

The second panel of Figure 4.5 shows the diurnal variation of SO_2 vertical profiles (number concentration) forecasted by the CAMS model and 1-D solver at every 3-hour interval during the rainy days of June 2020 over Kolkata. The maximum (minimum) SO_2 number concentration value determined by the CAMS model is 4.72×10^{18} molecules m^{-2} (3.27×10^{17} molecules m^{-2}) at 03 UTC (18 UTC) and 800 hPa (100 hPa) pressure level. The 1-D solver shows the maximum (minimum) SO_2 number concentration value of 1.25×10^{18} molecules m^{-2} (8.51×10^{16} molecules m^{-2}) at 09 UTC (18 UTC) and 800 hPa (100hPa) pressure level. Thus, the maximum and minimum number concentrations are underestimated in the forecast of a 1-D hybrid solver. The number concentration of SO_2 shows diurnal variation in the forecast of both the models at all pressure levels. The correlation coefficient (Table 4.2 (d)) between the CAMS model and 1-D hybrid solver is calculated for SO_2. Correlation coefficients at 03, 06, 09, 12, 15, and 18 UTC are 94.29%, 93.37%, 91.40%, 91.36%, 91.56%, and 92.14%, respectively (Patnaik et al., 2023).

Table 4.2. Correlation Matrix for Kolkata during non-rainy and rainy days. (a) CH4 (non-rainy) (b) SO2 (non-rainy) (c) CH4 (rainy) (d) SO2 (rainy)

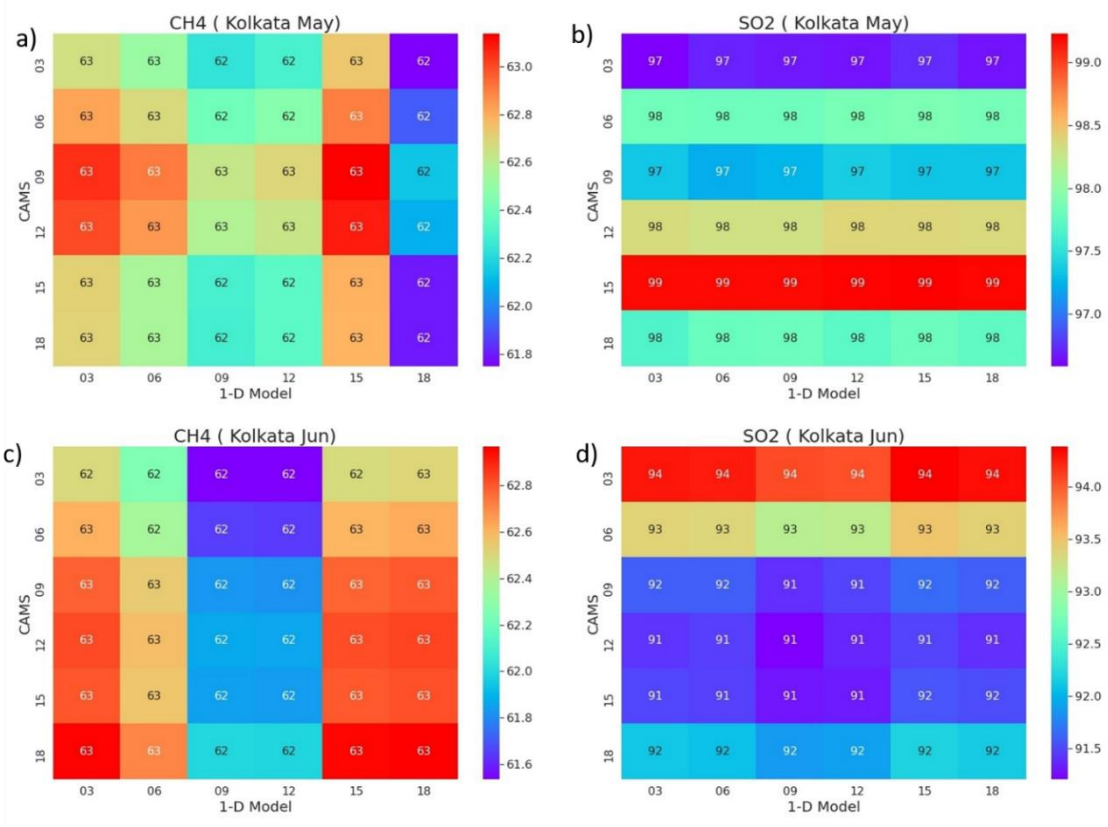

4.3.3. Chennai

The first panel of Figure 4.6 shows the diurnal variation of CH_4 vertical profiles (number concentration) forecasted by the CAMS model and 1-D solver at every 3-hour interval during the non-rainy days of May 2020 over Chennai. The CAMS forecasted maximum (minimum) CH_4 number concentration is 8.30×10^{21} molecules m^{-2} (2.3×10^{21} molecules m^{-2}) at 700 hPa (100 hPa) pressure level and on 03 UTC (03 UTC). The 1-D solver forecasted maximum (minimum) CH_4 number concentration is 10.07×10^{21} molecules m^{-2} (2.78×10^{21} molecules m^{-2}) at 800 hPa (100 hPa) pressure level and on 03 UTC (18 UTC). The number concentration of CH_4 shows almost a diurnal variation in the forecast of both models. The correlation coefficient (Table 4.3 (a)) between the CAMS model and 1-D hybrid solver is calculated for CH_4. Correlation coefficients at 03, 06, 09, 12, 15, and 18 UTC are 42.55%, 42.57%, 42.86%, 42.27%, 42.33%, and 42.71%, respectively (Patnaik et al., 2023).

The second panel of Figure 4.6 shows the diurnal variation of SO_2 vertical profiles (number concentration) forecasted by the CAMS model and 1-D solver at every 3-hour interval during the non-rainy days of May 2020 over Chennai. The maximum (minimum) SO_2 number concentration value determined by the CAMS model is 10.7×10^{18} molecules

m^{-2} (5.62×10^{16} molecules m^{-2}) at 09 UTC (12 UTC) and 800 hPa (100 hPa) pressure level. The 1-D solver shows the maximum (minimum) SO_2 number concentration value of 1.26×10^{18} molecules m^{-2} (8.50×10^{16} molecules m^{-2}) at 06 UTC (18 UTC) and 800 hPa (100hPa) pressure level. Thus, the maximum number concentration is underestimated, and the minimum number concentration is overestimated in the forecast of a 1-D hybrid solver. The number concentration of SO_2 shows diurnal variation in the forecast of both the models at all pressure levels. The correlation coefficient (Table 4.3 (b)) between the CAMS model and 1-D hybrid solver is calculated for SO_2. Correlation coefficients at 03, 06, 09, 12, 15, and 18 UTC are 96.48%, 96.69%, 94.31%, 95.83%, 95.33%, and 96.16%, respectively (Patnaik et al., 2023).

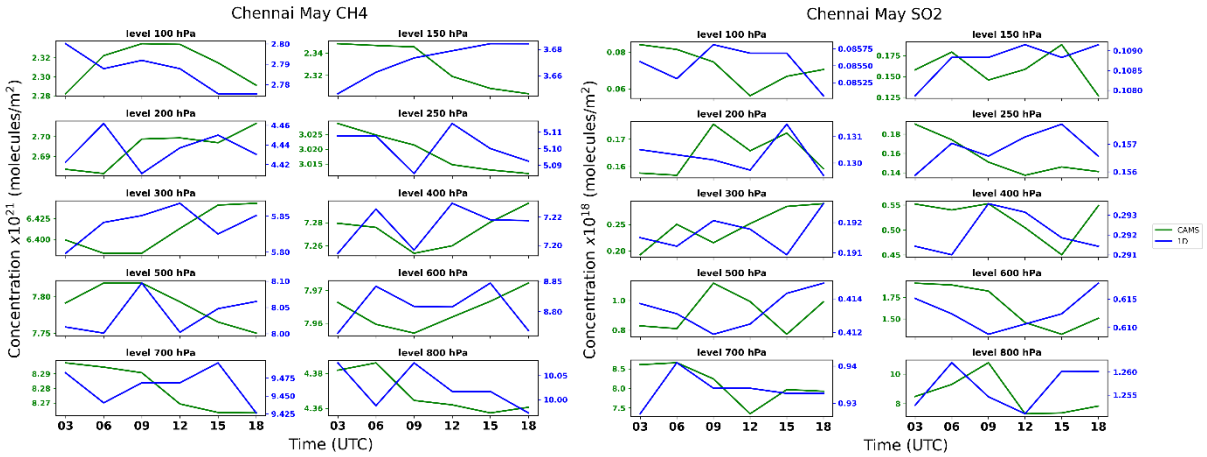

Figure 4.6. Mean diurnal variation of number concentration during non-rainy days over Chennai.

The first panel of Figure 4.7 shows the diurnal variation of CH_4 vertical profiles (number concentration) forecasted by the CAMS model and 1-D solver at every 3-hour interval during the rainy days of November 2020 over Chennai. The CAMS forecasted maximum (minimum) CH_4 number concentration is 8.44×10^{21} molecules m^{-2} (2.34×10^{21} molecules m^{-2}) at 700 hPa (150 hPa) pressure level and 06 UTC (12 UTC). The 1-D solver forecasted the maximum (minimum) CH_4 number concentration is 9.97×10^{21} molecules m^{-2} (2.73×10^{21} molecules m^{-2}) at 800 hPa (100 hPa) pressure level and on 12 UTC (12 UTC). The number concentration of CH_4 shows almost a diurnal variation in the forecast of both models. The correlation coefficient (Table 4.3c) between the CAMS model and the 1-D hybrid solver is calculated for CH_4. Correlation coefficients at 03, 06, 09, 12, 15, and 18 UTC are 40.16%, 41.34%, 41.13%, 38.83%, 42.98%, and 37.42%, respectively (Patnaik et al., 2023).

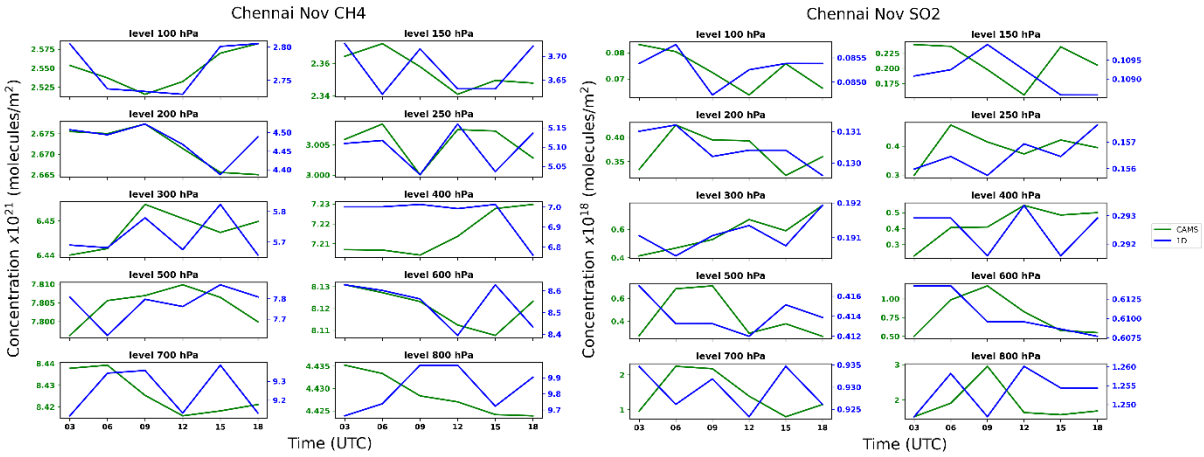

Figure 4.7. Mean diurnal variation of number concentration during rainy days over Chennai.

The second panel of Figure 4.7 shows the diurnal variation of SO_2 vertical profiles (number concentration) forecasted by the CAMS model and 1-D solver at every 3-hour interval during the rainy days of November 2020 over Chennai. The maximum (minimum) SO_2 number concentration value determined by the CAMS model is 2.95×10^{18} molecules m^{-2} (6.38×10^{16} molecules m^{-2}) at 09 UTC (12 UTC) and 800 hPa (100 hPa) pressure level. The 1-D solver shows the maximum (minimum) SO_2 number concentration value of 1.26×10^{18} molecules m^{-2} (8.47×10^{16} molecules m^{-2}) at 12 UTC (09 UTC) and 800 hPa (100hPa) pressure level. Thus, the maximum number concentration is underestimated, and the minimum number concentration is overestimated in the forecast of a 1-D hybrid solver. The number concentration of SO_2 shows diurnal variation in the forecast of both the models at all pressure levels. The correlation coefficient (Table 4.3 (d)) between the CAMS model and 1-D hybrid solver is calculated for SO_2. Correlation coefficients at 03, 06, 09, 12, 15, and 18 UTC are 84.39%, 87.43%, 89.97%, 86.96%, 88.18%, and 89.9%, respectively (Patnaik et al., 2023).

4.3.4. Mumbai

The first panel of Figure 4.8 shows the diurnal variation of CH_4 vertical profiles (number concentration) forecasted by the CAMS model and 1-D solver at every 3-hour interval during the non-rainy days of May 2020 over Mumbai. The CAMS forecasted maximum (minimum) CH_4 number concentration is 8.25×10^{21} molecules m^{-2} (2.39×10^{21} molecules m^{-2}) at 700 hPa (100 hPa) pressure level and on 03 UTC (03 UTC). The 1-D solver forecasted maximum (minimum) CH_4 number concentration is 10.24×10^{21}

molecules m^{-2} (2.75×10^{21} molecules m^{-2}) at 800 hPa (100 hPa) pressure level and on 12 UTC (03 UTC). The number concentration of CH_4 shows almost a diurnal variation in the forecast of both models. The correlation coefficient (Table 4.4 a) between the CAMS model and 1-D hybrid solver is calculated for CH_4. Correlation coefficients at 03, 06, 09, 12, 15, and 18 UTC are 39.05%, 39.49%, 38.74%, 39.37%, 38.32%, and 38.96%, respectively (Patnaik et al., 2023).

Table 4.3. Correlation Matrix for Chennai during non-rainy and rainy days. (a) CH_4 (non-rainy) (b) SO_2 (non-rainy) (c) CH_4 (rainy) (d) SO_2 (rainy)

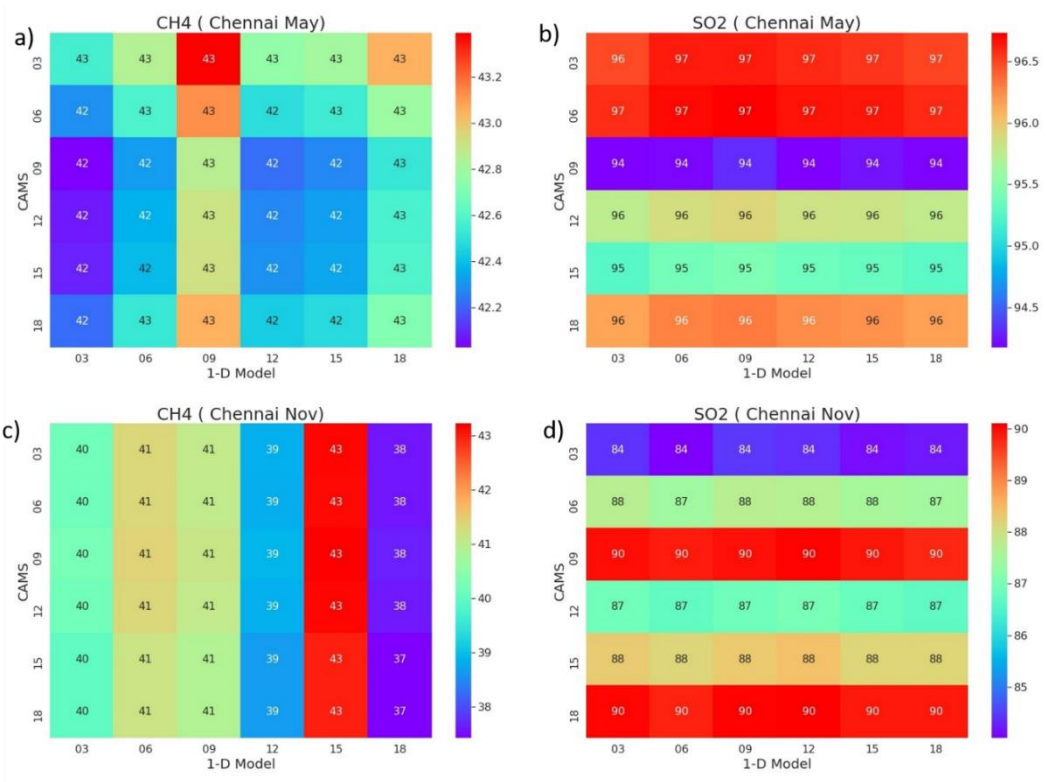

The second panel of Figure 4.8 shows the diurnal variation of SO_2 vertical profiles (number concentration) forecasted by the CAMS model and 1-D solver at every 3-hour interval during the non-rainy days of May 2020 over Mumbai. The maximum (minimum) SO_2 number concentration value determined by the CAMS model is 9.84×10^{18} molecules m^{-2} (3.65×10^{16} molecules m^{-2}) at 03 UTC (15 UTC) and 700 hPa (100 hPa) pressure level. The 1-D solver shows the maximum (minimum) SO_2 number concentration value of 1.95×10^{18} molecules m^{-2} (1.38×10^{17} molecules m^{-2}) at 09 UTC (18 UTC) and 800 hPa (100hPa) pressure level. Thus, the maximum number concentration is underestimated, and the minimum number concentration is overestimated in the forecast

of a 1-D hybrid solver. The number concentration of SO_2 shows diurnal variation in the forecast of both the models at all pressure levels. The correlation coefficient (Table 4.4b) between the CAMS model and 1-D hybrid solver is calculated for SO_2. Correlation coefficients at 03, 06, 09, 12, 15, and 18 UTC are 77.2%, 85.89%, 87.16%, 88.01%, 78.27%, and 77.57%, respectively (Patnaik et al., 2023).

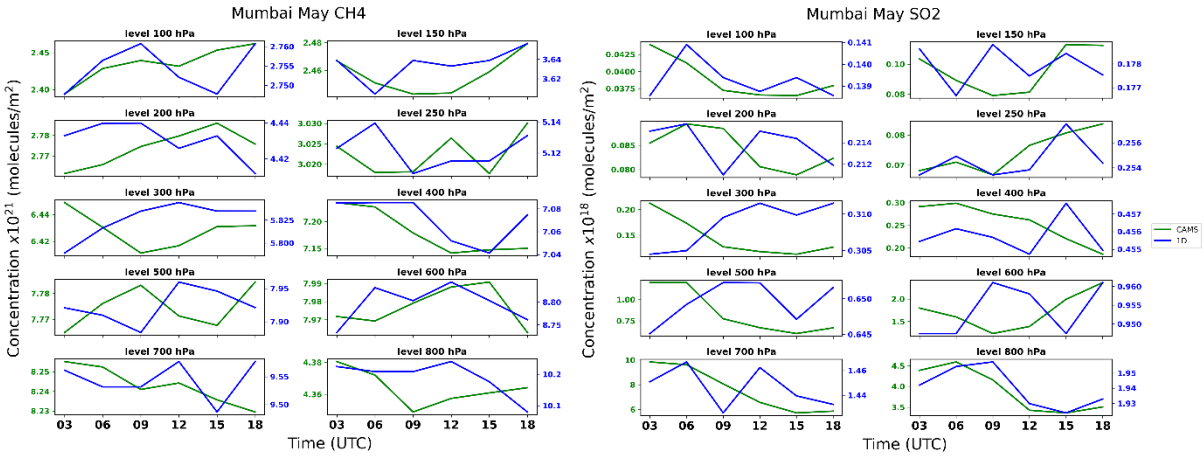

Figure 4.8. Mean diurnal variation of number concentration during non-rainy days over Mumbai.

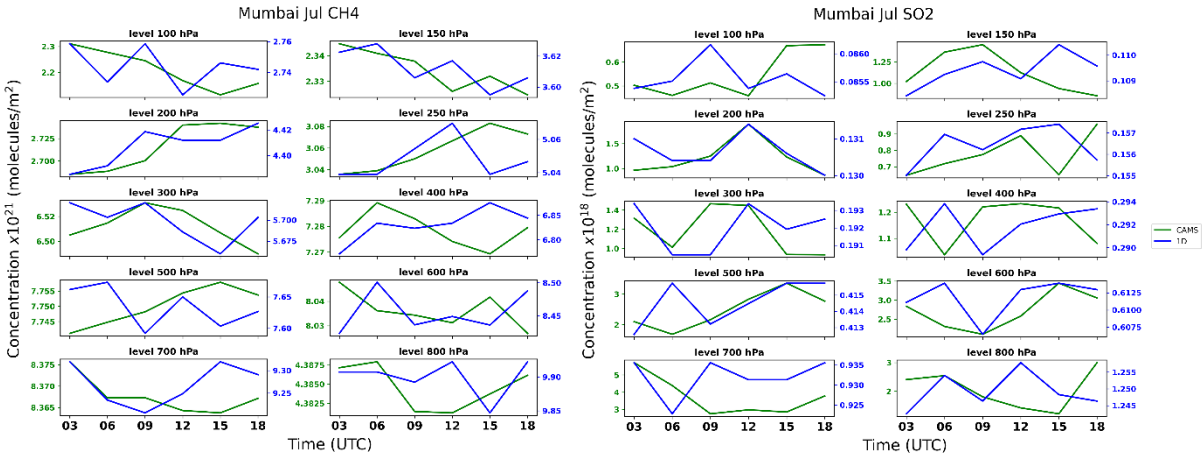

Figure 4.9. Mean diurnal variation of number concentration during rainy days over Mumbai.

The first panel of Figure 4.9 shows the diurnal variation of CH_4 vertical profiles (number concentration) forecasted by the CAMS model and 1-D solver at every 3-hour interval during the rainy days of July 2020 over Mumbai. The CAMS forecasted maximum (minimum) CH_4 number concentration is 8.38 × 10^{21} molecules m^{-2} (2.11 × 10^{21}

molecules m^{-2}) at 700 hPa (100 hPa) pressure level on 03 UTC (15 UTC). The 1-D solver forecasted maximum (minimum) CH_4 number concentration of 9.92×10^{21} molecules m^{-2} (2.72×10^{21} molecules m^{-2}) at 800 hPa (100 hPa) pressure level and on 12 UTC (12 UTC). The number concentration of CH_4 shows almost a diurnal variation in the forecast of both models. The correlation coefficient (Table 4.4c) between the CAMS model and 1-D hybrid solver is calculated for CH_4. Correlation coefficients at 03, 06, 09, 12, 15, and 18 UTC are 38.9%, 38.79%, 38.65%, 39.16%, 39.09%, and 39.71%, respectively (Patnaik et al., 2023).

Table 4.4. Correlation Matrix for Mumbai during non-rainy and rainy days. (a) CH_4 (non-rainy) (b) SO_2 (non-rainy) (c) CH_4 (rainy) (d) SO_2 (rainy)

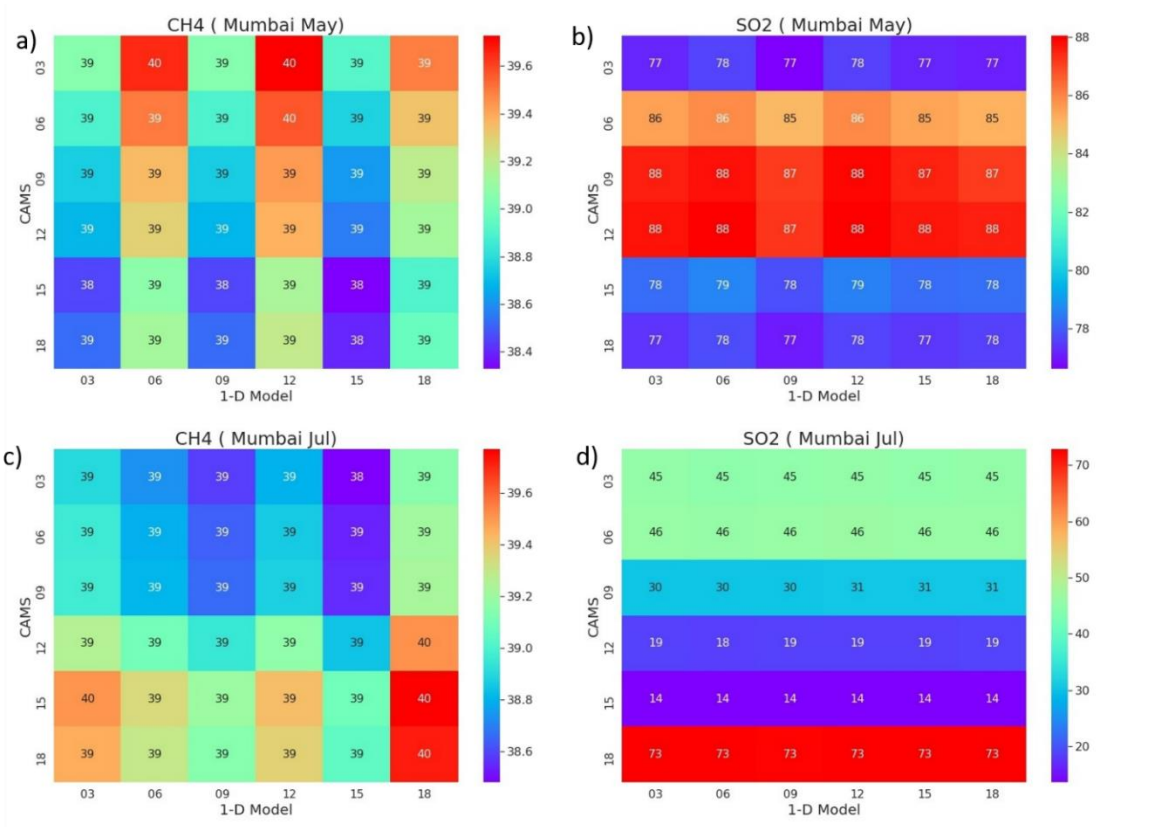

The second panel of Figure 4.9 shows the diurnal variation of SO_2 vertical profiles (number concentration) forecasted by the CAMS model and 1-D solver at every 3-hour interval during the rainy days of July 2020 over Mumbai. The maximum (minimum) SO_2 number concentration value determined by the CAMS model is 5.7×10^{18} molecules m^{-2} (4.58×10^{17} molecules m^{-2}) at 03 UTC (12 UTC) and 700 hPa (100 hPa) pressure level. The 1-D solver shows the maximum (minimum) SO_2 number concentration value of 1.26×10^{18} molecules m^{-2} (8.52×10^{16} molecules m^{-2}) at 12 UTC (18 UTC) and 800 hPa

(100hPa) pressure level. Thus, both the maximum and minimum number concentrations are underestimated in the forecast of a 1-D hybrid solver. The number concentration of SO_2 shows diurnal variation in the forecast of both the models at all pressure levels. The correlation coefficient (Table 4.4 d) between the CAMS model and 1-D hybrid solver is calculated for SO_2. Correlation coefficients at 03, 06, 09, 12, 15, and 18 UTC are 45.32%, 45.84%, 30.42%, 18.7%, 13.8%, and 72.7%, respectively (Patnaik et al., 2023).

The 1-D solver slightly overestimates the CH_4 number concentration compared to the CAMS model, while it underestimates the SO_2 number concentration. It is seen that after 18 UTC, the 1-D hybrid solver highly overestimates the number concentration of CH_4 and SO_2. Kavitha et al. (2018) studied the diurnal variation of CH_4 at a tropical coastal station in India. The CH_4 diurnal variation is observed to be low during the daytime and high during night-time. These changes are closely related to mesoscale circulations such as Sea Breezes and Land breezes. Also, in the Indian Subcontinent, fluxes and transport contribute to CH_4 seasonal variability. However, it is known that during the Asian summer monsoonal season, its intra-seasonal variability is also influenced by rains, which complicates the situation with CH_4, largely influenced by advection (Tiwari et al. 2020). These mesoscale circulations and advection processes are not considered in the 1-D solver, which may be the reason for the overestimation of CH_4 number concentration. Also, the atmospheric boundary layer is the lowest layer of the troposphere, where both temperature and wind speeds play a critical role in its vertical variation. The boundary layer can mix greenhouse gas emissions at the ground level up to a certain height and reduce their concentration near the ground. Hence, seasonal changes in the boundary layer can influence the concentration of greenhouse gases on the ground (Metya et al., 2021).

SO_2 having a significantly lower lifetime (typically two days), high solubility, and transportation from the place of emissions (Renuka et al. 2020) are the possible reasons for the underestimated values by the 1-D solver. The 1-D solver only relies on chemical transformation based on temperature changes, while the CAMS model considers all the factors, such as emissions and transportation. Without using an atmospheric chemistry-transport model, the complexity of evaluating the surface emissions as measured by columnar CH_4 has been highlighted by Chandra et al. (2017).

4.4. Conclusions

In this chapter, the monthly mean vertical number concentrations are obtained from the 1-D hybrid solver and compared with the CAMS model at 3-hour time intervals over the megacities, such as Delhi, Kolkata, Chennai, and Mumbai, during non-rainy days and rainy days. It has been seen that during non-rainy days over Delhi, Kolkata, Chennai, and Mumbai, the CAMS model shows a strong diurnal variation of CH_4 number concentration. The 1-D solver also shows a similar trend to the CAMS model at all pressure levels up to 18 UTC, and then there is a gradual increase in number concentration at 21 UTC over all four megacities, and the model blows off. Therefore, we have analyzed the output only up to 18 UTC, and the possible reasons for this model blow-off will be investigated in the future (Patnaik et al., 2023).

We have divided the time intervals into morning (03 UTC to 06 UTC), late morning (06 UTC to 09 UTC), afternoon (09 UTC to 12 UTC), evening (12 UTC to 15 UTC), late evening (15 UTC to 18 UTC) and night (18 UTC to 21 UTC). During non-rainy days over Delhi, Kolkata, Chennai, and Mumbai, the CAMS model and 1-D hybrid solver forecasted a strong diurnal variation of CH_4 number concentration at different pressure levels. Over Delhi, CAMS detects maxima (minima) in the late morning (night), whereas the 1-D hybrid solver shows maxima (minima) in the night (late evening) with a lag (lead) of 12 hours (3 hours). Over Kolkata, CAMS detects maxima (minima) in the late morning (evening), whereas 1-D hybrid solver shows maxima (minima) in the afternoon (morning) with a lag (lead) of 3 hours (9 hours). Over Chennai, CAMS detects maxima (minima) in the morning (morning), whereas the 1-D hybrid solver shows maxima (minima) in the morning (night) with a lag (lead) of 0 hours (15 hours). Over Mumbai, CAMS detects maxima (minima) in the morning (morning), whereas the 1-D hybrid solver shows maxima (minima) in the evening (morning) with a lag (lead) of 9 hours (0 hours). The Maxima of these two models for all four megacities is observed at a pressure difference of 100 hPa (Patnaik et al., 2023).

In the case of SO_2, during non-rainy days over Delhi, Kolkata, Chennai, and Mumbai, the CAMS model and the 1-D hybrid solver showed a strong diurnal pattern at all pressure levels. Over Delhi, CAMS detected maxima (minima) in the afternoon (morning), whereas the 1-D hybrid solver shows maxima (minima) in the night (morning)

with a lag (lead) of 9 hours (0 hours). Over Kolkata, CAMS detected maxima (minima) in the morning (morning), whereas 1-D hybrid solver shows maxima (minima) in the evening (late morning) with a lag (lag) of 9 hours (3 hours). Over Chennai, CAMS detects maxima (minima) in the afternoon (evening), whereas the 1-D hybrid solver shows maxima (minima) in the late morning (night) with a lead (lag) of 3 hours (6 hours). Over Mumbai, CAMS detects maxima (minima) in the morning (late evening), whereas the 1-D hybrid solver shows maxima (minima) in the afternoon (evening) with a lag (lag) of 6 hours (3 hours) (Patnaik et al. 2023).

During rainy days over Delhi, Kolkata, Chennai, and Mumbai, the CAMS model and 1-D hybrid solver forecasted a strong diurnal variation of CH_4 number concentration at different pressure levels. Over Delhi, CAMS detects maxima (minima) in the morning (evening), whereas the 1-D hybrid solver shows maxima (minima) in the late morning (late morning) with a lag (lead) of 3 hours (6 hours). Over Kolkata, CAMS detects maxima (minima) in the morning (night), whereas 1-D hybrid solver shows maxima (minima) in the late morning (morning) with a lag (lead) of 3 hours (15 hours). Over Chennai, CAMS detects maxima (minima) in the late morning (evening), whereas the 1-D hybrid solver shows maxima (minima) in the evening (evening) with a lag (lead) of 6 hours (0 hours). Over Mumbai, CAMS detects maxima (minima) in the morning (late evening), whereas the 1-D hybrid solver shows maxima (minima) in the evening (evening) with a lag (lead) of 9 hours (3 hours). The maxima of these two models for all four megacities are observed at a pressure difference of 100 hPa. In the case of SO_2, during rainy days over Delhi, Kolkata, Chennai, and Mumbai, the CAMS model and the 1-D hybrid solver showed a strong diurnal pattern at all pressure levels. Over Delhi, CAMS detects maxima (minima) in the morning (morning), whereas the 1-D hybrid solver shows maxima (minima) in the evening (late morning) with a lag (lag) of 9 hours (3 hours). Over Kolkata, CAMS detects maxima (minima) in the morning (night), whereas 1-D hybrid solver shows maxima (minima) in the afternoon (night) with a lag (lead) of 6 hours (0 hours). Over Chennai, CAMS detects maxima (minima) in the afternoon (evening), whereas the 1-D hybrid solver shows maxima (minima) in the evening (afternoon) with a lag (lead) of 3 hours (3 hours). Over Mumbai, CAMS detects maxima (minima) in the morning (evening), whereas 1-D hybrid solver shows maxima (minima) in the afternoon (night) with a lag (lag) of 9 hours (6 hours) (Patnaik et al. 2023).

During non-rainy days, the 1-D model overestimates the maximum number concentration of CH_4, while it underestimates the minimum number concentration over Delhi and overestimates the minimum and maximum number concentration over Kolkata, Chennai, and Mumbai. Over Delhi and Kolkata, the CAMS and 1-D hybrid solver exhibit a good correlation, whereas over Chennai and Mumbai, the CAMS and 1-D hybrid solver exhibit a weak correlation. During rainy days, the 1-D model overestimates the maximum and minimum number concentration of CH_4 over all four megacities. Over Delhi and Kolkata, the CAMS and 1-D hybrid solvers have a good correlation, whereas over Chennai and Mumbai, the CAMS and 1-D hybrid solvers exhibit a weak correlation (Patnaik et al., 2023).

During non-rainy days, the 1-D model overestimates the maximum number concentration of SO_2 over Delhi while underestimated over Kolkata, Chennai, and Mumbai, while the minimum number concentration is overestimated over all four megacities. Except for Delhi, other megacities correlate well with the CAMS and 1-D hybrid solver. During rainy days, the 1-D model underestimates the maximum number concentration of SO_2 over all four megacities. Except for Chennai, the minimum number concentration is underestimated over Delhi, Kolkata, and Mumbai. Except for Mumbai, for the other three megacities, a good correlation between CAMS and 1-D hybrid solver has been seen (Patnaik et al., 2023).

However, both models successfully simulate the diurnal variation. The 1-D hybrid solver uses only the chemical transformations dependent on vertical temperature profiles, while the CAMS model uses local emissions, advection, transportation, etc. The above are the possible reasons for overestimating or underestimating the CH_4 and SO_2 number concentration of the 1-D hybrid solver. This solver can be further modified by specifying prognostic sources and sinks of minor constituents, affecting CH_4 and SO_2 number concentrations at different model levels. Also, in the recent preprint, Mermigkas et al. (2023) have shown that the CAMS model underestimates the CH_4 number concentration. However, special observation campaigns for measuring vertical profiles of the number concentrations of these components are required to validate both these models.

Further, the influence of atmospheric dynamics is required to be represented explicitly. The sea and land breeze significantly influence Kolkata, Chennai, and Mumbai coastal cities. Local emissions, advection, convection, and transportation also play a significant role in these megacities. Also, the Indian Monsoon circulation, including the Southwest and Northeast monsoon, carries a large amount of water vapor, significantly influencing the circulation over these megacities. Therefore, we strongly feel that implementing this solver in a global model may provide robust estimates of the number of concentrations with better accuracy (Patnaik et al., 2023).

Chapter 5

5. Disturbed Weather Situations

5.1. Introduction

The concentrations of trace gases in the atmosphere over a region can be envisaged as an open system influenced by local and regional contributions (Mallik et al. 2014). Further, the knowledge of atmospheric chemistry of reactive minor constituents and their influence on cloud microphysics is essential to understanding the link between human activities and climate. However, monitoring the concentration of each minor constituent of the atmosphere and their chemistry is very difficult. Hence, it is paramount to develop a model that estimates their number concentration with substantial accuracy and variability.

The minor constituents such as methane (CH_4) are the second largest contributor to global warming among all anthropogenic species, with a positive radiative forcing of about 0.48 ± 0.05 W m^{-2}. Global models show that wetland emissions of CH_4 vary by ±3% yr^{-1} ($\sigma = 4.8$ Tg), mainly due to precipitation-induced changes. The rise in temperatures has significantly increased the wetland area, leading to the rise of CH_4 emissions, i.e., approximately +0.2%/year from 1999 to 2014 (McNorton et al. 2016). Nitrous oxide (N_2O) is another vital greenhouse gas with a Global warming potential (GWP) 273 times that of CO_2 for a 100-year timescale. It is produced in soil and aquatic ecosystems and is one of the main greenhouse gases known for its debilitating effect on Earth's ozone layer. The gas is produced naturally by microbial activity on land and in the oceans and artificially by emissions from human-made processes, such as fertilization or burning fossil fuels. As climate change continues, it is increasingly important to monitor and quantify greenhouse gases in the atmosphere using satellites (Wendel, 2014). Climate change is expected to aggravate disastrous weather, such as forest fires, hurricanes, and cloud bursts, with uncertain effects on atmospheric composition. The present ecosystem will evolve in response to changes in atmospheric composition and the behavior of global GHG emitters due to the expected increased frequency of disastrous events (Quebbeman et al., 2022).

Convective processes swiftly transport chemical constituents between the boundary layer and free troposphere and effectively clean the atmosphere via wet deposition. The knowledge of the vertical distribution of chemical species and the impact of convection on their concentrations is crucial for chemistry-climate research, air quality studies, and other chemistry-related investigations (Barth et al., 2007). Several studies have discussed the retrieval techniques of CH_4 and N_2O vertical profiles. The University of California Irvine's three-dimensional chemistry-transport model demonstrated that N_2O emissions reduce the amount of tropospheric CH_4 through a series of chemical processes. These processes include stratospheric ozone loss, modifications to solar ultraviolet radiation fluxes, modifications to ozone transport fluxes from the stratosphere to the troposphere, and an increased amount of tropospheric hydroxyl radicals (Prather & Hsu, 2010). Many models do not consider the formation of Secondary Organic Aerosols (SOAs) in cloud and aerosol water. The presence of organic aerosols in clouds and aerosol water contributes significantly to droplet mode, which field observations and laboratory studies have demonstrated. It is possible for semi-volatile compounds to increase the mass of SOA through further oxidation in the gas phase and re-condensation into particulate organic matter. However, this articulate organic matter can undergo oxidation and dissolve into the aqueous phase to produce SOA (Ervens et al. 2011).

Cloud microphysical and optical characteristics, such as water path, optical depth, particle size, and thermodynamic phase, are related to the radiative characteristics of clouds and are influenced by vertical profiles of atmospheric constituents. Cox et al. (2014) have used vertical profiles of temperature and trace gases such as ozone (O_3), nitrous oxide (N_2O), carbon monoxide (CO), and methane (CH_4), and input to Line-by-Line Radiative Transfer Model (LBLRTM), to study the cloud microphysical properties. Karppinen et al. (2020) have used data from a ground-based Fourier Transform Spectrometer (FTS) in Sodankylä, Northern Finland, from 2009 to 2018. They have developed a method that is an important addition to the CH_4 profile measurements. At first, the profile information is extracted using the dimension reduction retrieval methods. Since each measurement consists of three pieces of information between 0 and 40 km, it was compared to the measurements from the Atmospheric Chemistry Experiment Fourier Transform Spectrometer (ACE-FTS) satellite and the Air Core balloon. Below 20 km, ground-based FTS and ACE-FTS profiles agreed within 10%; between 20 and 40 km, it was within 30% in the stratosphere. This methodology is not very accurate compared to aircraft and

balloon measurements; however, it provides good temporal coverage. Li et al. (2023) have built a neural network based on the data of FY-3E/HIRAS-II to retrieve the atmospheric gas profiles, which have a faster retrieval ability. However, the above experiment was conducted over a fixed geographic area, and there is a need to remove the samples of polluted clouds, which makes it difficult to create an effective two-dimensional graphical structure. Xiong et al. (2014) have developed an algorithm to retrieve N_2O using the Atmospheric Infrared Sounder (AIRS) on EOS/Aqua and validated the same using aircraft measurements. The comparison of the AIRS retrieval mean profile and its standard deviation with aircraft measurements indicated that N_2O measured in the AIRS is two times higher than in aircraft measurements. Barret et al. (2021) have retrieved the N_2O profiles using Metop/IASI with the Software for the Retrieval of IASI Data (SOFRID) for the years from 2008 to 2018 and validated with FTIR data over 12 locations of the Network for the Detection of Atmospheric Composition Changes (NDACC). This study has shown that FTIR and SOFRID have a better agreement in the mid-troposphere (700 hPa -350 hPa), as compared to the upper (350 hPa- 110 hPa) and lower (surface – 700 hPa) troposphere, with correlation coefficients between 0.49-0.83. The correlation coefficient is greater than 0.77 for oceanic and coastal stations, while for continental stations, the correlation coefficient is less than 0.72. It is also suggested that inadequate estimation of the Land-Sea differences and day-night variations leads to large biases between FTIR and SOFRID. Such large biases lead to biases in estimating cloud condensation and ice nuclei. Hence, accurate estimation of vertical profiles of atmospheric minor constituents is required to reduce the biases of CCN and IN.

Patnaik et al. (2023) have developed a hybrid solver using Gear solution and the Monte Carlo method and integrated the gas-phase chemistry of CH4, N2O, and SO2 to estimate vertical profiles of minor constituents. The vertical profiles obtained from the solver have been validated using a merged product derived from satellite observations, viz., Community Long-term Infrared Microwave Coupled Atmospheric Product System (CLIMCAPS) dataset during non-rainy and rainy days over the megacities viz. Delhi, Kolkata, Chennai, and Mumbai. The chemical reactions and CH_4, N_2O, and SO_2 reaction rates were obtained from the Master Chemical Mechanism (MCM). Since reaction rates are temperature dependent, ERA5 temperature vertical profiles are taken and perturbed 1000 times using Maximum Likelihood Estimation (MLE) for Monte-Carlo simulations.

It was seen that CLIMCAPS and the collected profiles were in good agreement on rainy and non-rainy days. It was also noticed that the vertical number concentration of SO2 was in agreement with the CLIMCAPS as compared to the vertical number concentration of CH_4 and N_2O.

The Percentage Difference of Number Concentrations (PDNC) is calculated using $PDNC\ (\%) = 100\left(\frac{NCCD-ENC}{NCCD}\right)$ where NCCD is the number concentrations from the CLIMCAPS dataset, and ENC is the estimated number concentrations. PDNC of retrieved vertical profiles of CH_4 and N_2O during disturbed weather events, such as tropical cyclone Nivar and the rainfall associated with the northeast monsoon, was underestimated. Delhi showed higher values of PDNC, i.e., −18.49 % to −23.64 % (daytime of 23 April 2020) and −56.78 % to −60.8 % (night-time of 22 April 2020) during non-rainy days, and these variations were associated with the passage of western disturbances over Delhi, from 22 April 2020, 1300 UTC, to 23 April 2020, 2130 UTC. However, due to the development of super cyclonic storm "Nivar" (24 November 2020 and 25 November 2020) over the Bay of Bengal, near the Chennai coast, and on 15 November 2020, during the retreat of the Northeast monsoon, the error percentage was found to be higher between the observed and retrieved satellite profiles. Over these megacities, the passage of large-scale systems has caused a significant variation in the PDNC values. Otherwise, these profiles were in good agreement with the CLIMCAPS datasets. MLE was generated using mixed (fair and disturbed) weather conditions to develop a hybrid solver. The above may lead to erroneous MLE while simulating the number concentrations during disturbed weather conditions. Hence, we hypothesize that generating a separate MLE for the number concentrations of CH_4 and N_2O by considering only disturbed weather situations can reduce the errors in their predictions. Hence, this approach separates MLE for fair and disturbed weather situations. Here, we have used a modified 1-D model by incorporating another MLE for CH_4 and N_2O based on temperature profiles during western disturbances, rainy days for Delhi, rainy days for Chennai, and tropical cyclones for Chennai. As CH_4 vertical profiles were retrieved with good accuracies (Patnaik et al. 2023) during the rainy days over Kolkata and Mumbai, we have addressed the percentage errors of N_2O during rainy days over Kolkata and Mumbai in this chapter.

5.2. Data

5.2.1. CLIMCAPS Datasets

CLIMCAPS Version 2 Level-2 (**https://disc.gsfc.nasa.gov**) provides numerous geophysical parameters generated from IR/MW sounder observations made on board polar-orbiting satellites, including as AIRS/AMSU on Aqua, CrIS/ATMS on Suomi NPP, and NOAA20, which has been made available since 2012. Geophysical parameters such as temperature, water vapor, trace gas species (O_3, CO, CH_4, N_2O, HNO_3, and SO_2), cloud cover, and surface characteristics for six minutes of instrument observation at a time are provided by this satellite. Additionally, the Cross-Track IR Sounder (CrIS) sensor offers more precise, thorough observations of air temperature, moisture, and greenhouse gas concentrations for weather and climate applications. As infrared energy cannot penetrate dense clouds, it performs best in clear to partially cloudy circumstances. Since the Advanced Technology Microwave Sounder (ATMS)'s microwave energy can pass through cloud cover, it functions in conjunction with this device. On 37 fixed-pressure layers, this product has been used to initialize the O_3, CH_4, N_2O, HNO_3, and SO_2 concentrations on summer and rainy days in specific locations. Two times every day, at roughly 0800 UTC and 2000 UTC (0130 IST), this satellite passes over India. Hence, we have used CLIMCAPS data of number concentration around 0800 (2000) UTC for initialization only during weather conditions such as western disturbances, tropical cyclones, or heavy rains. The vertical profiles of number concentrations were estimated for each hour till up to 12 hours, and the simulated results have been validated with the next cycle of the CLIMCAPS dataset, i.e., if the model is initialized with 0800 (2000) UTC CLIMCAPS dataset, then it is validated with 2000 (0800) UTC dataset. In cities such as Delhi, Kolkata, Chennai, and Mumbai, ideal experiments have been conducted during disturbed weather events such as western disturbances, heavy rainfall, and tropical cyclones.

5.2.2. Master Chemical Mechanism (MCM)

The tropospheric degradation process described by MCM (http://mcm.york.ac.uk/) involves several primary released volatile organic compounds (VOCs) and gas-phase chemical reactions. MCM was initially developed to deliver precise, current, and thorough information on the function of certain organic chemicals at the ground level. Additionally, MCM provides a research tool for looking into many topics where a

thorough explanation of the chemistry is needed, such as creating distributions of speciated radicals and closed-shell intermediates produced during VOC degradation. This dataset includes thermal and photochemical reactions and accompanying temperature-dependent reaction rates for gas-phase atmospheric constituents. In the current work, we have chosen chemical reactions and kinematic reaction rates using MCM version 3.3.1, as described in Patnaik et al. (2023). While the CLIMCAPS dataset provides the number concentrations of O_3, CO, CH_4, N_2O, HNO_3, H_2O, and SO_2 for model initialization, the chemical reactions, as well as the rate of reactions for these atmospheric constituents, have been obtained from the MCM dataset.

5.2.3. ERA5 Reanalysis Dataset

ERA5 provides hourly estimates of different atmospheric, terrestrial, and oceanic climate variables. The atmosphere is divided into 137 levels from the surface to an altitude of 80 km based on the IFS Cy41r2 Integrated Forecasting System. At lower spatial and temporal resolutions, this dataset additionally offers details on the uncertainty of all variables. As described earlier, we have obtained vertical temperature profiles at 37 different pressure levels for the days of the simulation months in this work. These temperature profiles are the inputs to Monte Carlo simulations, which are then used to determine the thermal reaction rates of the chemical reactions taken from MCM.

5.3. Methodology

5.3.1 Monte Carlo simulations

In order to get deterministic results, Monte Carlo simulations employ randomization in their computing processes. These techniques are used to handle uncertainty indeterministic problem estimations by initializing a set of the most probable initial circumstances. Multiple probabilistic simulations are done to estimate the results, using these approaches with initialization provided by random seeds within the acceptable range. The simulation of atmospheric chemistry in general and chemical processes at the cloud level yields the vertical profiles of the number concentrations of the minor atmospheric constituents. Since the surrounding temperature influences reaction rates for chemical reactions, we have generated 1000 random samples by varying the temperature from the ERA5 dataset at 37 pressure levels using Maximum Likelihood Estimation (MLE). The uncertainty in the number concentrations of minor atmospheric elements can

be determined by altering the reaction rates (which rely on temperature) for suitable samples with an appropriate range. It will be helpful to establish probabilistic estimations of the highest likely temperature profiles in the atmosphere (Patnaik et al., 2023).

5.3.2 Gear's solution method

The chemical ordinary differential equations are solved using Gear's solver (Jacobson, 2005) to ascertain the concentration of CH_4, N_2O, and SO_2 molecules at each pressure level. This method uses the backward differentiation formula (5.1)

$$\frac{dN_{i,t}}{dt} = \frac{N_{i,t} - \alpha_{s,1}N_{i,t-h} - \alpha_{s,2}N_{i,t-2h} \ldots\ldots \alpha_{s,s}N_{i,t-sh}}{h\beta_s} = \frac{N_{i,t} - \sum_{j=1}^{s} \alpha_{s,j}N_{i,t-jh}}{h\beta_s} \ldots\ldots\ldots (5.1)$$

s is the order of approximation of the method, and α and β are scalar multipliers, j=1, 2,…,s. $N_{i,t}$ is the concentration for individual species i at a time 't' and $\widehat{N}_{i,t}$ is for the set of species. $N_{i,t-\mathrm{j}h}$ is the concentration of species i at a time (*t-jh*). We have to examine the local error following each iteration. Moreover, depending on the order of approximation, a global error test is carried out once the local error test has been satisfied to determine whether the cumulative normalized root-mean-square error (NRMS) obtained exceeds another parameterized number. If the global error check is unsuccessful, a subsequent time step, with a lower approximation order, is taken into account. If the global test is successful, the time step is also successful, and the final concentrations are set to the $N_{t,m+1}$ values at iteration m from the previous iteration. In the dynamical models, the disturbed weather conditions can be identified if Relative Vorticity at 850, 500, and 200 hPa is more than 10^{-3} s^{-1}. Hence, the above condition is implemented to differentiate the normal and disturbed weather conditions in this algorithm. In this work, the methodology described in Patnaik et al. (2023) has been further extended and improved by calculating the Maximum Likelihood Estimation (MLE) temperature profiles during disturbed weather conditions mentioned above. The bias correction in the number concentration of CH_4 and N_2O has been carried out using the CLIMCAPS dataset during disturbed weather events from 2012 to 2019, shown in Figure 5.1.

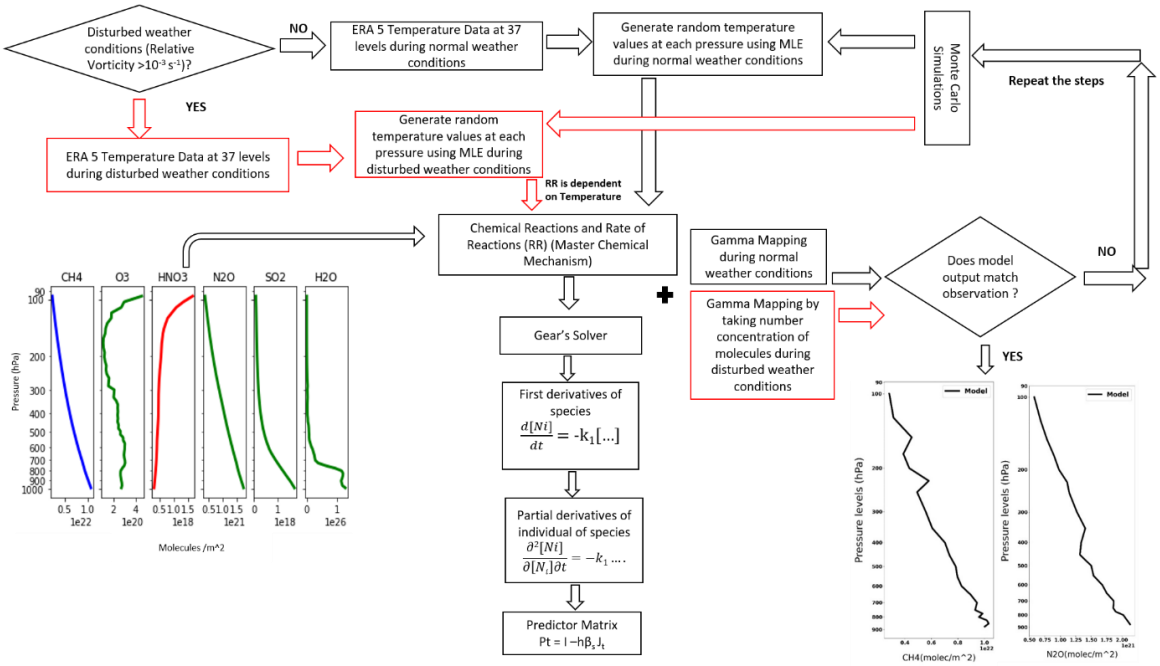

Figure 5.1. Graphical representation of the proposed methodology.

5.4. Results and Discussions

In Figure 5.2, the first row shows the number concentrations of CH_4 from the CLIMCAPS dataset (NCCD), estimated number concentrations (ENC), and percentage difference of number concentrations (PDNC) of CH_4 during the daytime for April 2020 over Delhi. The modified methodology has been implemented to reduce errors in number concentration during the passage of western disturbance over the Delhi region, i.e., on 22 April 2020 and 23 April 2020. It is seen that on and after 23 April 2020, there was a reduction in the error percentage during the daytime. The minimum PDNC using the new methodology is found to be -19.04 %, which was -24.18 % without these corrections (Patnaik et al., 2023).

The number concentrations from the CLIMCAPS dataset NCCD, ENC, and PDNC of CH_4 during April 2020 over Delhi at night time are shown in the second row of Figure 5.2. The night-time simulations showed a very small reduction in the error percentage on 22 April 2020. Using the methodology described in Patnaik et al. (2023), the PDNC was -60.8% and -56.78% at 850 and 825 hPa, respectively. After implementing the modified methodology, the PDNC has changed to -60.5 % and -56.04 % (Patnaik et al., 2023).

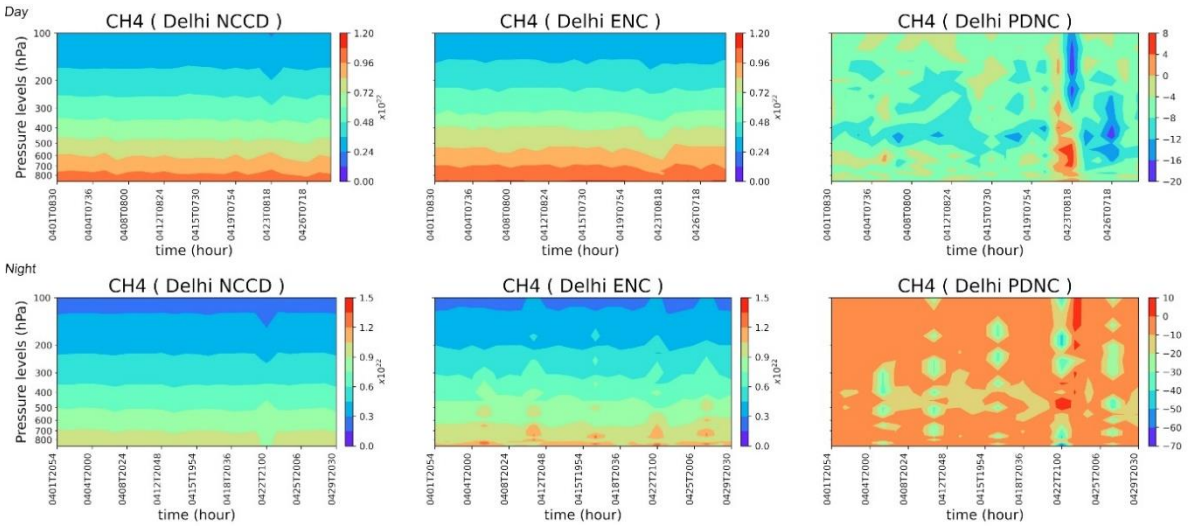

Figure 5.2. Vertical profile of NCCD, ENC, and PDNC of CH_4 over Delhi during April 2020.

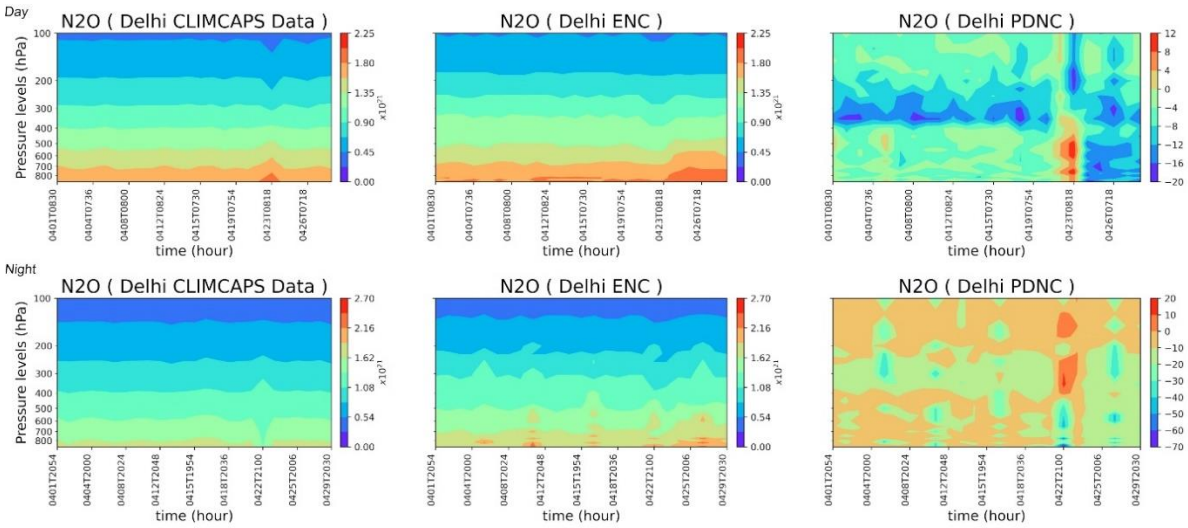

Figure 5.3. Vertical profile of NCCD, ENC, and PDNC of N_2O over Delhi during April 2020.

In Figure 5.3, the first row shows the NCCD, ENC, and PDNC of N_2O during April 2020 over Delhi during the day. Previously, in Patnaik et al. (2023), it was found that % on 23 April 2020, PDNC was -26.47 %, which is now reduced to -18.5 % after implementing the new methodology (Patnaik et al. 2023).

In Figure 5.3, the second row shows the NCCD (ENC) and PDNC of N_2O during April 2020 over Delhi at night. Earlier, the minimum PDNC was found to be between -63.8 %

and -65.43 % in Patnaik et al. (2023), which is now reduced to -62.4 % and -64.25 %, respectively.

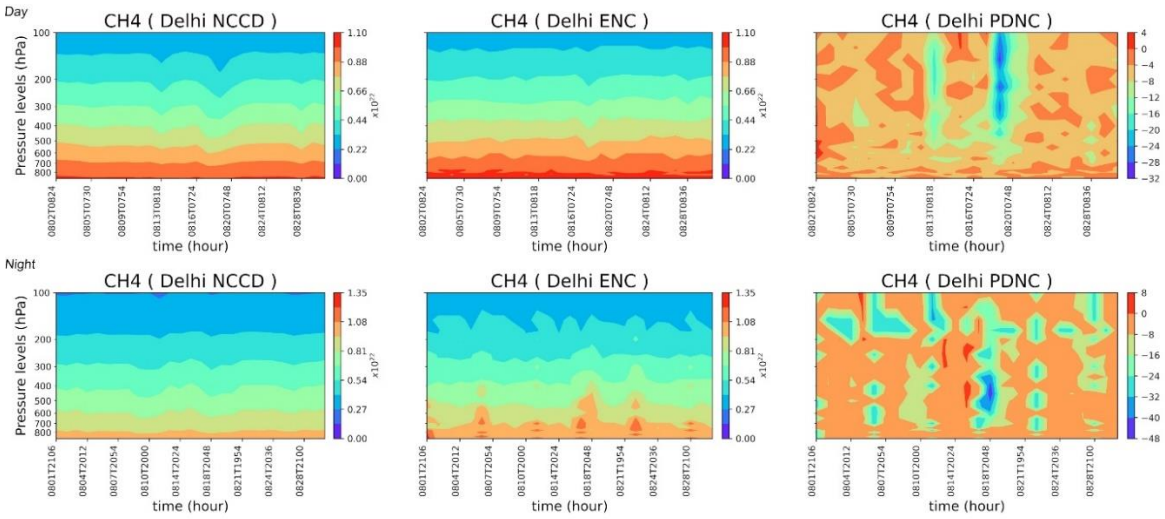

Figure 5.4. Vertical profile of NCCD, ENC, and PDNC of CH_4 over Delhi during August 2020.

The first row of Figure 5.4 shows the NCCD, ENC, and PDNC of CH_4 during August 2020 over Delhi during the day. While the minimum PDNC on 19 Aug 2020 was -29.82 % (Patnaik et al. 2023) earlier, the same is now reduced to -10.25 % (Patnaik et al. 2023).

The second row of Figure 5.4 shows the NCCD, ENC, and PDNC of CH_4 during the night of August 2020 over Delhi. PDNC at 450 hPa, on 18 Aug 2020, has been changed to -46.81 % from -16.12%.

The first row of Figure 5.5 shows the NCCD, ENC, and PDNC of N_2O during August 2020 over Delhi during the day. PDNC of N_2O was -110.96 % (Patnaik et al. 2023) on 13 Aug 2020, which is now reduced to -16.55 %. On 19 Aug 2020, PDNC between 500 hPa and 875 hPa was between -23.63 % and -57.94 %, which has now changed to -21.03% and -58.15 %. The second row, Figure 5.5, shows the NCCD, ENC, and PDNC of N_2O during August 2020 over Delhi at night. PDNC of N_2O was -94.01% (Patnaik et al. 2023) on 9 Aug 2020, which is now reduced to -16.98 %, while there is an overall reduction in PDNC at all pressure levels (Patnaik et al. 2023).

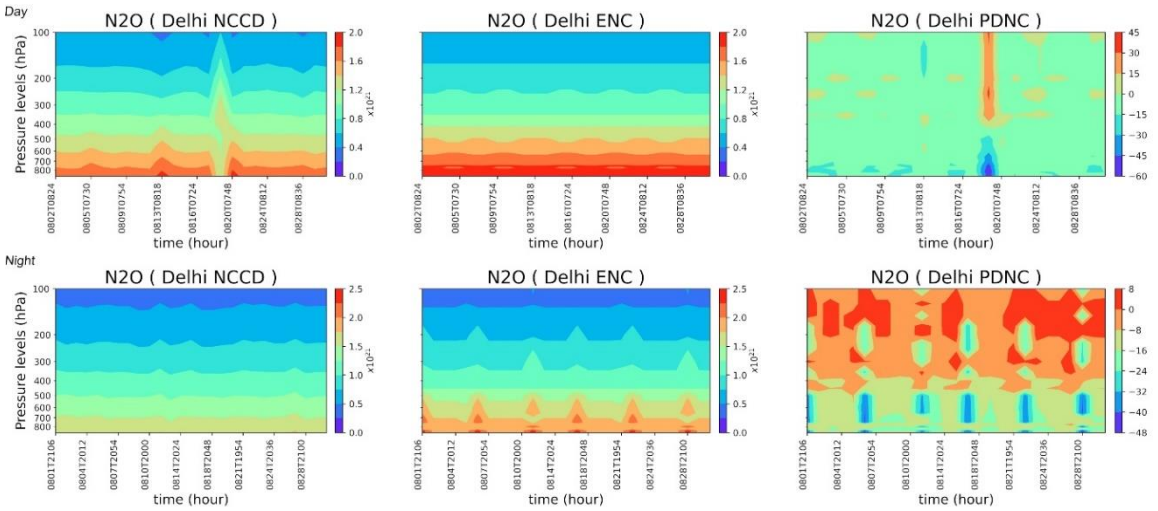

Figure 5.5. Vertical profile of NCCD, ENC, and PDNC of N_2O over Delhi during August 2020

In Figure 5.6, the first row shows the NCCD, ENC, and PDNC of N_2O during June 2020 over Kolkata during the day. N_2O had a maximum PDNC of 46.38 % (Patnaik et al. 2023) on 15 Jun 2020, which has now been reduced to 33.19%. In Figure 5.6, the second row shows the NCCD, ENC, and PDNC of N_2O during June 2020 over Kolkata at night. PDNC is reduced to -38.19 % from -44.39 %. There is a reduction in PDNC across all pressure levels (Patnaik et al., 2023).

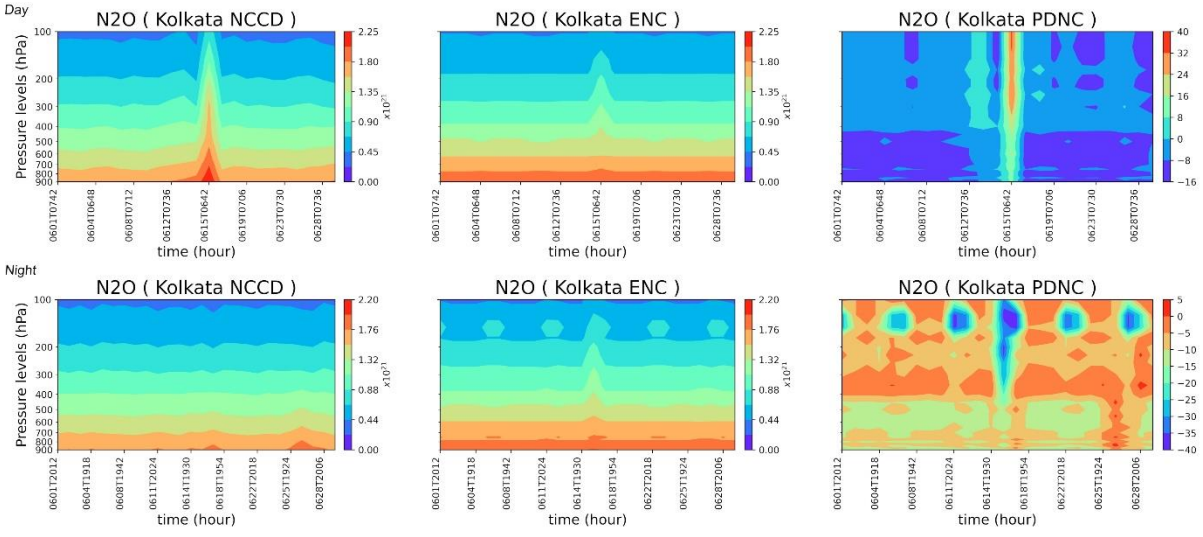

Figure 5.6. Vertical profile of NCCD, ENC, and PDNC of N_2O over Kolkata during June 2020.

In Figure 5.7, the first row shows the NCCD, ENC, and PDNC of CH_4 during November 2020 over Chennai during the daytime. On 16 Nov 2020, there was no significant difference in the PDNC of CH_4. However, on 24 and 25 Nov 2020, the PDNC changed from -17.48 % and -15.3% (Patnaik et al. 2023) to -17.25 % and -13.1 %, respectively between 300 hPa to 400 hPa (Patnaik et al. 2023).

Also, in Figure 5.7, the second row shows the NCCD, ENC PDNC of CH_4 during November 2020 over Chennai at night. While on 15 Nov 2020, the minimum PDNC during night-time was -47.35 % (Patnaik et al. 2023), which is now reduced to -28.18 %. On 24 Nov 2020 and 25 Nov 2020, the PDNC decreased from -44.1 % and -38.5 % to -15.12 % and -19.36 %, respectively, between 100 and 300 hPa (Patnaik et al., 2023).

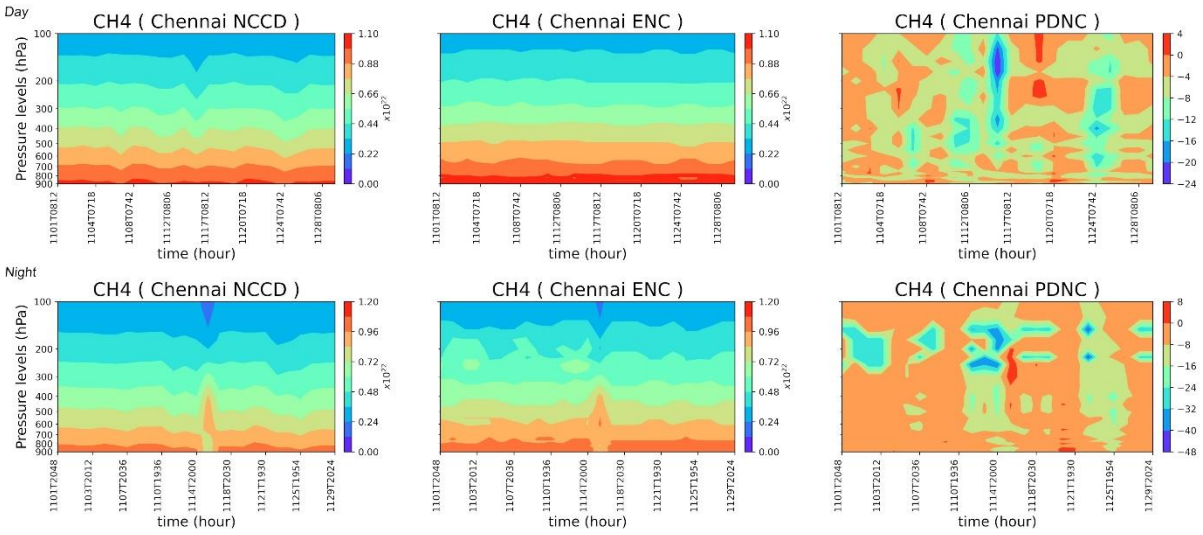

Figure 5.7. Vertical profile of NCCD, ENC, and PDNC of CH_4 over Chennai during November 2020.

In Figure 5.8, the first row shows the NCCD, ENC, and PDNC of N_2O during November 2020 over Chennai during the day. On 16 Nov 2020, N_2O had a minimum PDNC of -94.9 % (Patnaik et al. 2023), now reduced to -11.15 %. In Figure 5.8, the second row shows the NCCD, ENC, and PDNC of N_2O during November 2020 over Chennai at night. The PDNC on 15 Nov 2020 was -130.04 % (Patnaik et al. 2023), and is now reduced to -19.5% (Patnaik et al. 2023).

In Figure 5.9, the first row shows the NCCD, ENC, and PDNC of N_2O during July 2020 over Mumbai during the day. From 23 July 2020 to 30 July 2020, N_2O had a PDNC between -48.73 % to 20.12 % (Patnaik et al. 2023), which is now changed to -16.41 % to

-7.27 %. In Figure 5.9, the second row shows the NCCD), ENC, and PDNC of N_2O during July 2020 over Mumbai at night. The PDNC of N_2O was found between -56.4 % to -71.85 % from 26 to 27 July 2020 (100 hPa to 300 hPa), and on 23 July 2020, PDNC was -22.52 % to -63.31 % between 950 hPa to 550 hPa (Patnaik et al. 2023). Now, after the implementation of the modified methodology, PDNC has changed between -27.61 % and -28.65 % (100 hPa to 300 hPa) on 26 and 27 July 2020, while on 23 July 2020, PDNC has changed between -11.81 % and -53.94 % (Patnaik et al. 2023).

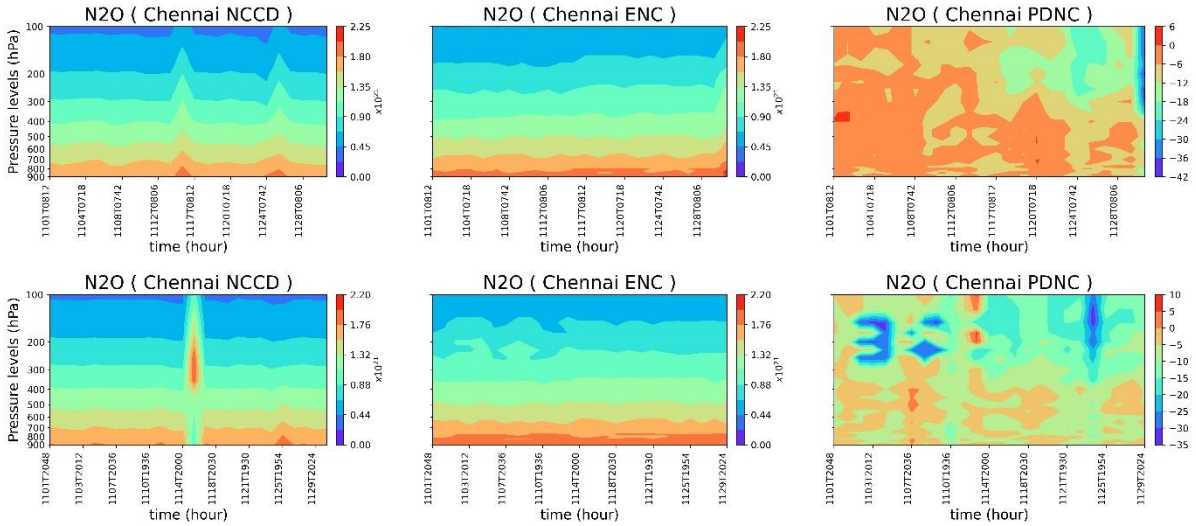

Figure 5.8. Vertical profile of NCCD, ENC, and PDNC of N_2O over Chennai during November 2020.

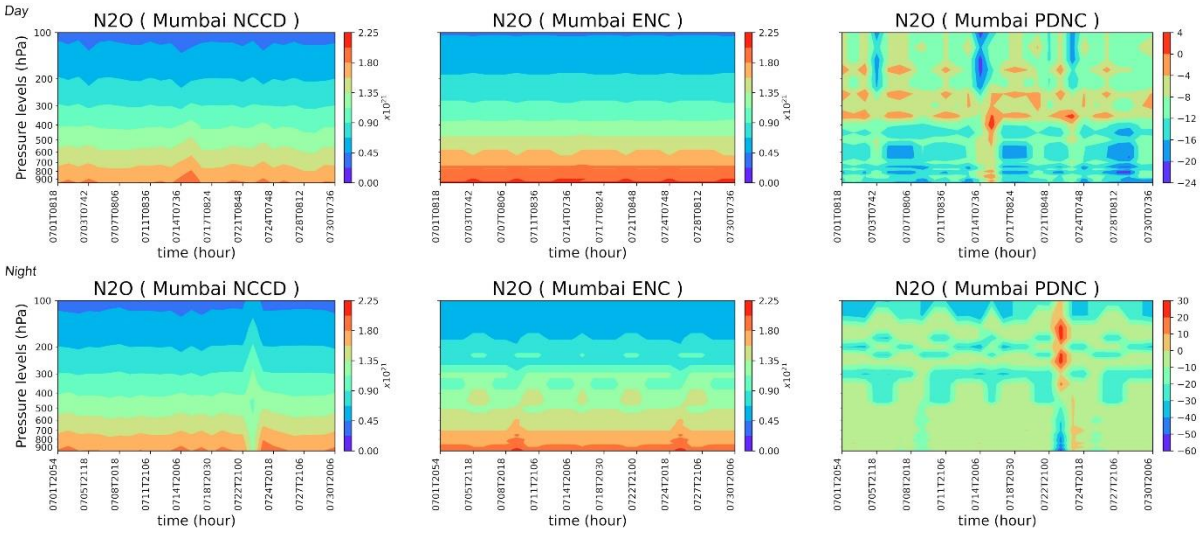

Figure 5.9. Vertical profile of NCCD, ENC, and PDNC of N_2O over Mumbai during July 2020.

Over India, monsoons' dynamics significantly impact CH_4 variability (Guha et al. 2018). High concentrations in the tropics and subtropics, with strong maxima in the middle and upper troposphere, are observed in atmospheric N_2O measurements covering altitudes from surface to 14 km and latitudes from 67° S to 85° N (Kort et al. 2011). The observed N_2O distribution as a function of latitudes, altitudes, and time has yet to be accurately captured in global simulations. The results show that the observed vertical and latitudinal distribution of N_2O depends on vital episodic inputs of nitrous oxide from the tropical regions. These findings highlight the strong tropical sources of N_2O, with high temporal variability and the need to utilize complete vertical profile observations to derive emissions from atmospheric measurements.

With the increasing intensity of tropical cyclones, the effective diameter of ice particles near the center increased gradually while the temperature decreased gradually (Q. Liu et al. 2020). Methane's shortwave absorption counteracts about 30% of the surface heating associated with its longwave radiation effects, and a larger effect occurs in precipitation, as shortwave absorption of methane offsets about 60% of the increase in rainfall as compared to the effect of longwave radiation. Shortwave cooling by methane is primarily due to rapid cloud adjustments, such as an increase in low-level clouds that increase the reflection of incoming shortwave radiation and a decrease in high-level clouds that rise outgoing longwave radiation. The cloud response is related to the solar heating profile in the atmosphere and the corresponding changes in temperature and relative humidity (Allen et al., 2023). In the Arabian Sea, tropical cyclones and southwest monsoons trigger the significant production of N2O in the atmosphere (Patra & Maksyutov, 2004). From the above studies, it is evident that it is imperative to analyze the vertical distribution of these molecules during severe weather conditions to understand their role in cloud microphysical processes. Using the modified methodology, it is evident that there is a reduction in PDNC of CH_4 and N_2O during disturbed weather events, such as western disturbances, heavy rainfall, and the formation of tropical cyclones (Patnaik et al. 2023).

5.5. Conclusions

In this chapter, we have modified the methodology described in Patnaik et al. (2023) by calculating Maximum Likelihood Estimation (MLE) during disturbed weather systems separately, using the temperature values from ERA5. The relative vorticity can

differentiate disturbed and normal weather conditions at 850, 500, and 200 hPa. If relative vorticity at these pressure levels is more than 10^{-3} s^{-1}, the algorithm can identify it as disturbed weather conditions. Furthermore, we also consider the number concentration of CH_4 and N_2O molecules individually for western disturbances, rainfall, and tropical cyclones, separately, for bias correction, for all four megacities. We have compared the CH_4 and N_2O number concentrations obtained from the 1-D model using the old methodology as well as a modified methodology over Delhi and Chennai and also calculated the percentage difference $\left(100 \times \left(\frac{Modified\ Methodology - Old\ Methodology}{Modified\ Methodology}\right)\right)$.

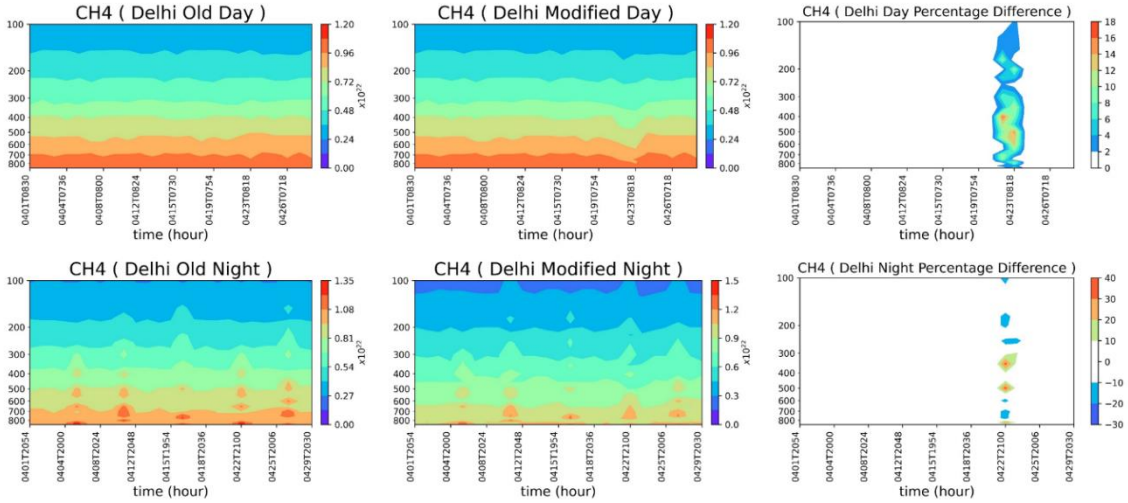

Figure 5.10. Comparison of CH_4 number concentration between the 1-D model outputs of old methodology and modified methodology over Delhi.

The first row of Figure 5.10 shows the ENC of CH_4 using both old and modified methodologies over Delhi during the daytime, whereas the second row shows the same during the night-time. Over Delhi, on normal days, the CH_4 percentage error of both methodologies during daytime (night-time) is less than 1.5% (-10 % and +10 %), whereas during western disturbances, percentage error varies between 1.5% and 17.5% (-24% and 38%). The first row of Figure 5.11 shows the ENC of N_2O using both old and modified methodologies over Delhi during the daytime, whereas the second row shows the ENC during the nighttime. Over Delhi, on normal days, the N_2O percentage error of both methodologies during daytime (night-time) is less than 3% (-10 % and +10 %), whereas during western disturbances, the percentage error varies between 5% and 23.5% (-19.5% and 47%) (Patnaik et al. 2023).

The first row of Figure 5.12 shows the ENC of CH_4 using both old and modified methodologies over Chennai during the daytime, whereas the second row shows the same during the night-time. Over Chennai, on normal days, the CH_4 percentage error of both methodologies during daytime (night-time) is between -1% and 1% (-4.5 % and +8 %), whereas during tropical cyclone days, the percentage error varies between -5.2% and 6% (-22% and 35%) (Patnaik et al. 2023).

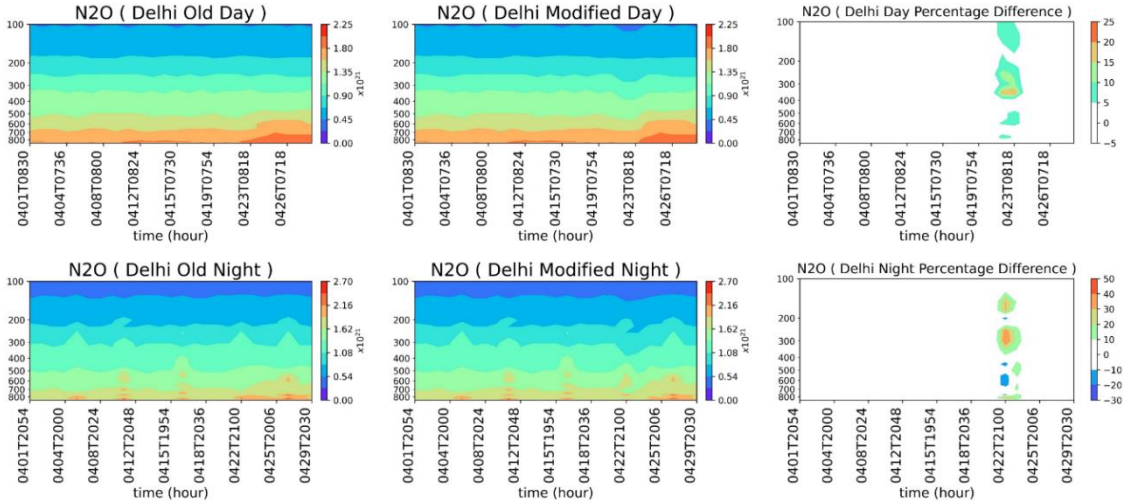

Figure 5.11. Comparison of N_2O number concentration between the 1-D model outputs of old methodology and modified methodology over Delhi.

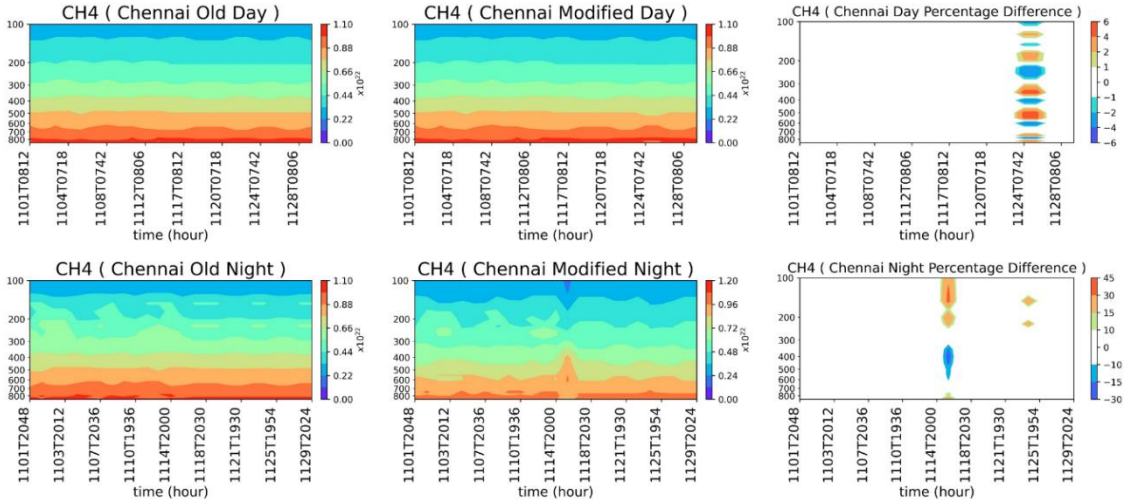

Figure 5.12. Comparison of CH_4 number concentration between the 1-D model outputs of old methodology and modified methodology over Chennai.

The first row of Figure 5.13 shows the ENC of N_2O using both old and modified methodologies over Chennai during the daytime, whereas the second row shows the same

during the night-time. Over Chennai, on normal days from 1 Nov 2023 till 28 Nov 2023, during the daytime between 400 hPa to 100 hPa pressure levels, the percentage error varies between 22% and 24%, whereas on tropical cyclone days, the percentage difference lies between 24% to 131%. During night-time, on normal days as well as tropical cyclone days, the percentage difference below 400 hPa pressure level is less than 20%, whereas, above 400 hPa, the percentage difference varies between 24.7 % to 36.4% (Patnaik et al. 2023).

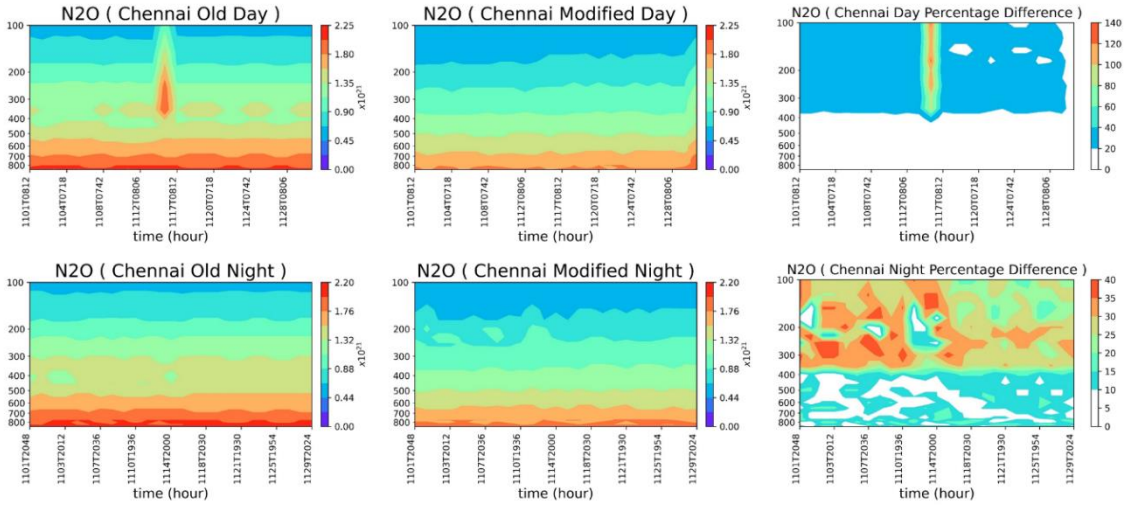

Figure 5.13. Comparison of N_2O number concentration between the 1-D model outputs of old methodology and modified methodology over Chennai.

It is seen from the results of this chapter that there is a reduction in percentage error during day and night time while implementing this methodology during disturbed weather conditions. Over Delhi, there was a reduction in PDNC of CH_4 and N_2O on 22 and 23 April 2020 (western disturbance). During the rainfall month of August 2020, a significant decrease of PDNC of CH_4 and N_2O is seen over Delhi at all pressure levels. Similarly, the error percentage was reduced over Kolkata during the rainy month of June 2020. Since a super cyclonic storm, "Nivar," was formed near the Chennai coast in November 2020, a considerable reduction in percentage error of N_2O was found on 24 and 25 Nov 2020. After implementing the modified methodology, a massive reduction in PDNC of N_2O is observed. Also, there is a significant decrease in CH_4 percentage error during the tropical cyclone. Also, due to the Northeast monsoon during November, there was a heavy rainfall event over Chennai on 15 Nov 2020. The percentage error of CH_4 and N_2O is reduced by implementing the latter methodology.

Similarly, during the passage of the Southwest monsoon in July 2020, the PDNC of N2O was reduced over Mumbai. Overall, there is significantly reduction in PDNC during rainy days, western disturbances, and tropical cyclonic storms after implementing this modified methodology. The advection of minor constituents and moisture have not been considered in the 1-D model and can be improved by incorporating this 1-D model in the Global Circulation Models (GCMs) (Patnaik et al., 2023).

Chapter 6

6. Summary and Future Scope

6.1. Summary

Several natural and anthropogenic activities are responsible for the generation of Methane (CH4), Sulphur dioxide (SO2), and nitrous oxide (N2O) in the atmosphere. Indian megacities such as Delhi, Kolkata, Mumbai, and Chennai are India's major commercial and cultural centers and are part of the Golden Quadrilateral. The Golden Quadrilateral, with 5846 km, is a national highway network connecting India's major industrial, agricultural, and cultural centers. They form a quadrilateral with all four major metro cities of India forming the vertices, namely, Delhi (north), Kolkata (east), Mumbai (west), and Chennai (south). Moreover, these megacities, which have a population of about 56 million, are responsible for high vehicular emissions, dust generation - particularly from construction sites, crop burning from nearby villages, depleting tree covers, and poor waste management. Since these minor constituents affect the radiation budget and air quality and pose health hazards, it is important to determine their number concentrations. For this purpose, a 1-D hybrid Monte-Carlo Gear's solver is developed and tested.

A one-dimensional model has been developed to retrieve the vertical profiles of the number of concentrations of minor constituents in the atmosphere. The CH4, N2O, and SO2 gas phase chemistry obtained from MCM has been used as input to this hybrid Monte Carlo-Gear's solver. Vertical profiles of temperature at different pressure levels are taken from ERA5 to calculate the rate of reactions. Further, MLE has been used to generate the 1000 temperature values at each pressure level for the Monte Carlo simulations. Also, the chemical ODE's Gear Solver is used in the hybrid model. CLIMCAPS satellite datasets are used to initialize (validate) the model around 0800 UTC (2000 UTC). Further, idealized experiments have been carried out over the four megacities during normal and disturbed weather situations and for both daytime and night-time. It is seen from the results that the 1-D hybrid solver performs better in retrieving the vertical profiles of CH4, N2O, and SO2 during normal days than in disturbed weather situations.

Further, the mean diurnal variation of number concentration during rainy and non-rainy days of CH4 and SO2 are calculated for these megacities and compared with the CAMS model. It is seen that up to 18 UTC, both models are in good agreement; however, after 18 UTC, the number concentration determined by the 1-D hybrid solver increases rapidly due to model blow-off.

Since the number concentrations predicted by the 1-D hybrid solver during disturbed weather situations does not agree with the CLIMCAPS, we have modified the methodology by separating the disturbed weather event days from the normal days. Relative vorticity fields at 850, 500, and 200 hPa can be used to distinguish between disturbed and normal weather situations. Relative vorticity values higher than 10-3 s^{-1} at these pressure levels can be identified as disturbed weather situations. Hence, we have generated separate MLE for disturbed weather events in this study. It is seen that after modifying the methodology, the number concentrations of these minor constituents are predicted reasonably well with good accuracy.

6.2. Future Scope

Kommula et al. (2021) have studied the effect of marine influx on the enhanced Secondary Organic Aerosol (SOA) fraction over Chennai. The results highlight that marine winds and weather conditions influence the chemical composition and ambient aerosol mass burden at the coastal site. In addition, the study stresses that local pollution can be decreased because of marine influx and may show distinctive chemical composition with an impact on aerosol properties. Prabhakar et al. (2014) have aimed to determine the sources of NO_3^- in stratocumulus clouds and the factors, which determine their influence on concentrations, using airborne chemical measurements, off the coast of California. Over the Indian region, such campaigns should be proposed to study the impact of minor constituents in cloud microphysics. Thompson and Eidhammer (2014) have modified bulk microphysical parameterization with explicit cloud droplet nucleation and ice activation by aerosols, as shown in equations 6.1, 6.2, and 6.3, which do not include the change in number concentration due to chemistry.

$$\frac{dN_c}{dt} = -(rain, snow, graupel\ collecting\ droplets) - (freezing\ into\ cloud\ ice) - (collide\ or\ coalesce\ into\ rain) - (evaporation) + (CCN\ activation) - (cloud\ ice\ melting) \quad \ldots\ldots\ldots (6.1)$$

$$\frac{dN_{wfa}}{dt} = -(rain, snow, graupel\ collecting\ aerosols) - (homogeneous\ nucleated\ deliquesced\ aerosols) - (collide\ or\ coalesce\ into\ rain) - (CCN\ activation) - (cloud\ and\ rain\ evaporation) + (surface\ emissions) \quad \ldots.(6.2)$$

$$\frac{dN_{ifa}}{dt} = -(rain, snow, graupel\ collecting\ aerosols) - (IN\ activation) - (cloud\ ice\ sublimation) + (surface\ emissions) \quad \ldots.(6.3)$$

where N_c is Cloud droplet number concentration and number of each aerosol species (N_{wfa} and N_{ifa}), where wfa is water friendly aerosol (hygroscopic), ifa is ice friendly aerosol (nonhygroscopic)

Hence, including the number concentration obtained from the 1-D hybrid solver can improve the cloud droplet number concentration forecast, as shown in equations 6.4, 6.5, and 6.6. $N_{chemistry}$ is number concentration due to chemistry.

$$\frac{dN_c}{dt} = -(rain, snow, graupel\ collecting\ droplets) - (freezing\ into\ cloud\ ice) - (collide\ or\ coalesce\ into\ rain) - (evaporation) + (CCN\ activation) - (cloud\ ice\ melting) + \frac{dN_{chemistry}}{dt} \quad \ldots\ldots\ldots(6.4)$$

$$\frac{dN_{wfa}}{dt} = -(rain, snow, graupel\ collecting\ aerosols) - (homogeneous\ nucleated\ deliquesced\ aerosols) - (collide\ or\ coalesce\ into\ rain) - (CCN\ activation) - (cloud\ and\ rain\ evaporation) + (surface\ emissions) + \frac{dN_{chemistry}}{dt} \ldots.(6.5)$$

$$\frac{dN_{ifa}}{dt} = -(rain, snow, graupel\ collecting\ aerosols) - (IN\ activation) - (cloud\ ice\ sublimation) + (surface\ emissions) + \frac{dN_{chemistry}}{dt} \ldots\ldots\ldots(6.6)$$

It is also important to include the chemistry of other minor constituents so that the rapid increase in number concentrations can be adressed. Further, It will be of great help to improve the prediction of the microphysical parameterization, especially during heavy rainfall situations. Further, there will be an improvement in the simulation of the number concentration of aerosols, contributing to the formation of IN and CCN and their direct and indirect impacts. It will further help to address the issues related to anthropogenic impacts on clouds and precipitation processes.

References

Alexander, B., Savarino, J., Kreutz, K. J., & Thiemens, M. H. (2004). Impact of preindustrial biomass-burning emissions on the oxidation pathways of tropospheric sulfur and nitrogen. *Journal of Geophysical Research: Atmospheres*, *109*(D8). https://doi.org/10.1029/2003JD004218

Allen, R. J., Zhao, X., Randles, C. A., Kramer, R. J., Samset, B. H., & Smith, C. J. (2023). Surface warming and wetting due to methane's long-wave radiative effects muted by short-wave absorption. *Nature Geoscience*, *16*(4), 314–320. https://doi.org/10.1038/s41561-023-01144-z

Atkinson, R., Baulch, D. L., Cox, R. A., Crowley, J. N., Hampson, R. F., Hynes, R. G., ... & Troe, J. (2004). Evaluated kinetic and photochemical data for atmospheric chemistry: Volume I-gas phase reactions of Ox, HOx, NOx and SOx species. Atmospheric chemistry and physics, 4(6), 1461-1738.Bange, H. W., Arévalo-Martínez, D. L., de la Paz, M., Farías, L., Kaiser, J., Kock, A., Law, C. S., Rees, A. P., Rehder, G., Tortell, P. D., Upstill-Goddard, R. C., & Wilson, S. T. (2019). A Harmonized Nitrous Oxide (N2O) Ocean Observation Network for the 21st Century. Frontiers in Marine Science, 6. https://doi.org/10.3389/fmars.2019.00157

Barret, B., Gouzenes, Y., Le Flochmoen, E., & Ferrant, S. (2021). Retrieval of Metop-A/IASI N2O Profiles and Validation with NDACC FTIR Data. *Atmosphere*, *12*(2), 219. https://doi.org/10.3390/atmos12020219

Barth, M. C., Kim, S.-W., Wang, C., Pickering, K. E., Ott, L. E., Stenchikov, G., Leriche, M., Cautenet, S., Pinty, J.-P., Barthe, C., Mari, C., Helsdon, J. H., Farley, R. D., Fridlind, A. M., Ackerman, A. S., Spiridonov, V., & Telenta, B. (2007). Cloud-scale model intercomparison of chemical constituent transport in deep convection. *Atmospheric Chemistry and Physics*, *7*(18), 4709–4731. https://doi.org/10.5194/acp-7-4709-2007

Bell, B., Hersbach, H., Simmons, A., Berrisford, P., Dahlgren, P., Horányi, A., Muñoz-

Sabater, J., Nicolas, J., Radu, R., Schepers, D., Soci, C., Villaume, S., Bidlot, J., Haimberger, L., Woollen, J., Buontempo, C., & Thépaut, J. (2021). The ERA5 global reanalysis: Preliminary extension to 1950. *Quarterly Journal of the Royal Meteorological Society*, *147*(741), 4186–4227. https://doi.org/10.1002/qj.4174

Bhate, J., & Kesarkar, A. (2019). Sensitivity of diurnal cycle of simulated rainfall to cumulus parameterization during Indian summer monsoon seasons. *Climate Dynamics*, *53*(5–6), 3431–3444. https://doi.org/10.1007/s00382-019-04716-1

Bhate, J., Kesarkar, A., & Rajasree, V. P. M. (2019). Simulation of the diurnal cycle of rainfall during Indian summer monsoon season using mesoscale model. *Theoretical and Applied Climatology*, *138*(1–2), 185–200. https://doi.org/10.1007/s00704-019-02777-0

BIrd. (n.d.). *Molecular Gas Dynamics and the Direct Simulation of Gas Flows* (1976th ed.). Retrieved November 27, 2020, from https://global.oup.com/academic/product/molecular-gas-dynamics-and-the-direct-simulation-of-gas-flows-9780198561958?cc=in&lang=en&

Byun, D., & Schere, K. L. (2006). Review of the Governing Equations, Computational Algorithms, and Other Components of the Models-3 Community Multiscale Air Quality (CMAQ) Modeling System. *Applied Mechanics Reviews*, *59*(2), 51–77. https://doi.org/10.1115/1.2128636

Caffrey, P. F., Hoppel, W. A., & Shi, J. J. (2006). A one-dimensional sectional aerosol model integrated with mesoscale meteorological data to study marine boundary layer aerosol dynamics. *Journal of Geophysical Research*, *111*(D24), D24201. https://doi.org/10.1029/2006JD007237

Cariolle, D., Moinat, P., Teyssèdre, H., Giraud, L., Josse, B., & Lefèvre, F. (2017). ASIS v1.0: an adaptive solver for the simulation of atmospheric chemistry. *Geoscientific Model Development*, *10*(4), 1467–1485. https://doi.org/10.5194/gmd-10-1467-2017

Chandra, N., Hayashida, S., Saeki, T., & Patra, P. K. (2017). What controls the seasonal

cycle of columnar methane observed by GOSAT over different regions in India? *Atmospheric Chemistry and Physics*, *17*(20), 12633–12643. https://doi.org/10.5194/acp-17-12633-2017

Chin, M., Rood, R. B., Lin, S.-J., Müller, J.-F., & Thompson, A. M. (2000). Atmospheric sulfur cycle simulated in the global model GOCART: Model description and global properties. *Journal of Geophysical Research: Atmospheres*, *105*(D20), 24671–24687. https://doi.org/10.1029/2000JD900384

Chutia, L., Ojha, N., Girach, I., Pathak, B., Sahu, L. K., Sarangi, C., Flemming, J., da Silva, A., & Bhuyan, P. K. (2022). Trends in sulfur dioxide over the Indian subcontinent during 2003–2019. *Atmospheric Environment*, *284*, 119189. https://doi.org/10.1016/j.atmosenv.2022.119189

DeMott, P. J., Sassen, K., Poellot, M. R., Baumgardner, D., Rogers, D. C., Brooks, S. D., Prenni, A. J., & Kreidenweis, S. M. (2003). African dust aerosols as atmospheric ice nuclei. *Geophysical Research Letters*, *30*(14). https://doi.org/10.1029/2003GL017410

Efendiev, Y., & Zachariah, M. R. (2002). Hybrid Monte Carlo Method for Simulation of Two-Component Aerosol Coagulation and Phase Segregation. *Journal of Colloid and Interface Science*, *249*(1), 30–43. https://doi.org/10.1006/jcis.2001.8114

Ervens, B., Turpin, B. J., & Weber, R. J. (2011). Secondary organic aerosol formation in cloud droplets and aqueous particles (aqSOA): a review of laboratory, field and model studies. *Atmospheric Chemistry and Physics*, *11*(21), 11069–11102. https://doi.org/10.5194/acp-11-11069-2011

Fitzgerald, J. W., Hoppel, W. A., & Gelbard, F. (1998). A one-dimensional sectional model to simulate multicomponent aerosol dynamics in the marine boundary layer: 1. Model description. *Journal of Geophysical Research: Atmospheres*, *103*(D13), 16085–16102. https://doi.org/10.1029/98JD01019

Gaur, A., Tripathi, S. N., Kanawade, V. P., Tare, V., & Shukla, S. P. (2014). Four-year measurements of trace gases (SO2, NOx, CO, and O3) at an urban location, Kanpur, in Northern India. *Journal of Atmospheric Chemistry*, *71*(4), 283–301. https://doi.org/10.1007/s10874-014-9295-8

Gear, C. W. (1971). The automatic integration of ordinary differential equations. *Communications of the ACM*, *14*(3), 176–179. https://doi.org/10.1145/362566.362571

Gelbard, F., Fitzgerald, J. W., & Hoppel, W. A. (1998). A one-dimensional sectional model to simulate multicomponent aerosol dynamics in the marine boundary layer: 3. Numerical methods and comparisons with exact solutions. *Journal of Geophysical Research: Atmospheres*, *103*(D13), 16119–16132. https://doi.org/10.1029/98JD01017

Guha, T., Tiwari, Y. K., Valsala, V., Lin, X., Ramonet, M., Mahajan, A., Datye, A., & Kumar, K. R. (2018). What controls the atmospheric methane seasonal variability over India? *Atmospheric Environment*, *175*, 83–91. https://doi.org/10.1016/j.atmosenv.2017.11.042

Hakami, A., Henze, D. K., Seinfeld, J. H., Singh, K., Sandu, A., Kim, S., Byun, & Li, Q. (2007). The Adjoint of CMAQ. *Environmental Science & Technology*, *41*(22), 7807–7817. https://doi.org/10.1021/es070944p

Hersbach, H., Bell, B., Berrisford, P., Hirahara, S., Horányi, A., Muñoz-Sabater, J., Nicolas, J., Peubey, C., Radu, R., Schepers, D., Simmons, A., Soci, C., Abdalla, S., Abellan, X., Balsamo, G., Bechtold, P., Biavati, G., Bidlot, J., Bonavita, M., … Thépaut, J. (2020). The ERA5 global reanalysis. *Quarterly Journal of the Royal Meteorological Society*, *146*(730), 1999–2049. https://doi.org/10.1002/qj.3803

Hertel, O. (1994). Modelling of the end products of the chemical decomposition of DMS in the marine boundary layer. *Atmospheric Environment*, *28*(15), 2431–2449. https://doi.org/10.1016/1352-2310(94)90395-6

Hertel, O., Berkowicz, R., Christensen, J., & Hov, Ø. (1993). Test of two numerical schemes for use in atmospheric transport-chemistry models. *Atmospheric Environment. Part A. General Topics*, *27*(16), 2591–2611. https://doi.org/10.1016/0960-1686(93)90032-T

Hong, Q., Liu, C., Hu, Q., Xing, C., Tan, W., Liu, T., & Liu, J. (2021). Vertical distributions of tropospheric SO2 based on MAX-DOAS observations: Investigating the impacts of regional transport at different heights in the boundary layer. *Journal*

of Environmental Sciences, *103*, 119–134. https://doi.org/10.1016/j.jes.2020.09.036

Hov, Ø. (1983). One-dimensional vertical model for ozone and other gases in the atmospheric boundary layer. *Atmospheric Environment (1967)*, *17*(3), 535–549. https://doi.org/10.1016/0004-6981(83)90127-0

Huijnen, V., Pozzer, A., Arteta, J., Brasseur, G., Bouarar, I., Chabrillat, S., Christophe, Y., Doumbia, T., Flemming, J., Guth, J., Josse, B., Karydis, V. A., Marécal, V., & Pelletier, S. (2019). Quantifying uncertainties due to chemistry modelling – evaluation of tropospheric composition simulations in the CAMS model (cycle 43R1). *Geoscientific Model Development*, *12*(4), 1725–1752. https://doi.org/10.5194/gmd-12-1725-2019

Ishizaka, Y., & Adhikari, M. (2003). Composition of cloud condensation nuclei. *Journal of Geophysical Research: Atmospheres*, *108*(D4). https://doi.org/10.1029/2002JD002085

Jacobson, M. Z. (2005). *Fundamentals of Atmospheric Modeling*. Cambridge University Press. https://doi.org/10.1017/CBO9781139165389

Jaruga, A., & Pawlowska, H. (2018). libcloudph++ 2.0: aqueous-phase chemistry extension of the particle-based cloud microphysics scheme. *Geoscientific Model Development*, *11*(9), 3623–3645. https://doi.org/10.5194/gmd-11-3623-2018

Jha, C. S., Rodda, S. R., Thumaty, K. C., Raha, A. K., & Dadhwal, V. K. (2014). Eddy covariance based methane flux in Sundarbans mangroves, India. *Journal of Earth System Science*, *123*(5), 1089–1096. https://doi.org/10.1007/s12040-014-0451-y

Jonson, J. E., & Isaksen, I. S. A. (1992). Parameterization of episodical cloud and rainout events in large-scale atmospheric chemistry models. *Atmospheric Environment. Part A. General Topics*, *26*(11), 2019–2029. https://doi.org/10.1016/0960-1686(92)90086-Z

K. PATRA, P., TAKIGAWA, M., ISHIJIMA, K., CHOI, B.-C., CUNNOLD, D., J. DLUGOKENCKY, E., FRASER, P., J. GOMEZ-PELAEZ, A., GOO, T.-Y., KIM, J.-S., KRUMMEL, P., LANGENFELDS, R., MEINHARDT, F., MUKAI, H., O'DOHERTY, S., G. PRINN, R., SIMMONDS, P., STEELE, P., TOHJIMA, Y., … NAKAZAWA, T. (2009). Growth Rate, Seasonal, Synoptic, Diurnal Variations and

Budget of Methane in the Lower Atmosphere. *Journal of the Meteorological Society of Japan. Ser. II*, *87*(4), 635–663. https://doi.org/10.2151/jmsj.87.635

Karppinen, T., Lamminpää, O., Tukiainen, S., Kivi, R., Heikkinen, P., Hatakka, J., Laine, M., Chen, H., Lindqvist, H., & Tamminen, J. (2020). Vertical Distribution of Arctic Methane in 2009–2018 Using Ground-Based Remote Sensing. *Remote Sensing*, *12*(6), 917. https://doi.org/10.3390/rs12060917

Kavitha, M., Nair, P. R., Girach, I. A., Aneesh, S., Sijikumar, S., & Renju, R. (2018). Diurnal and seasonal variations in surface methane at a tropical coastal station: Role of mesoscale meteorology. *Science of The Total Environment*, *631–632*, 1472–1485. https://doi.org/10.1016/j.scitotenv.2018.03.123

Kelp, M. M., Jacob, D. J., Lin, H., & Sulprizio, M. P. (2022). An Online-Learned Neural Network Chemical Solver for Stable Long-Term Global Simulations of Atmospheric Chemistry. *Journal of Advances in Modeling Earth Systems*, *14*(6). https://doi.org/10.1029/2021MS002926

Keppler, F., Hamilton, J. T. G., Braß, M., & Röckmann, T. (2006). Methane emissions from terrestrial plants under aerobic conditions. *Nature*, *439*(7073), 187–191. https://doi.org/10.1038/nature04420

Kirschke, S., Bousquet, P., Ciais, P., Saunois, M., Canadell, J. G., Dlugokencky, E. J., Bergamaschi, P., Bergmann, D., Blake, D. R., Bruhwiler, L., Cameron-Smith, P., Castaldi, S., Chevallier, F., Feng, L., Fraser, A., Heimann, M., Hodson, E. L., Houweling, S., Josse, B., … Zeng, G. (2013). Three decades of global methane sources and sinks. *Nature Geoscience*, *6*(10), 813–823. https://doi.org/10.1038/ngeo1955

Koehler, K. A., Kreidenweis, S. M., DeMott, P. J., Petters, M. D., Prenni, A. J., & Carrico, C. M. (2009). Hygroscopicity and cloud droplet activation of mineral dust aerosol. *Geophysical Research Letters*, *36*(8), L08805. https://doi.org/10.1029/2009GL037348

Kommula, S. M., Upasana, P., Sharma, A., Raj, S. S., Reyes-villegas, E., Liu, T., Allan, J. D., Jose, C., Pöhlker, M. L., Ravikrishna, R., Liu, P., Su, H., Martin, S. T., Pöschl, U., Mcfiggans, G., Coe, H., & Gunthe, S. S. (2021). Chemical Characterization and

Source Apportionment of Organic Aerosols in the Coastal City of Chennai, India: Impact of Marine Air Masses on Aerosol Chemical Composition and Potential for Secondary Organic Aerosol Formation. *ACS Earth and Space Chemistry*, *5*(11), 3197–3209. https://doi.org/10.1021/acsearthspacechem.1c00276

Kort, E. A., Patra, P. K., Ishijima, K., Daube, B. C., Jiménez, R., Elkins, J., Hurst, D., Moore, F. L., Sweeney, C., & Wofsy, S. C. (2011). Tropospheric distribution and variability of N_2O: Evidence for strong tropical emissions. *Geophysical Research Letters*, *38*(15). https://doi.org/10.1029/2011GL047612

Kroese, D. P., Brereton, T., Taimre, T., & Botev, Z. I. (2014). Why the Monte Carlo method is so important today. *WIREs Computational Statistics*, *6*(6), 386–392. https://doi.org/10.1002/wics.1314

Kruza, M., Shaw, D., Shaw, J., & Carslaw, N. (2021). Towards improved models for indoor air chemistry: A Monte Carlo simulation study. *Atmospheric Environment*, *262*, 118625. https://doi.org/10.1016/j.atmosenv.2021.118625

La, I., Yum, S. S., Yeom, J. M., & Shaw, R. A. (2022). Influence of Entrainment on Centimeter-Scale Cloud Microphysics in Marine Stratocumulus Clouds Observed during CSET. *Journal of the Atmospheric Sciences*, *79*(11), 2935–2948. https://doi.org/10.1175/JAS-D-22-0005.1

Levy, H. (1971). Normal Atmosphere: Large Radical and Formaldehyde Concentrations Predicted. *Science*, *173*(3992), 141–143. https://doi.org/10.1126/science.173.3992.141

Liao, H. (2004). Global radiative forcing of coupled tropospheric ozone and aerosols in a unified general circulation model. *Journal of Geophysical Research*, *109*(D16), D16207. https://doi.org/10.1029/2003JD004456

Lin, X., Indira, N. K., Ramonet, M., Delmotte, M., Ciais, P., Bhatt, B. C., Reddy, M. V., Angchuk, D., Balakrishnan, S., Jorphail, S., Dorjai, T., Mahey, T. T., Patnaik, S., Begum, M., Brenninkmeijer, C., Durairaj, S., Kirubagaran, R., Schmidt, M., Swathi, P. S., … Gaur, V. K. (2015). Long-lived atmospheric trace gases measurements in liCyclone Temperature Profiles and Cloud Macro-/Micro-Physical Properties Based on AIRS Data. *Atmosphere*, *11*(11), 1181. https://doi.org/10.3390/atmos11111181

Liu, T., Chan, A. W. H., & Abbatt, J. P. D. (2021). Multiphase Oxidation of Sulfur Dioxide in Aerosol Particles: Implications for Sulfate Formation in Polluted Environments. *Environmental Science & Technology*, *55*(8), 4227–4242. https://doi.org/10.1021/acs.est.0c06496

Locatelli, R., Bousquet, P., Saunois, M., Chevallier, F., & Cressot, C. (2015). Sensitivity of the recent methane budget to LMDz sub-grid-scale physical parameterizations. *Atmospheric Chemistry and Physics*, *15*(17), 9765–9780. https://doi.org/10.5194/acp-15-9765-2015

Lu, R., Turco, R. P., & Jacobson, M. Z. (1997). An integrated air pollution modeling system for urban and regional scales: 2. Simulations for SCAQS 1987. *Journal of Geophysical Research: Atmospheres*, *102*(D5), 6081–6098. https://doi.org/10.1029/96JD03502

Mallik, C., Ghosh, D., Ghosh, D., Sarkar, U., Lal, S., & Venkataramani, S. (2014). Variability of SO2, CO, and light hydrocarbons over a megacity in Eastern India: effects of emissions and transport. *Environmental Science and Pollution Research*, *21*(14), 8692–8706. https://doi.org/10.1007/s11356-014-2795-x

Martin, R. V. (2002). An improved retrieval of tropospheric nitrogen dioxide from GOME. *Journal of Geophysical Research*, *107*(D20), 4437. https://doi.org/10.1029/2001JD001027

McMeeking, G. R., Good, N., Petters, M. D., McFiggans, G., & Coe, H. (2011). Influences on the fraction of hydrophobic and hydrophilic black carbon in the atmosphere. *Atmospheric Chemistry and Physics*, *11*(10), 5099–5112. https://doi.org/10.5194/acp-11-5099-2011

McNorton, J., Gloor, E., Wilson, C., Hayman, G. D., Gedney, N., Comyn-Platt, E., Marthews, T., Parker, R. J., Boesch, H., & Chipperfield, M. P. (2016). Role of regional wetland emissions in atmospheric methane variability. *Geophysical Research Letters*, *43*(21). https://doi.org/10.1002/2016GL070649

Metya, A., Datye, A., Chakraborty, S., Tiwari, Y. K., Sarma, D., Bora, A., & Gogoi, N. (2021). Diurnal and seasonal variability of CO2 and CH4 concentration in a semi-

urban environment of western India. *Scientific Reports*, *11*(1), 2931. https://doi.org/10.1038/s41598-021-82321-1

Ming, Y., & Russell, L. M. (2001). Predicted hygroscopic growth of sea salt aerosol. *Journal of Geophysical Research: Atmospheres*, *106*(D22), 28259–28274. https://doi.org/10.1029/2001JD000454

Mitchell, P., & Frenklach, M. (2003). Particle aggregation with simultaneous surface growth. *Physical Review E*, *67*(6), 061407. https://doi.org/10.1103/PhysRevE.67.061407

Mochida, M., Nishita-Hara, C., Furutani, H., Miyazaki, Y., Jung, J., Kawamura, K., & Uematsu, M. (2011). Hygroscopicity and cloud condensation nucleus activity of marine aerosol particles over the western North Pacific. *Journal of Geophysical Research*, *116*(D6), D06204. https://doi.org/10.1029/2010JD014759

Modala, N. R. (2017). *Assessing the impacts of climate change on cotton production in the Texas High Plains and Rolling Plains*. https://www.researchgate.net/publication/292992461

Moumen, A., Azizi, G., Chekroun, K. Ben, & Baghour, M. (2016). The effects of livestock methane emission on the global warming: a review. *International Journal of Global Warming*, *9*(2), 229. https://doi.org/10.1504/IJGW.2016.074956

Ojha, N., Sharma, A., Kumar, M., Girach, I., Ansari, T. U., Sharma, S. K., Singh, N., Pozzer, A., & Gunthe, S. S. (2020). On the widespread enhancement in fine particulate matter across the Indo-Gangetic Plain towards winter. *Scientific Reports*, *10*(1), 5862. https://doi.org/10.1038/s41598-020-62710-8

Patnaik, K., Kesarkar, A. P., Rath, S., Bhate, J. N., Panchal, A., Chandrasekar, A., & Giri, R. (2023). A 1-D model to retrieve the vertical profiles of minor atmospheric constituents for cloud microphysical modeling: I. Formulation and validation. *Science of The Total Environment*, *881*, 163360. https://doi.org/10.1016/j.scitotenv.2023.163360.

Patnaik, K., Kesarkar, A. P., Rath, S., Bhate, J. N., & Chandrasekar, A. (2023). A 1-D model to retrieve the vertical profiles of minor atmospheric constituents for cloud microphysical modeling: II. Simulation of diurnal cycle. *Science of The Total*

Environment, 905, 167377. https://doi.org/10.1016/j.scitotenv.2023.167377.

Patnaik, K., Kesarkar, A. P., Rath, S., Bhate, J. N., & Chandrasekar, A. (2024). A 1-D model to retrieve the vertical profiles of minor atmospheric constituents for cloud microphysical modelling: III. Disturbed weather situations. *Science of The Total Environment, 907, 167959.* https://doi.org/10.1016/j.scitotenv.2023.167959.

Patra, P. K., & Maksyutov, S. (2004). Severe weather conditions in the Arabian Sea and their impact on atmospheric N2O budget NASA Land-Cover and Land-Use Change-Regional and Global Climate and Societal Impacts of Land-Use and Land-Cover Change in Northern Eurasia: A Synthesis Study Using Remote Sensing Data and An Integrated Global System Model View project Atmospheric O2/N2 observation View project. In *Article in Indian Journal of Geo-Marine Sciences*. https://www.researchgate.net/publication/242072099

Peel, M. C., Finlayson, B. L., & McMahon, T. A. (2007). Updated world map of the Köppen-Geiger climate classification. *Hydrology and Earth System Sciences*, *11*(5), 1633–1644. https://doi.org/10.5194/hess-11-1633-2007

Prabhakar, G., Ervens, B., Wang, Z., Maudlin, L. C., Coggon, M. M., Jonsson, H. H., Seinfeld, J. H., & Sorooshian, A. (2014). Sources of nitrate in stratocumulus cloud water: Airborne measurements during the 2011 E-PEACE and 2013 NiCE studies. *Atmospheric Environment*, *97*, 166–173. https://doi.org/10.1016/j.atmosenv.2014.08.019

Prather, M. J., & Hsu, J. (2010). Coupling of Nitrous Oxide and Methane by Global Atmospheric Chemistry. *Science*, *330*(6006), 952–954. https://doi.org/10.1126/science.1196285

Quebbeman, A. W., Menge, D. N. L., Arellano, G., Hall, J., Wood, T. E., Zimmerman, J. K., & Uriarte, M. (2022). A Severe Hurricane Increases Carbon Dioxide and Methane Fluxes and Triples Nitrous Oxide Emissions in a Tropical Forest. *Ecosystems*, *25*(8), 1754–1766. https://doi.org/10.1007/s10021-022-00794-1

Ramachandran, A., & Anushiya, J. (2015). Long-term rainfall trends of Indian urban station and its variation in different phases and seasons. *International Journal of Global Warming*, *7*(3), 307. https://doi.org/10.1504/IJGW.2015.069364

Ramachandran, S., & Rupakheti, M. (2022). Trends in physical, optical and chemical columnar aerosol characteristics and radiative effects over South and East Asia: Satellite and ground-based observations. *Gondwana Research*, *105*, 366–387. https://doi.org/10.1016/j.gr.2021.09.016

Rastogi, N., Satish, R., Singh, A., Kumar, V., Thamban, N., Lalchandani, V., Shukla, A., Vats, P., Tripathi, S. N., Ganguly, D., Slowik, J., & Prevot, A. S. H. (2021). Diurnal variability in the spectral characteristics and sources of water-soluble brown carbon aerosols over Delhi. *Science of The Total Environment*, *794*, 148589. https://doi.org/10.1016/j.scitotenv.2021.148589

Raychaudhuri, S. (2008). Introduction to Monte Carlo simulation. *2008 Winter Simulation Conference*, 91–100. https://doi.org/10.1109/WSC.2008.4736059

Renuka, K., Gadhavi, H., Jayaraman, A., Rao, S. V. B., & Lal, S. (2020). Study of mixing ratios of SO2 in a tropical rural environment in south India. *Journal of Earth System Science*, *129*(1), 104. https://doi.org/10.1007/s12040-020-1366-4

Sander, R., Baumgaertner, A., Gromov, S., Harder, H., Jöckel, P., Kerkweg, A., Kubistin, D., Regelin, E., Riede, H., Sandu, A., Taraborrelli, D., Tost, H., & Xie, Z.-Q. (2011). The atmospheric chemistry box model CAABA/MECCA-3.0. *Geoscientific Model Development*, *4*(2), 373–380. https://doi.org/10.5194/gmd-4-373-2011

Santillana, M., Le Sager, P., Jacob, D. J., & Brenner, M. P. (2010). An adaptive reduction algorithm for efficient chemical calculations in global atmospheric chemistry models. *Atmospheric Environment*, *44*(35), 4426–4431. https://doi.org/10.1016/j.atmosenv.2010.07.044

Singh, V., Singh, S., & Biswal, A. (2021). Exceedances and trends of particulate matter (PM2.5) in five Indian megacities. *Science of The Total Environment*, *750*, 141461. https://doi.org/10.1016/j.scitotenv.2020.141461

Smith, M., & Matsoukas, T. (1998). Constant-number Monte Carlo simulation of population balances. In *Chemical Engineering Science* (Vol. 53, Issue 9).

Smith, N., & Barnet, C. D. (2020). CLIMCAPS observing capability for temperature, moisture, and trace gases from AIRS/AMSU and CrIS/ATMS. *Atmospheric Measurement Techniques*, *13*(8), 4437–4459. https://doi.org/10.5194/amt-13-4437-

2020

Sun, J., & Ariya, P. A. (2006). Atmospheric organic and bio-aerosols as cloud condensation nuclei (CCN): A review. In *Atmospheric Environment* (Vol. 40, Issue 5). https://doi.org/10.1016/j.atmosenv.2005.05.052

Sun, Z., Axelbaum, R. L., & Huertas, J. I. (2004). Monte Carlo simulation of multicomponent aerosols undergoing simultaneous coagulation and condensation. *Aerosol Science and Technology*, *38*(10), 963–971. https://doi.org/10.1080/027868290513847

Suneja, J., Kotnala, G., Kaur, A., Mandal, T. K., & Sharma, S. K. (2020). Long-Term Measurements of SO2 Over Delhi, India. *MAPAN*, *35*(1), 125–133. https://doi.org/10.1007/s12647-019-00349-1

THOM, H. C. S. (1958). A NOTE ON THE GAMMA DISTRIBUTION. *Monthly Weather Review*, *86*(4), 117–122. https://doi.org/10.1175/1520-0493(1958)086<0117:ANOTGD>2.0.CO;2

Thompson, G., & Eidhammer, T. (2014). A Study of Aerosol Impacts on Clouds and Precipitation Development in a Large Winter Cyclone. Journal of the Atmospheric Sciences, 71(10), 3636–3658. https://doi.org/10.1175/JAS-D-13-0305.1

Tiwari, Y. K., Guha, T., Valsala, V., Lopez, A. S., Cuevas, C., Fernandez, R. P., & Mahajan, A. S. (2020). Understanding atmospheric methane sub-seasonal variability over India. *Atmospheric Environment*, *223*, 117206. https://doi.org/10.1016/j.atmosenv.2019.117206

Trenberth, K. E., Dai, A., Rasmussen, R. M., & Parsons, D. B. (2003). The Changing Character of Precipitation. *Bulletin of the American Meteorological Society*, *84*(9), 1205–1218. https://doi.org/10.1175/BAMS-84-9-1205

Tsai, T. R., Rose, R. A., Weidmann, D., & Wysocki, G. (2012). Atmospheric vertical profiles of O_3, N_2O, CH_4, CCl_2F_2, and H_2O retrieved from external-cavity quantum-cascade laser heterodyne radiometer measurements. *Applied Optics*, *51*(36), 8779. https://doi.org/10.1364/AO.51.008779

van Peborgh Gooch, J. R., & Hounslow, M. J. (1996). Monte Carlo simulation of size-

enlargement mechanisms in crystallization. *AIChE Journal*, *42*(7), 1864–1874. https://doi.org/10.1002/aic.690420708

Verwer, J. G., Blom, J. G., van Loon, M., & Spee, E. J. (1996). A comparison of stiff ODE solvers for atmospheric chemistry problems. *Atmospheric Environment*, *30*(1), 49–58. https://doi.org/10.1016/1352-2310(95)00283-5

Wagh, S. P., Joge, S. D., Singh, S., Mali, P., Beirle, S., Wagner, T., Bucci, S., Saiz-Lopez, A., Bhawar, R., & Mahajan, A. S. (2023). Year-long ground-based observations of bromine oxide over Bharati Station, Antarctica. *Polar Science*, 100977. https://doi.org/10.1016/j.polar.2023.100977

Wang, Z.-P., & Han, X.-G. (2005). Diurnal variation in methane emissions in relation to plants and environmental variables in the Inner Mongolia marshes. *Atmospheric Environment*, *39*(34), 6295–6305. https://doi.org/10.1016/j.atmosenv.2005.07.010

Wang, Z., Huang, X., & Ding, A. (2018). Dome effect of black carbon and its key influencing factors: a one-dimensional modelling study. *Atmospheric Chemistry and Physics*, *18*(4), 2821–2834. https://doi.org/10.5194/acp-18-2821-2018

Wendel, J. (2014). Improved measurements of atmospheric nitrous oxide. *Eos, Transactions American Geophysical Union*, *95*(42), 388–388. https://doi.org/10.1002/2014EO420013

Xiong, X., Maddy, E. S., Barnet, C., Gambacorta, A., Patra, P. K., Sun, F., & Goldberg, M. (2014). Retrieval of nitrous oxide from Atmospheric Infrared Sounder: Characterization and validation. *Journal of Geophysical Research: Atmospheres*, *119*(14), 9107–9122. https://doi.org/10.1002/2013JD021406

Yan, H., Qian, Y., Zhao, C., Wang, H., Wang, M., Yang, B., Liu, X., & Fu, Q. (2015). A new approach to modeling aerosol effects on East Asian climate: Parametric uncertainties associated with emissions, cloud microphysics, and their interactions. *Journal of Geophysical Research: Atmospheres*, *120*(17), 8905–8924. https://doi.org/10.1002/2015JD023442

Yirdaw Berhe, T., Mengistu Tsidu, G., Blumenstock, T., Hase, F., & Stiller, G. P. (2020). Methane and nitrous oxide from ground-based FTIR at Addis Ababa: observations, error analysis, and comparison with satellite data. *Atmospheric Measurement*

Techniques, *13*(7), 4079–4096. https://doi.org/10.5194/amt-13-4079-2020

Yoo, J.-M., Lee, Y.-R., Kim, D., Jeong, M.-J., Stockwell, W. R., Kundu, P. K., Oh, S.-M., Shin, D.-B., & Lee, S.-J. (2014). New indices for wet scavenging of air pollutants (O3, CO, NO2, SO2, and PM10) by summertime rain. *Atmospheric Environment*, *82*, 226–237. https://doi.org/10.1016/j.atmosenv.2013.10.022

Z. Jacobson, M., & Turco, R. P. (1994). SMVGEAR: A sparse-matrix, vectorized gear code for atmospheric models. *Atmospheric Environment*, *28*(2), 273–284. https://doi.org/10.1016/1352-2310(94)90102-3

Zhao, H., & Zheng, C. (2006). Monte Carlo solution of wet removal of aerosols by precipitation. *Atmospheric Environment*, *40*(8), 1510–1525. https://doi.org/10.1016/j.atmosenv.2005.10.043